University College London

Computational Studies of the Properties of Molecular Dications

Philip Champkin

Thesis submitted in partial fulfilment of the degree of Doctor of Philosophy

2000

Abstract

Computational methods have been used to investigate properties of the doubly charged molecules (dications), SiF_3^{2+}, O_3^{2+} and BCl^{2+}. *Ab Initio* electronic structure calculations have been performed on all systems to provide information on equilibrium geometries and ground and excited state energies. Other computational techniques have also been used dependent on the system under study.

For SiF_3^{2+}, relative product ion intensities following electron-transfer reactions between SiF_3^{2+} and the rare gases neon, argon, krypton and xenon have been rationalised using a combination of *ab initio* electronic structure techniques and Landau-Zener reaction window theory. The calculations show that the experimentally observed products derived from the dications (SiF_3^+, SiF_2^+ and SiF^+) require the ions in the dication beam to be present in three different electronic states. The predicted and experimental product ion distributions, given this energy distribution, are in very close agreement. The combined computational approach adopted in this study is valuable for large molecular systems where the reactant molecules have several degrees of freedom and adopt markedly different equilibrium geometries depending on the degree of ionisation.

The theoretical study of the ozone dication O_3^{2+} was prompted by experimental studies into the double ionisation of neutral ozone. No stable O_3^{2+} ions were detected in the experiments and this study determines a possible mechanism for the rapid dissociation of the ozone dication upon formation via double ionisation of neutral O_3. The dication ground singlet state is found to have a linear equilibrium geometry that is stable with respect to dissociation to O^+ and O_2^+. However at the Franck-Condon zone for formation of O_3^{2+} from the neutral molecule the singlet potential energy surface intersects with a dissociative triplet state. It is proposed that crossing to this dissociative triplet state can account for the absence of any long lived O_3^{2+} ions in the electron impact mass spectrum of ozone.

For BCl^{2+} state averaged complete active space, SA-CAS, calculations have been used to determine the stabilities of the ground electronic state and 34 excited states. Vibrational level energies and tunnelling lifetimes have been determined for those states found to be quasibound. The majority of the states are found to be unbound, and of the bound states the ground $^1\Sigma^+$ state has the largest barrier to dissociation at 2.57 eV. Nine other excited states are found to be quasibound, although crossing to unbound states through strong spin orbit coupling is likely to reduce the lifetime of these states. The long lifetime of the ground state and the presence of other low lying quasibound states suggest that BCl^{2+} could be made and studied successfully in electron ionisation experiments.

Table of Contents

Publications

The following publications are based on the work discussed in this thesis

"Laser photofragmentation and collision-induced reactions of SiF_2^{2+} and SiF_3^{2+}", Yin-Yu Lee, Stephen R Leone, Philip Champkin, Nikolas Kaltsoyannis, Stephen D Price. *Journal of Chemical Physics*, **106(19)** (1997) 7981.

"A theoretical investigation of the electron-transfer reactions of the SiF_3^{2+} dication with the rare gases, neon, argon, krypton and xenon", Philip Champkin, Nikolas Kaltsoyannis, Stephen D Price. *International Journal of Mass Spectrometry and Ion Processes,* **172** (1998) 57.

"On the dissociation of the ozone dication", Philip Champkin, Nikolas Kaltsoyannis, Stephen D. Price, *Journal of Electron Spectroscopy and Related Phenomena,* **105**, (1999) 21.

Acknowledgements

I would like to thank my supervisors Dr. Stephen Price and Dr. Nikolas Kaltsoyannis for all their help, advice and patience during my studies and also their proof reading and corrections of the many drafts of this thesis. Thanks also go to UCL and Professor David Clary for the computational facilities necessary for my studies and to Dr. David Lauvergnat for help in using MOLPRO and state averaging CAS. Special thanks must of course go to Claire for her exceptional patience and support, to my parents for their continued loving encouragement and to Mr William Hedley for helping resurrect my computer and supplying me with a printer.

Chapter 1

Introduction

1.1 Introduction

In this thesis *ab initio* computational calculations have been used to investigate properties of the doubly charged molecules SiF_3^{2+}, O_3^{2+} and BCl^{2+}. For SiF_3^{2+} the calculations have allowed the interpretation of experiments investigating the collision between this doubly charged molecule and rare gas atoms. The O_3^{2+} molecule decays rapidly when formed experimentally, and computational investigations are used to discover a likely decay pathway for the molecule. BCl^{2+} has not been studied experimentally and the calculations are used to predict its likely stability when BCl is doubly ionised.

Singly charged positive ions have been studied extensively [1] and there exists a substantial amount of data on many of these species. Doubly charged positive ions, dications, due to the relatively high energies required for their formation and an inherent instability complicating experimental studies, have only recently been intensively studied. Hence, the amount of information on dicationic properties is relatively small compared to that on singly charged ions, although it is increasing rapidly due to advances in experimental techniques and an increased interest in dicationic properties.

Experiments on highly reactive or unstable molecules, such as dications, are often complicated and the experimental information obtained can be limited or complicated to interpret. Computational studies can be particularly useful for these experiments, providing information on molecular properties to aid the experimental set-up and also in interpreting inconclusive experimental results. The calculations performed for the studies in this thesis are geared toward the interpretation of

particular experimental results concerning dications and show the power of a combined experimental and computational approach to solving problems in chemical physics.

1.2 Computers and Chemistry

In the past two decades, the computational prediction of chemical properties has become an increasingly powerful tool for work in chemistry, producing a shift in emphasis away from chemistry being a purely experimental subject. The increasing power and reduced cost of computers has encouraged theoretical chemists and later physical, organic and inorganic chemists to use and develop sophisticated computational techniques. The subject of computational chemistry has become distinct from theoretical chemistry as it uses known theory to develop computer software to solve chemical problems. Computational chemistry is performed on all sizes of computer from desktop personal computers and workstations up to super computers. The size of the system under study or the required accuracy of the results is the guiding factor for which computer to use, but cost and the time available are also important. Generally, personal computers are not powerful enough to perform sophisticated calculations but they allow graphical representations of the results of calculations, manipulation of data and restricted calculations which can be used as a starting point for subsequent larger calculations. Workstations costing a few thousand pounds can be used for almost the entire range of computational chemistry and have become widely used by many research groups. Also, by linking several workstations together it is possible to achieve as much computational power as larger mainframes without the large cost.

Supercomputers, costing millions of pounds are at the top end of computational power and are used for studies on particularly large systems of thousands of molecules or to obtain results to very high accuracy. Such results can then be used as benchmark figures for subsequent studies. The power of supercomputers also

means that they can have hundreds of different users and each user can then use a small fraction of the computing power for smaller, but still sophisticated, calculations. Computational chemists are amongst the largest users of super computing time and some of the leading industrial companies own the most powerful machines in order to serve the chemists' needs.

1.2.1 Types of Calculation [2-4]

Single molecules: calculations on a single molecule can in principle give information on almost any physical observable. Molecular properties that are typically calculated include stable geometries (i.e. bond lengths and angles), barriers to internal rotation about bonds, vibrational frequencies, electron distribution, ionisation potentials, electron affinities, dipole moments and spin orbit coupling constants. The software to calculate these properties is often provided as a single package containing a suite of different programs. The packages used for the calculations in this thesis are capable of calculating many of the properties given above and are described in Chapter 2.

Molecular Assemblies: when calculations are performed on a large number of molecules, particularly solvent molecules, it is possible to determine thermodynamic properties, such as enthalpies, free energies, heat capacities and equilibrium constants. The binding energy between small molecules can be determined, as can partition coefficients, ionisation constants, potentials of mean force and free energy as a function of a particular co-ordinate.

Molecular reactions: The calculation of absolute rate constants for chemical reactions performed on a macroscopic scale is beyond the capability of computational chemistry, but it is possible to gain an idea of relative rate constants and the structure of transition states. Solvent effects in simple reactions have been

determined and the behaviour of macromolecules over time of a few hundred picoseconds.

1.3 Properties of doubly charged ions

Molecular ions with two positive charges, dications, are thought to play a role in atmospheric chemistry[5], combustion chemistry[6] and in the interstellar medium[7]. There is also interest in dications because small molecular dications display unusual bonding properties. Experimental studies of dications are difficult though, due to their high reactivity and the short lifetimes of many of their electronic states, and hence the information that can be obtained by experimental studies is often limited and hard to interpret[8]. Studies have also tended to concentrate on diatomic dications, although recent advances in experimental apparatus have allowed triatomics and larger dications to be studied in detail [9].

1.4 Stability of Dications

Molecular dications are energy rich species with the two positive charges producing an internal energy of 20-30 eV. The coulomb repulsion between the two positive charges would be expected to result in rapid fragmentation of the molecular dication and indeed a large number of dications are highly unstable, dissociating to two singly charged ions and, in some cases, additional neutral molecules, Eqns 1.1 & 1.2.

$$XY^{2+} \rightarrow X^{+} + Y^{+} \qquad 1.1$$

$$XY_2^{2+} \rightarrow X^{+} + Y^{+} + Y \qquad 1.2$$

However, a significant number of molecular dications with long-lived electronic states do exist, the first long-lived molecular dication, CO^{2+}, being observed in 1930 [10], and many more have been observed and studied since [11-16].

Molecular dications are often detected in mass spectrometric studies in which the ions must survive for at least 1×10^{-6} s in order to be observable. Thus the ions must possess at least one electronic state which has a barrier with respect to charge-separating dissociation, Eqns 1.1 & 1.2. These electronic states often lie at energies above the charge-separation asymptote and are thus termed metastable. In Figure 1.1 a typical metastable dication potential curve is shown, along with a purely repulsive curve and a stable bonding curve for comparison.

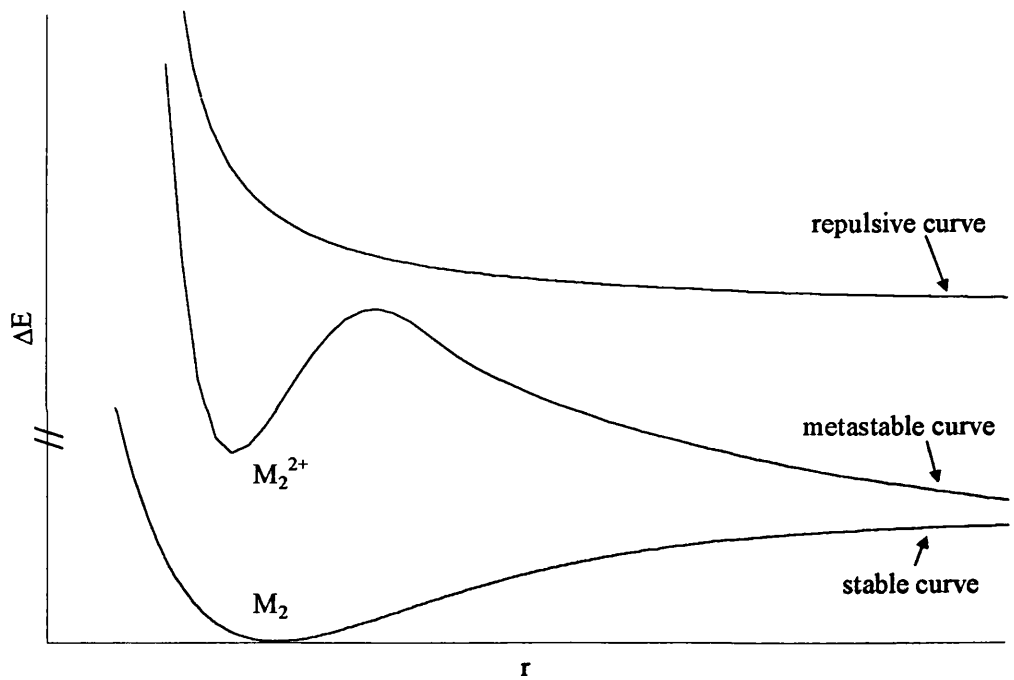

Fig 1.1 *Plot of repulsive, metastable and stable potential curves. Bond length, r, is plotted on the x axis and the energy, E, on the y axis.*

There are two theories currently proposed to account for the metastability of molecular dications. The first theory considers metastable states to arise from an avoided crossing between an attractive electronic state converging to a fragment dication plus neutral, (X^{2+} + Y), and a purely repulsive state correlating to the charge separation asymptote, (X^{+} + Y^{+}). This is shown schematically in Figure 1.2. An alternative explanation is proposed by O'Neill and co-workers from computational studies of F_2^{2+}; the potential curves for the F_2^{2+} dication were found to be well reproduced by combining the well-established curves of isoelectronic O_2

with a coulomb repulsion [17]. From this, they proposed that dication states can be pictured as arising from the combination of an ordinary chemical binding potential and the constituent ion Coulomb repulsion potential. Thus metastable states will exist when the chemical bond is strong enough to overcome the repulsion of the two positive charges. But, studies on some heteronuclear diatomics such as HCl^{2+} have shown that the positive charges can both reside on one atom at small internuclear separation [18], the additive model is thus inappropriate for these systems and they are better described by the avoided crossing theory.

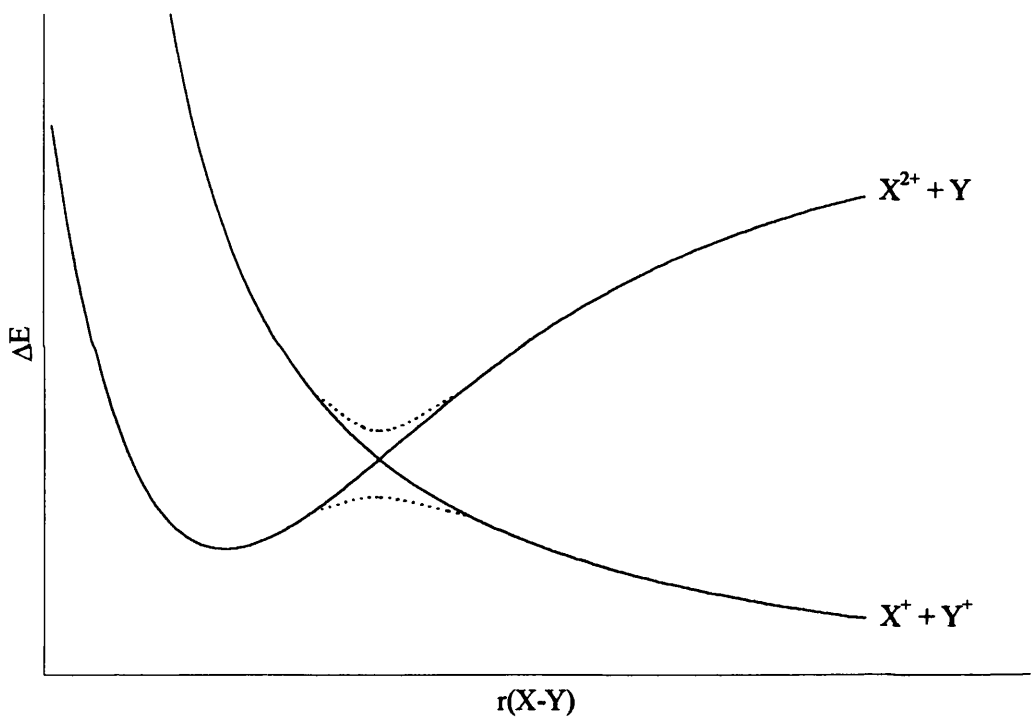

Fig 1.2 *Schematic potential energy curves showing a metastble dication state arising from the avoided crossing (dashed lines) of potential energy curves which correlate with the charge separated $X^{+} + Y^{+}$ and neutral loss $X^{2+} + Y$ asymptotes.*

1.5 Experimental studies of dications

Although many dications have been detected experimentally, detailed studies of their electronic structures are hampered by the dication's high reactivity, short lifetimes and limited accessibility of electronic states suitable for high resolution studies. Laser spectroscopic studies have provided detailed information on the

structures and energetics of many monocations [19] but similar studies on dications are limited to only a handful of molecules.

Metastable electronic states of N_2^{2+} have been studied with rotational resolution by laser predissociation spectroscopy [20-26]. This technique detects photoabsorption between metastable dication electronic states by monitoring the fragment ions from the photoinduced unimolecular charge separation of the upper state as in equation 1.3.

$$N_2^{2+}(X) + h\nu \rightarrow N_2^{2+}(A) \rightarrow N^+ + N^+ \qquad 1.3$$

No other dications have yielded such detailed information on their excited electronic states from spectroscopic studies although recently the first high resolution IR laser predissociation spectra of DCl^{2+} have been recorded, which resolve several vibrational levels [27]. The carbon monoxide dication has been studied with vibrational resolution [15] and the dications NO^{2+} and CF^{2+} are thought to be good candidates for spectroscopic studies, but as yet no spectra have been recorded [28,29].

Experimental information on the electronic structure of three and four atom molecular dications is less detailed, with most information obtained from collisional studies, and some from threshold electron spectroscopy experiments. These techniques provide information on electronic energy levels and their stability, double ionisation potentials and kinetic energy release, and are described below. Collisional studies are discussed in detail in Chapter 3. Larger polyatomic dications have only been studied by analysis of the fragmentation products observed upon double ionisation of the neutral [30,31]. These studies determine the double ionisation potential, kinetic energy release and fragmentation pathways of the dication.

1.6 Experimental Techniques

Many techniques have been developed to study dicationic molecules and their reactions, and a detailed discussion of all these techniques is beyond the scope of this thesis. But, as the experimental studies of the dications SiF_3^{2+} and O_3^{2+} are relevant to the calculations described in Chapters 3 & 4, some discussion of the techniques used in these studies is given below, along with descriptions of some of the current state of the art techniques for high resolution studies of dications.

1.6.1 Dication formation

The experimental studies of dications commonly form the ions by one of three different methods:-

(i) Electron-impact ionisation forms the ions by passing the neutral molecules through a region where they collide with fast moving electrons and the impact ionizes the molecules.

(ii) Photoionisation uses a photon of a known energy to ionise electrons from the molecule.

(iii) Collisional ionisation forms the ions by colliding the neutral molecules with high energy ions.

As well as the dications that are desired, these processes often form many other ions such as singly or triply charged species and also charged fragments of the precursor molecules, as the high energy processes are capable of breaking up the molecules as well as ionising them. The required dications are extracted from these other ions by mass spectrommetric techniques that separate the ions by their mass to charge ratio. The experimental studies of SiF_3^{2+} and O_3^{2+} both form the ions by electron impact ionisation.

1.6.2 Time of flight mass spectrometry

Many dication experiments use the mass spectrometric technique of time of flight mass spectrometry. This technique identifies ions by the length of time they take to travel a set distance within the mass spectrometer. Ions are accelerated by passing them through a controlled potential difference and their resulting velocity is dependent on the ion's mass to charge ratio. The ions produced in the SiF_3^{2+} experiments are identified and studied by time of flight spectroscopy [32].

1.6.3 Coincidence techniques

In the mass spectrometric study of doubly charged molecules, identifying the ions by their mass to charge ratio encounters problems for a doubly charged diatomic such as N_2^{2+}, as the parent dication has the same mass to charge ratio as the fragment ion N^+. The signal for N_2^{2+} then overlaps with any N^+ signal, making it hard to obtain useful information on the dication. To overcome this problem coincidence techniques have been developed to study molecular dication dissociation [33]. Coincidence techniques are used in time of flight mass spectrometric studies and measure the difference between the flight times of selected dissociation products of an unstable dication. These techniques are used to study both electron ionisation and photoionisation of the neutral molecule. Coincidence experiments yield information on the dynamics of the double ionisation process, electronic information on the dications and fragmentation pathways.

1.6.3.1 Ion-Ion Coincidence and PIPICO

In an electron impact time of flight mass spectrometer the ion-ion coincidence technique [34-36] is used to investigate the following dissociation process.

$$e^- + XY \rightarrow XY^{2+} + 3e^- \rightarrow X^+ + Y^+ + 3e^- \qquad 1.4$$

Ion pairs detected within a certain time of each other are assumed to both be the dissociation products of the same molecule. From this technique, the kinetic energy release upon dissociation can be determined, as well as branching ratios for various dissociation routes and the mechanism of the dissociation reaction. The ion-ion coincidence technique is used in the O_3^{2+} experiment (see chapter 4), identifying the dications dissociation products and determining the double ionisation potential and kinetic energy release [37]. Where the dication is formed by photoionisation the technique is called photoion - photoion coincidence (PIPICO) [8,38-40]. These techniques have the advantage that the energy of the ionizing photon is known.

1.6.3.2 PEPIPICO

As the ion-ion coincidence and PIPICO experiments measure the time of flight difference between fragment ion pairs, when these two particle coincidence techniques are applied to ion pairs of equal mass the time difference is zero and the identity of the ion pair cannot be determined. Also, complex polyatomic dications may have a number of fragmentation channels that yield ion pairs with the same time of flight difference, so the ions are not unambiguously identified. For such cases, triple coincidence techniques have been developed which, as well as the fragment ion pair, also detect one or more of the ejected electrons. These photoelectron - photoion - photoion coincidence (PEPIPICO) [41,42] techniques record the actual ion flight times, thus allowing the fragments to be identified.

1.6.3.3 TPEsCO

When forming dications by photoionisation techniques, if the photon is of the correct energy to doubly ionise the neutral species and form the dication exactly at a specific electronic state then there is no excess energy to go into the kinetic energy of the ejected electrons, so the photoelectrons detected will have zero energy. This Threshold Photo Electrons COincidence, TPEsCO, technique [43] detects the pair of ejected electrons whilst the ionising photon's energy is varied

scanning for zero energy electrons. This technique provides information on the electronic energy levels and some vibrational levels. The resolution of this technique is limited by the choice of zero energy actually being as close to zero as is feasible with the experimental set-up. The closer to zero energy, the higher the resolution of the experiment but the weaker the electron signal that is detected.

1.6.4 DFKER

Due to the thermal motion of the parent molecule, the results of experiments using the techniques described above suffer from Doppler broadening which limits the energy resolution of the kinetic energy release spectra. However, using the technique Doppler Free Kinetic Energy Release spectroscopy (DFKER) [44] the Doppler broadening is eliminated through simultaneous measurement of both fragment ions energies. The kinetic energy release spectra recorded contain vibrational fine structure and this technique allows detailed investigation of the electronic and vibrational states of the dications, DFKER has been used to study the dications N_2^{2+}, O_2^{2+} and NO^{2+} [12,45,46] .

1.6.5 Double charge transfer

Another method used to investigate dications is the Double Charge Transfer (DCT) technique [47], where a monocation, P^+, is collided with the neutral, AB at keV energies. In the reaction

$$P^+ + AB \rightarrow P^- + AB^{2+} \qquad 1.5$$

the anion P^- is monitored, and providing the transition $P^+ \rightarrow P^-$ is well understood, kinetic energy analysis of the anion gives concise information about the various electronic states of the dication AB^{2+}. Unfortunately the DCT techniques can only be applied to neutral molecules which exist as bulk compounds and the dication is only probed indirectly as it is the anion P^- which is detected.

1.6.6 Collisional studies

As well as probing the properties of the isolated dication, experiments have recently been developed to investigate the reactions of dications upon collision with neutral species [48]. The early studies focused on the collisions between CO^{2+} and rare gas atoms at high collision energies (keV) in conventional mass spectrometers [49-52]. However, for a more chemically realistic study, lower collision energies (eV) need to be employed requiring specialist spectrometers [9]. The collision studies using rare gases observe an electron-transfer reaction occurring where the dication strips an electron from the rare gas. The electron-transfer reaction is discussed in more detail in Chapter 3 which investigates collisions between the dication SiF_3^{2+} and rare gas atoms. In the collision reaction with neutral molecules bond forming reactions have been observed. A wide variety of dications have been found to form chemical bonds upon low energy collisions with D_2 and O_2 of which typical reactions observed are:

$$CF^{2+} + D_2 \rightarrow DCF_2^{+} + D^{+}$$

$$CF_3^{2+} + D_2 \rightarrow DCF_2^{+} + [F + D]^{+}$$

$$OCS^{2+} + D_2 \rightarrow DS^{+} + [D + O + C]^{+}$$

$$CF^{2+} + O_2 \rightarrow CO^{+} + [F + O]^{+}.$$

The reactions occur more readily with D_2 and recent analysis has determined that reactions with D_2 occur via hydride, D^-, transfer from the neutral molecule to the dication [9].

The SiF_3^{2+} experiments investigate the charge transfer reaction that occurs between the SiF_3^{2+} dication and rare gas atoms and are described in more detail in chapter 3.

1.7 *Ab initio* calculations on dications

Computational studies of dications require sophisticated quantum chemistry calculations due to their unusual bonding properties. The formation of the potential

well due to competition between an ordinary bond and electrostatic repulsion, as described earlier, complicates calculations as the coulomb component is described very accurately by the *ab initio* calculations, but the chemical bonding term is described with less accuracy. In neutral systems the error in the bonding potential is tolerable, but in dications the coulomb term cancels most of the binding energy, thus the error is magnified as it is now a larger fraction of the well depth [53,54].

Although the error in the *ab initio* calculations of the dication potential curves is small it can result in the barrier heights and widths being underestimated, with the result that experiments have observed vibrational levels for dication electronic states above the highest predicted by calculation [53]. In addition, underestimating the barrier width resulted in calculations on N_2^{2+} predicting that the predominant decay route for certain electronic states would be tunnelling through the potential barrier [55]. Subsequent high resolution experiments on N_2^{2+} though, determined that the electronic states actually decayed via crossing to other electronic states [20], indicating that the tunnelling lifetimes, and thus the barrier widths, were greater than the calculations suggested. But high level calculations on dications do achieve good agreement with experimental transition frequencies and equilibrium bond lengths [55-57], and the discrepancies described above are only noticed in detailed comparisons of calculation and experimental results. The information gained from computational studies of dications is still of great use for studying dication properties and as a guide to experimental studies.

1.8 Chapter Summaries

1.8.1 Molecular electronic structure theory

The basic principles behind the current molecular electronic structure theories and how they are applied in computational calculations are presented in Chapter 2. The

software packages used for the calculations performed in this thesis are discussed along with the computational resources used.

1.8.2 Electron transfer reactions of the SiF_3^{2+} dication with the rare gases neon, argon, krypton and xenon

Recent advances in experimental techniques have allowed the reactive properties of some dications to be studied mass spectrometrically. Typically, dications are found to undergo a charge transfer reaction where the high positive charge of dications can strip an electron off a neutral species. Experimental studies of the charge transfer reactions of OCS^{2+}, CO_2^{2+} and SiF_2^{2+} with rare gas atoms found good agreement with the current theories to model the charge transfer reaction and the experimental results. However, the experimental results for SiF_3^{2+} were found to show marked discrepancies from the theory predictions [58].

In Chapter 3, *ab initio* calculations of the equilibrium geometries and excited state energies of SiF_3^+ and SiF_3^{2+} provide vital information for use in Landau-Zener calculations. These calculations are used to predict the experimental product ion yields following the reaction of SiF_3^{2+} with the rare gases, and good agreement is found with the experimental results.

1.8.3 On the dissociation of the ozone dication

Dications are thought to play an important part in atmospheric chemistry, and so the dication of ozone, O_3^{2+}, is likely to be important in the atmospheric ozone cycle. However, recent experiments to form O_3^{2+} by electron impact ionisation did not detect any O_3^{2+}, only the dissociation products O_2^+ and O^+, showing that any dications produced are formed in an unstable state with lifetimes $< 10^{-6}$ s [36].

In Chapter 4, *ab initio* calculations on the ground singlet and first excited triplet states are used to create potential energy surfaces for the ozone dication

dissociating to O_2^+ and O^+. From these surfaces, a dissociation mechanism is proposed where the ozone dication rapidly crosses from a quasibound singlet state to weakly bound triplet state. The singlet and triplet states are found to lie close in energy at the geometry at which the dication is formed in experiments; the calculations suggest that forming the dication via single ionisation of O_3^+ could result in long lived O_3^{2+} ions.

1.8.4 An *ab initio* study of the structure and stability of low lying electronic states of the dication BCl^{2+}

The BCl^{2+} dication has not been studied experimentally, so in Chapter 5 a series of *ab initio* calculations are performed on the dication to provide information on its likely stability to aid possible experiments. Potential curves of the 35 electronic states that dissociate to first six dissociation asymptotes of BCl^{2+} have been calculated, and the molecular orbital configurations that make up the electronic states are determined. The calculations suggest that BCl^{2+} ions should be observable in mass spectrometric studies due to the presence of metastable electronic states and some discussion of the possible origin of this metastability is undertaken.

References

(1) Eland J. H. D. *Photoelectron Spectroscopy*; Second ed.; Butterworth and Co.:, 1984.

(2) Grant G. H. and Richards W. G. *Computational Chemistry*; OUP: Oxford, 1995.

(3) Jensen F. *Introduction to Computational Chemistry*; Wiley: Chichester, 1999.

(4) Atkins P. W. *Molecular Quantum Mechanics*; Third ed.; OUP: Oxford, 1997.

(5) Prasad S. and Furman D. R. *J. Geophys. Res.* **80** (1975) 1360.

(6) Safvan C. P. and Mathur D. *J. Phys. B* **26** (1993) L793.

(7) Leach S. *J. Elect. Spectr. Relat. Phenom.* **41** (1985) 427.

(8) Curtis D. M. and Eland J. H. D. *Int. J. Mass Spectrom. Ion Proc.* **63** (1985) 241.

(9) Price S. D. *J. Chem. Soc., Faraday Trans.* **93** (1997) 2451.

(10) Conrad R. *Physik Z* **31** (1930) 888.

(11) Hall R. I., Avaldi L., Dawber G., McConkey A. G., MacDonald M. A. and King G. C. *Chem. Phys.* **187** (1994) 125.

(12) Lundqvist M., Edvardsson D., Baltzer P., Larsson M. and Wannberg B. *J. Phys. B* **29** (1996) 499.

(13) Dejarme L. E., Cooks R. G. and Ast T. *Org. Mass Spectrom.* **27** (1992) 667.

(14) Mathur D., Anderson L. H., Hvelplund P., Kella D. and Safvan C. P. *J. Phys. B* **28** (1995) 3415.

(15) Hochlaf M., Hall R. I., Penet F., Kjeldson H., Lablanquie P., Lavollee M. and Elland J. H. D. *Chem. Phys.* **207** (1996) 159.

(16) Hsieh S. and Eland J. H. D. *J. Chem. Phys.* **103** (1995) 1006.

(17) Senekowitsch J. and O'neil S. *J. Chem. Phys.* **95** (1991) 1847.

(18) Bennett F. R. and McNab I. R. *Chem. Phys. Lett.* **251** (1996) 405.

(19) Maier J. P. *J. Elect. Spectr. Relat. Phenom.* **66** (1993) 15.

(20) Mullin A. S., Szaflarski D. M., Yokoyama K., Gerber G. and Lineberger W. C. *J. Chem. Phys.* **96** (1992) 3636.

(21) Szaflarski D. M., Mullin A. S., Yokoyama K., Ashford M. N. F. and Lineberger W. C. *J. Phys. Chem.* **95** (1991) 2122.

(22) Masters T. E. and Sarre P. J. *J. Chem. Soc., Faraday Trans.* **86** (1990) 2005.

(23) Martin P. A., Bennett F. R. and Maier J. P. *J. Chem. Phys.* **100** (1994).

(24) Cosby P. C., Moller R. and Helm H. *Phys. Rev. A* **28** (1983) 766.

(25) Larsson M., Sundstrom G., Brostrom L. and Mannervik S. *J. Chem. Phys.* **97** (1992) 1750.

(26) Sundstrom G., Carlson M., Larsson M. and Brostrom L. *Chem. Phys. Lett.* **218** (1994) 17.

(27) Abusen R., Bennett F. R., McNabb I. R., Sharp D. N., Sheill R. C. and Woodward G. A. *J. Chem. Phys.* **180 No. 5** (1998) 1761.

(28) Senekowitsch J., ONeil S. V., Knowles P. and Werner H.-J. *J. Chem. Phys.* **93** (1990) 562.

(29) Pettersson L. G. M., Karlsson L., Keane M. P., Debrito A. N., Correia N., Larsson M., Brostrom L., Mannervik S. and Svenson S. *J. Chem. Phys.* **96** (1992) 4884.

(30) O'Connor C. and Price S. D. *Int. J. Mass Spectrom. Ion Proc.* **177** (1998) 119.

(31) O'Conner C., Jones N. C. and Price S. D. *Chem. Phys.* **214** (1997) 131.

(32) Champkin P., Kaltsoyannis N. and Price S. D. *Int. J. Mass Spectrom. Ion Proc.* **172** (1998) 57.

(33) Eland J. H. D. *Vacuum Ultraviolet Photoionization and Photodissociation of Molecules and Clusters*; C. Y. Ng ed.; World Scientific: Singapore, 1991.

(34) McCulloh K. E., Sharp T. E. and Rosenstock H. M. *J. Chem. Phys.* **42** (1965) 3501.

(35) Brehm B. and deFrênes G. *Int. J. Mass Spectrom. Ion Proc.* **26** (1978) 251.

(36) Newson K. A. and Price S. D. *Int. J. Mass Spectrom. Ion Proc.* **153** (1996) 151.

(37) Champkin P., Kaltsoyannis N. and Price S. D. *J. Elect. Spectr. Relat. Phenom.* **105** (1999) 21.

(38) Lablanquie P., Nenner I., Millie P., Morin P., Eland J. H. D., Hubin-Franksin M. J. and Delwiche J. *J. Chem. Phys.* **82** (1985) 2951.

(39) Masuoka T. *Phys. Rev. A* **48** (1993) 1955.

(40) Dujardin G., Leach S., Dutuit O., Guyon P. M. and Richardviard M. *Chem. Phys.* **88** (1984) 339.

(41) Eland J. H. D., Wort F. S. and Royds R. N. *J. Elect. Spectr. Relat. Phenom.* **41** (1986) 297.

(42) Frasinski L. J., Stankiewicz M., Randall K. J., Hatherly P. A. and Codling K. *J. Phys. B* **19** (1986) L819.

(43) McConky A. G., Dawber G., Avoldi L., MacDonald M. A. and King G. C. *J. Phys. B.* **27** (1994) 271.

(44) Lundqvist M., Baltzer P., Edvardsson D., Karlsson L. and Wannberg B. *Phys. Rev. Lett.* **75** (1995) 1058.

(45) Edvardsson D., Lundqvist M., Baltzer P., Wannberg B. and Lunell S. *Chem. Phys. Lett.* **256** (1996) 341.

(46) Lundqvist M., Edvardsson D., Baltzer P. and Wannberg B. *J. Phys. B* **29** (1996) 499.

(47) Harris F. M. *Int. J. Mass Spectrom. Ion Proc.* **120** (1992) 1.

(48) Herman Z. *Int. Reviews in Phys. Chem.* **15** (1996) 299.

(49) Hamdan M. and Brenton A. G. *J. Phys. B* **22** (1989) L45.

(50) Curtis J. M. and Boyd R. K. *J. Chem. Phys.* **80** (1984) 1150.

(51) Krishnamurthi V., Negasha K., Marathe V. R. and Mathur D. *Phys. Rev. A* **44** (1991) 5460.

(52) Herman Z., Jonathon P., Brenton A. G. and Beynon J. H. *Chem. Phys. Lett.* **141** (1987) 433.

(53) Bennett F. R. *Chem. Phys.* **190** (1995) 53.

(54) Bennett F. R. *J. Chem. Phys.* **103 (9)** (1995) 3613.

(55) Senekowitsch J., ONeil S. V., Knowles P. and Werner H.-J. *J. Phys. Chem.* **95** (1991) 2125.

(56) Pettersson L. G. M., Siegbahn P. E. M., Böstrom L., Mannervik S. and Larsson M. *Chem. Phys. Lett.* **191** (1992) 279.

(57) Taylor P. R. and Partridge H. *J. Phys. Chem.* **91** (1987) 6148.

(58) Lee Y.-Y., Leone S. R., Champkin P., Kaltsoyannis N. and Price S. D. *J. Chem. Phys.* **106** (1997) 7981.

Chapter 2

Molecular electronic structure theory

2.1 Introduction

Modern electronic structure theory has become a powerful tool for the solution of many chemical problems, often enabling the determination of molecular properties that can be very difficult or impossible to probe experimentally. The use of computers is essential to most modern work with different techniques available allowing the accuracy of the calculations to be balanced with computational resources available.

Studies on large molecular systems may use techniques such as Extended Hückel Theory [1] that employ extensive approximations to produce a simplified description of the system under study; here the interaction between electrons in different orbitals is not calculated but replaced by an experimentally determined constant. For smaller systems the more accurate *ab initio* computational techniques can be used; here an attempt is made to solve the Schrödinger equation from first principles, treating the molecule as a collection of positive nuclei and negative electrons moving under a coulomb potential. In these methods some initial approximations are made. The first is the Born-Oppenheimer approximation in which the motion of the nuclei is considered to be so slow (relative to electronic motion) that it has no effect on the motion of the electrons (i.e. the electrons move in the potential field of the fixed nuclei). Also relativistic effects are ignored, the particles are influenced only by electrostatic forces. In the *ab initio* techniques the important aspect is that the molecular properties are calculated without using any prior knowledge of the species' chemical behaviour. Unfortunately *ab initio* studies require large calculations but with the power of modern computers molecular

systems of tens of atoms can be studied to a very high accuracy and calculations on three to five atom molecules are routine.

Underlying many of the computational techniques is the Variation Principle [2] which states that so long as the equations used to model the systems under study conform to certain rules then an approximate wavefunction used to calculate the energy of a system will never give a value lower than that possible with the 'perfect' wavefunction. This principle is important to many of the techniques in computational chemistry because with the power of modern computers it is possible to create highly flexible wavefunctions with literally thousands of variables. If the wavefunction conforms to the Variation Principle then providing there is sufficient computer power to efficiently vary all the parameters in the wavefunction it is possible to come close to the 'perfect' wavefunction and obtain highly accurate results.

2.2 Hartree-Fock equations

The Schrödinger equation, Eqn 2.1, provides a theoretical basis for determining the properties of almost any chemical system, but an exact solution of the equation for a system with any more than one electron is not possible due to the complication of solving the electron-electron interaction. However, computational techniques have been developed that are able to give very detailed and reliable numerical solutions to the Schrödinger equation for many systems.

$$H\Psi = E\Psi \qquad 2.1$$

Douglas Hartree originally introduced these techniques before the advent of computers [3] then they were subsequently modified by Vladimer Fock to correctly account for the Pauli exclusion principle [4], hence they are known now as Hartree-Fock equations.

The full derivation of the Hartree-Fock equations from the Schrödinger equation is non-trivial [2] and has the Schrödinger equation expressed as

$$H^{SCF}\phi_i = \varepsilon_i\phi_i \qquad 2.2$$

where H^{SCF} is in the form necessary to be used in the Self Consistent Field equations described later, and ϕ_i are the one electron molecular orbitals. H^{SCF} contains the kinetic and potential energy terms of the system and is given by

$$H^{\mathrm{SCF}} = \left\{ H^{\mathrm{N}} + \sum_{\mathrm{i}} J - \sum_{\mathrm{j}}{}' K \right\} \qquad 2.3$$

where H^N describes the electrons moving in the electronic field of the nuclei, and J and K represent the electron / electron interaction.

In $\sum_{\mathrm{i}} J$ J is a shorthand notation for the coulombic repulsion between two electrons in orbitals ϕ_i and ϕ_j where the second electron is represented as a spherical charge distribution; the fully expanded form of J is given in Eqn. 2.4. The second summation term $\sum_{\mathrm{j}}{}' K$ is performed over pairs of electrons with the same spin and is necessary so that the equations obey the Pauli exclusion principle. Again, K is shorthand notation, the expanded form of K is given in Eqn. 2.5.

$$J_{\mathrm{j}}\phi_{\mathrm{i}}(1) = \left(\int \phi_{\mathrm{j}}^2(2) \frac{1}{r_{12}} \mathrm{d}v_2 \right) \phi_{\mathrm{i}}(1) \qquad 2.4$$

$$K_{\mathrm{j}}\phi_{\mathrm{i}}(1) = \left(\int \phi_{\mathrm{j}}(1)\phi_{\mathrm{i}}(2) \frac{1}{r_{12}} \mathrm{d}v_2 \right) \qquad 2.5$$

The $\sum_{\mathrm{j}}{}' K$ summation is generally called an exchange term and is purely a quantum mechanical artifact with no direct classical analogue, although it can be thought of as a modification of the coulomb potential to take account of like spin electrons' increased tendency to avoid each other. In Eqn. 2.4 J is described as 'local' because the calculation of $J_j\phi_i$ requires the knowledge of ϕ_i only at a single point in space, whereas K is 'non-local' because $K_j\phi_i$ has ϕ_i within the integral so a knowledge of ϕ_i over all space is required.

2.3 Self Consistent Field Calculations

In the Hartree Fock form of the Schrödinger equation, Eqn. 2.2, a description of the molecular orbitals of the system, ϕ_i, is required to solve the equations and obtain the energy of the molecular system. This introduces a problem because to obtain an accurate energy, accurate molecular orbitals for the system are required, but before performing calculations on a system it is not possible to know what the accurate orbitals of the system will be, as they are an integral part of the results expected from the calculations. To address this problem an initial guess of the form of the molecular orbitals is made to act as a starting point for the calculations. Then, using an iterative process a cyclical series of calculations gradually improves the molecular orbitals, and thus the energy, until the energy difference between successive calculations is within a specified limit.

The general scheme can be neatly represented as the sequence below.

Start,	*1*	*Guess initial molecular orbitals,* $\Psi=\phi_1, \phi_2, \phi_3 \ldots \phi_n$
	2	*Solve Hartree-Fock equation for* ϕ_1 *in the field of electrons in* $\phi_2, \phi_3 \ldots \phi_n$
	3	*Obtain* $\phi'_1, \phi_2, \phi_3 \ldots \phi_n$
	4	*Solve Hartree-Fock equation for* ϕ_2 *in the field of electrons in* $\phi'_1, \phi_3 \ldots \phi_n$
	5	*Obtain* $\phi'_1, \phi'_2, \phi_3 \ldots \phi_n$
	6	*Repeat process to find* $\phi'_1, \phi'_2, \phi'_3 \ldots \phi'_n$
	7	*Compare* $\phi_1, \phi_2, \phi_3 \ldots \phi_n$ *with* $\phi'_1, \phi'_2, \phi'_3 \ldots \phi'_n$
	8	*If difference is small and within set limits end cycle, otherwise let* $\phi'_n = \phi_n$ *repeat steps 2 to 8*

In its simplest form the Hartree-Fock equation can only be used on closed shell systems where all the electrons are paired, this is called Restricted Hartree-Fock, RHF, theory. To allow calculations on open shell systems the more sophisticated Unrestricted Hartree-Fock, UHF, theory uses two sets of orbitals, one representing the alpha spin electrons and the other the beta spin electrons. Each set of UHF orbitals is represented by a different spatial wavefunction, thus unpaired electrons are created by occupying one spin molecular orbital and not its corresponding opposite spin orbital. Paired alpha and beta spin orbitals correspond to the doubly occupied orbitals of the RHF system. Unfortunately the UHF wavefunction for a given system contains contributions from higher spin states of the same symmetry, a problem called spin contamination. Energies obtained from UHF calculations can sometimes be more negative than a corresponding RHF calculation, thus creating difficulties if the neutral and ionized versions of a molecule need to be compared. To counter the problem of spin contamination in open shell calculations the Restricted Open shell Hartree-Fock, ROHF, method has been developed; here the doubly occupied orbitals are constrained to be identical for alpha and beta spin preventing the mixing of higher spin states.

2.3.1 Molecular orbitals

In producing a molecular wavefunction, Ψ, to adequately describe the molecular system under study, accurate molecular orbitals, ϕ, are required. Ψ represents the molecular wavefunction,

$$\Psi = \phi_1\phi_2\phi_3\ldots\phi_n \qquad 2.6$$

where each ϕ_i can be considered as a three dimensional function which determines the properties of an individual electron in the molecule. There are certain constraints necessary on Ψ in Eqn 2.6. The Pauli Exclusion Principle tells us that the total wavefunction must be anti-symmetric, change sign, upon the interchange

of any two electron co-ordinates as the electron has a spin of ½. To conform to these requirements Ψ is expressed as a Slater determinant where the columns for the determinant are single electron wavefunctions, orbitals, and the rows are the electron co-ordinates. Expressing Ψ is in the form of Eqn 2.6 is short hand notation for the leading diagonal of the Slater determinant (i.e. Ψ is not a simple product wavefunction).

In most *ab initio* studies the molecular orbitals are unknown and are created using a linear combination of known atomic orbitals, the LCAO method. Using the LCAO method each molecular orbital, ϕ_i, can be written as

$$\phi_i = \sum_k C_{ik}\chi_k \qquad 2.7$$

where χ_k is a one electron atomic wavefunction and C an expansion coefficient which describes the extent of the contribution of the atomic orbital to the molecular orbital. Bonding molecular orbitals are created when the atomic orbitals add constructively, increasing the electron density between the atoms. Conversely, anti-bonding molecular orbitals can be formed when the atomic orbitals sum destructively reducing the electron density between the atoms. So for the simple case of a molecular orbital, ϕ, created from the combination of a 1*s* atomic orbital on atom *A*, $\chi_{1s}(A)$, and a 1*s* atomic orbital on atom *B*, $\chi_{1s}(B)$, the bonding molecular orbital would be

$$\phi = C_1\chi_{1s}(A) + C_2\chi_{1s}(B) \qquad 2.8$$

and the antibonding molecular orbital would be

$$\phi = C_1\chi_{1s}(A) - C_2\chi_{1s}(B) \qquad 2.9$$

The extent to which atomic orbitals will interact, constructively or destructively, is governed by the overlap between the orbitals, the overlap integral *S*. For two orbitals $\chi(A)$ and $\chi(B)$

$$S = \int \chi(A)\chi(B)\mathrm{d}v \qquad 2.10$$

and in some cases simple formulae can be written for overlap integrals, for example for two hydrogenic 1*s* orbitals on nuclei at a separation *R*

$$S = \left\{ 1 + \frac{ZR}{a_0} + \frac{1}{3}\left(\frac{ZR}{a_0}\right)^2 \right\} e^{-ZR/a_0}. \qquad 2.11$$

Here *Z* is the nuclear charge and a_0 the Bohr radius, (5.292 x 10^{-11} m). For two 1*s* orbitals at the equilibrium bond length of H_2^+, 1.06 x 10^{-10} m, [5] $S = 0.59$, which is unusually large, generally for higher lying atomic orbitals *S* is in the range 0.2 to 0.3. The extent to which orbitals overlap is obviously dependent on separation but also on the energy of the orbitals and their symmetry. Only orbitals of the same symmetry can overlap and also the greater the energy difference between the orbitals the smaller the overlap. Also, the more terms in the molecular orbital expansion, Eqn 2.7, the more flexible the wavefunction and so by the variation principle an infinite expansion would give an energy which is the largest negative number possible for the SCF process, this energy is commonly called the Hartree-Fock limit.

2.3.2 Atomic orbitals and basis sets

By creating the molecular orbitals from a combination of atomic orbitals in the LCAO method described above it is obvious that the atomic orbitals used are important. The most sensible atomic orbitals, χ_k, to use in the molecular orbital expansion are the exponential functions suggested by Slater [6]. These Slater type orbitals, STO's, have the form,

$$\chi_k = C_e^{-\zeta r} Y_{lm} \qquad 2.12$$

where *C* is a normalising constant, Y_{lm}, a spherical harmonic function describing the angular dependence of the orbital and ζ is the orbital exponent. STO's are used because they describe the atomic orbitals in the exact solution of the Schrödinger equation for the hydrogen atom. But integrals involving exponentials of the form present in STO's are at best expensive computationally and at worst can be

intractable for molecules, so Gaussian functions are actually used in calculations. The use of Gaussian functions was suggested by Boys [7] because they are more practical for computer calculations being easily and effectively evaluated and efficient routines exist for the analytic evaluation of integrals over Gaussian functions.

Wavefunctions created from either Gaussian type orbitals (GTOs) or STO's have the same angular dependence (i.e. *s*, *p*, *d*, etc.) and thus GTOs and STOs differ only in their radial part. The Gaussian radial dependence has the form $exp(-ar^2)$ which is a poor description of the atomic orbital both near and far from the nucleus. To produce a satisfactory atomic orbital several Gaussian functions are combined to give a best fit to an STO, and it is found that the ratio of the number of Gaussians to the number of STO's required to obtain comparable accuracy is not very large. Although four Gaussians are needed to obtain energies within 10^{-3} hartrees, (0.002 eV), of the exact energy of the hydrogen atom, for atoms further down the periodic table the ratio is reduced i.e. for argon the ratio is around 2.6 : 1.

The set of atomic orbitals used in a calculation is called the *basis set*. The use of basis sets is essentially another approximation used in *ab initio* methods. Expanding an unknown molecular orbital as a set of known atomic orbitals, as described above, is not an approximation if the basis set is complete but a complete basis is one that is infinite. To use an infinite number of functions in actual calculations would be impossible so a compromise is made, balancing the size of the basis with computational resources.

As well as representing the occupied atomic orbitals on an atom extra functions are often added to a basis set to improve the accuracy of calculations, these are polarisation and diffuse functions. Polarisation functions are atomic orbitals of a

higher angular momentum than is normally occupied on an atom, so *p* type orbitals on hydrogen or *d* orbitals on *p*-block elements, *f* orbitals on *d*-block etc. The polarization functions are important as bonding between atoms often involves contribution from higher lying orbitals. Also, the asymmetry in the charge density around an atom that is introduced by the presence of other atoms cannot always be described properly without the flexibility provided by polarisation functions. Diffuse functions are functions with small exponents and are needed for systems with loosely bound electrons such as anions or excited states or for determining properties such as polarisability.

There are many different basis sets available for use in *ab initio* calculations, often with distinctive names that outline the complexity of the basis. The simplest basis sets are the STO-nG series where the name means Slater type orbitals consisting of n Gaussians [8]. The STO-nG are called a minimal type basis as they only use one STO for each atomic orbital. An STO function is not actually used; as mentioned above the STO is created by fitting n Gaussian functions to it. Basis sets with $n = 2 - 6$ have been derived but it was found that using more than 3 Gaussians gives little improvement and the STO-3G basis was the most widely used of this type. However, computers today are so fast the minimal basis set calculations have been superseded by more sophisticated basis sets.

Basis sets using two STO's to represent each atomic orbital is the obvious way to improve the flexibility of the basis. These are called double zeta (DZ) type bases, the term zeta comes from the exponent in the STO function, Eqn. 2.12, which is often represented by the Greek letter zeta, ζ. If there are three STOs are used per atomic orbital then the basis is called a triple zeta (TZ).

As chemical bonding occurs between valence orbitals, increasing the flexibility of the description of core orbitals close to the nucleus is not as important as

improving the description of the valence orbitals. To account for the importance of valence orbitals a variety of basis sets are available that use two STO's for the valence orbitals and one for the core orbitals, these are called split valence basis sets (technically these are valence double zeta bases: there are also split valence versions of TZ basis sets called triple split valence). The split valence basis sets have the general name k-nlmG where k is the number of Gaussians representing core orbitals and nlm represents both how many STO functions the valence orbitals are split into and how many Gaussians are used for their representations. If there are two values after the hyphen, i.e. nl, then it is a split valence basis set and if there are three values, i.e. nlm, this is a triple split valence basis. An example of a split valence basis set is 6-31G, here the core orbitals are described by one STO approximated by 6 Gaussians and the valence orbitals by 2 STO's created from 3 and 1 Gaussian functions respectively. A triple split valence basis set is 6-311G where again the core orbitals are represented by one STO created from 6 Gaussians but the valence orbitals are three STOs created by 3,1 and 1 Gaussians respectively.

The addition of diffuse and/or polarization functions to split valence basis sets is indicated by symbols added just before or after the G. The general notation for diffuse orbitals is to use a + or ++ before the G as they are usually *s* or *p* functions, the first + indicates one set of diffuse *s*- and *p*- functions on heavy atoms, the second + shows diffuse *s*- functions added to hydrogen. Polarisation functions are either written explicitly in brackets after the G or as one or two *. The 6-31G** is identical to 6-31G(d,p) both representing *d* polarisation functions on heavy atoms and *p* on hydrogen. In the brackets the heavy atom polarisation functions are written first then the hydrogen polarisation functions after the comma.

2.3.3 Contracted basis sets

Valence electrons are more important in chemistry than the core electrons but as they contribute little to the energy, optimizing the energy of the system will not effectively optimise the valence orbitals. Thus an energy optimized basis set which gives a good description of the valence orbitals needs to be very large. But in a large basis the majority of the functions are used to describe the energetically important but chemically uninteresting core orbitals. To minimize the computational effort used to calculate these 'uninteresting' core orbitals the method of basis set contraction was introduced by Clementi [9] and Whitten [10].

A typical basis set for carbon may have 10 Gaussian *s* functions, six of which describe the 1*s* orbital, three describe the 'inner' part of the 2*s* orbital and the remaining orbital actually describes the chemically important 'outer' region of the 2*s* orbital. As the computing power required for Hartree-Fock calculations increases with the fourth power of the number of basis functions, having 8 of the 10 functions describing the inner region of the *s* orbitals is inefficient. In a contracted basis set the first six functions, called primitives, are described by one variational parameter. Thus, the 1*s* orbital is described by a fixed linear combination of six primitives. Similarly the next three functions are combined, describing the inner region of the 2*s* orbital, the remaining function describing the outer region. The number of parameters to be optimized is thus reduced from 10 to 3 reducing the computational load but also increasing the energy of the system as the flexibility of the wavefunction is reduced. The resulting functions created by contracting the primitive Gaussians are called the contracted Gaussian orbitals. A similar contraction process is applied to *p* orbitals but rarely to *d* or higher orbitals.

Typically the number of primitives making up a contracted orbital is between 1 and 10, and the specification of a basis set in terms of primitive and contracted functions is given by the notation (10*s*4*p*1*d*/4*s*1*p*) → [3*s*2*p*1*d*/2*s*1*p*]. Here the

number of primitives is on the left hand side and the contracted orbitals on the right hand side, the numbers before the slash are for heavy atoms (non hydrogen), and for hydrogen after the slash.

2.4 Electron correlation

Solving the Schrödinger equation for a molecular system using the Hartree-Fock method introduces some fundamental errors due to the way the electron / electron repulsion is handled. From Eqns 2.4 and 2.5 it can be seen that the electron potential energy functions J and K contain terms of the form $\frac{1}{r_{1,2}}$ to describe the inter-electron repulsion. Describing the electrons in this way has each electron moving in an average electron density representing the other electrons, but the electrons are better described as point charges which will try to avoid each other resulting in the motion of one electron being correlated to the other's position. The error in the calculated energy introduced by describing the electrons in this way is called the correlation energy [11] and its magnitude is generally taken to be the difference between the RHF energy and the exact non-relativistic energy of a particular system. A Hartree-Fock calculation with a sufficiently large basis set accounts for ~99 % of the total energy of the system, but the remaining 1 % is often the same magnitude as a chemical bond.

Electron correlation can be broadly divided into two types, static and dynamic, where dynamic correlation is the error introduced by the average electron density assumption described above. Static correlation is an error caused by Hartree-Fock theory inaccurately describing a molecule over a range of bond lengths. Although these two types of electron correlation have two distinct causes, techniques to recover electron correlation do not recover solely static or dynamic. Generally a mixture of static or dynamic correlation is recovered with certain methods often recovering a majority of one type. For example the Configuration Interaction technique recovers mostly static correlation and some dynamic whereas the

Complete Active Space method efficiently recovers dynamic correlation. These techniques are discussed in detail in subsequent sections.

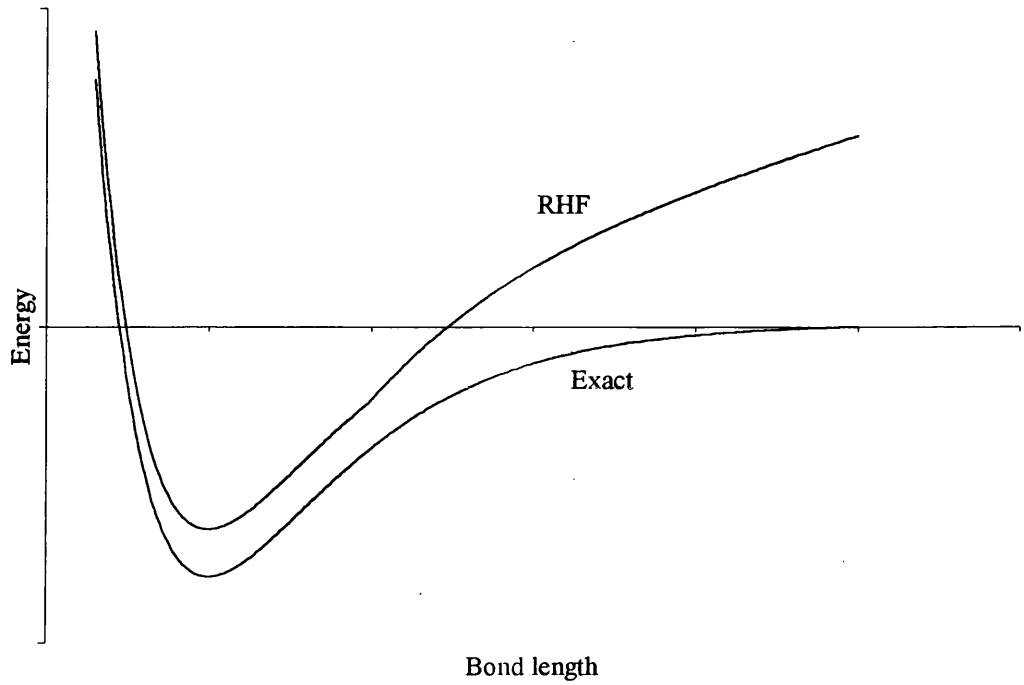

Fig 2.1 *Potential energy curves for an RHF calculation and an 'exact' calculation showing the failure of a single determinant calculation as the calculations approach dissociation.*

Static correlation is particularly noticeable in SCF calculations of molecular dynamics. In Fig 2.1 the dissociation curve of a typical molecule is well represented by an RHF calculation around the equilibrium bond length but at large bond-lengths the RHF curve overestimates the dissociation energy by a large extent; the curve becomes characteristic of ionic interaction rather than neutral molecules. The reason for the static correlation error can be seen by considering the RHF wavefunction of the $X^1\Sigma^+_g$ ground state of H_2. The H_2 ground state wavefunction has the form

$$\Psi_X = A\sigma_g^{\alpha}(1)\sigma_g^{\beta}(2) \qquad 2.13$$

where A is required to make the molecular wavefunction anti-symmetric, α and β are one electron spin functions and σ_g is the bonding orbital $\chi_A + \chi_B$ with χ_A an *s*-like orbital centered on atom A and χ_B an *s*-like orbital centered on atom B. At

infinite separation χ_A becomes the $1s$ orbital of atom A, $1s_A$, and χ_B the $1s$ orbital of atom B, $1s_B$ thus expansion of Eqn.2.13 gives

$$\Psi_X \approx \left(1s_A^\alpha 1s_B^\beta + 1s_B^\alpha 1s_A^\beta + 1s_A^\alpha 1s_A^\beta + 1s_B^\alpha 1s_B^\beta\right). \qquad 2.14$$

The terms $1s_A^\alpha 1s_B^\beta$ and $1s_B^\alpha 1s_A^\beta$ represent one electron located on atom A and one on atom B, which is a correct description of H_2 separated to two H atoms. But the $1s_A^\alpha 1s_A^\beta$ and $1s_B^\alpha 1s_B^\beta$ terms represent both electrons either on atom A or both on atom B, so a $H^+ H^-$ ion pair, thus the H_2 molecule is 50 % covalent and 50 % ionic. The overall energy of Ψ_X is greater than the energy of two H atoms by half the difference of the ionization energy and electron affinity of H, i.e. ~6.4 eV, and at large bond lengths the wavefunction has an inaccurate R^{-1} behaviour.

2.5 Configuration Interaction

A frequently used method to regain the correlation energy is the technique of configuration interaction, CI, [12]. In the Hartree-Fock equation the wavefunction is created from a single Slater determinant, i.e. one particular configuration of the electrons in the molecular orbitals. For a closed shell RHF calculation the Hartree-Fock wavefunction is the ground state configuration of two electrons in each occupied molecular orbital, with the molecular orbitals filled in order of increasing energy. In a calculation with N electrons and M basis functions there will be N/2 occupied molecular orbitals and M-N/2 unoccupied (virtual) orbitals. Except for a minimal basis calculation there will always be more virtual than occupied molecular orbitals. Using the virtual orbitals new configurations can be created by taking electrons out of occupied molecular orbitals and placing them in virtual orbitals, and the new configurations can be denoted by the number of electrons excited out of the original configuration to create the new configuration, i.e. singly, doubly, triply excited configurations. In the CI method a wavefunction is created using a linear combination of different configurations (each of which is described by a single Slater determinant) with coefficients determined by the variation method. The CI wavefunction has the form

$$\Psi_{CI} = \sum_i C_i \phi_i \qquad 2.15$$

where C_i is the coefficient and ϕ_i the electron configurations (Slater determinants).

The flexibility of a CI wave function is demonstrated by considering the ground state wave function of H_2, Eqn. 2.14 and an excited state of H_2, Ψ_E, made from the anti-bonding orbital, σ_u. The excited state is

$$\Psi_E = A\sigma_u^{\alpha}(1)\sigma_u^{\beta}(2) \qquad 2.16$$

where A is required to make the equation anti-symmetric and σ_u is an anti-bonding orbital made by the destructive combination of the *s*-like orbitals centered on atoms A and B, $\sigma_u = \chi_A - \chi_B$.

At infinite separation the χ_A is again essentially the 1*s* orbital on atom A, $1s_A$, and χ_B the 1*s* orbital on atom B, $1s_B$, and the expansion of Eqn 2.16 is

$$\Psi_E \approx \left(-1s_A^{\alpha}1s_B^{\beta} - 1s_B^{\alpha}1s_A^{\beta} + 1s_A^{\alpha}1s_A^{\beta} + 1s_B^{\alpha}1s_B^{\beta}\right) \qquad 2.17$$

Like Ψ_X, (Eqn 2.14), Ψ_E contains a mixture of covalent and ionic terms, but by taking a linear combination of Ψ_X and Ψ_E either the covalent $1s_A^{\alpha}1s_B^{\beta}$ or the ionic $1s_A^{\alpha}1s_A^{\beta}$ terms will cancel. For H_2 a CI wave function, Ψ_{CI}, can be constructed

$$\Psi_{CI} = C_X\Psi_X + C_E\Psi_E \qquad 2.18$$

where C_X and C_E coefficients are allowed to vary. Thus, a correct description of H_2 at dissociation is given by $C_X = -C_E$ i.e. $\Psi_X - \Psi_E$ as the ionic $1s_A^{\alpha}1s_A^{\beta}$ and $1s_B^{\alpha}1s_B^{\beta}$ terms are removed. But near equilibrium the RHF wave function is a good approximation so the C_E coefficient is small.

As important chemical changes generally involve the valence orbitals, configurations involving excitation from core orbitals contribute little to the CI wave function. So most calculations will only use configurations where the core orbitals are kept doubly occupied, frozen. The small influence of the core orbitals on the CI energy can be seen in Fig 2.2 where the energy of a CI calculation on SiF_3^{2+} is plotted against the number of frozen molecular orbitals, the energy

improvement for configurations from core orbital excitation rapidly decreases. Also the highest energy unoccupied virtual molecular orbitals are excluded from the calculations as configurations involving excitations to these orbitals also contribute little to the CI energy.

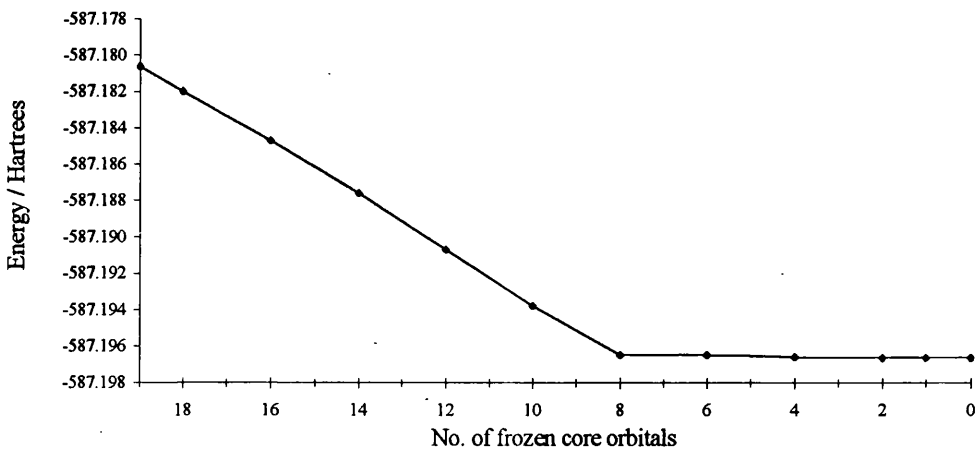

Fig 2.2 *Energy of SiF_3^+ for a series of CI calculations using decreasing number of frozen core orbitals showing the small improvement in energy achieved using the core molecular orbitals.*

As the CI wave function is a sum of configurations which are themselves a combination of molecular orbitals which are a sum of atomic orbitals, CI calculations require the evaluation of a large number of integrals and are computationally expensive. Fortunately there are rules within CI theory that restrict the number of configurations included in a calculation and also methods to choose which molecular orbitals are used to create the configurations. In CI calculations only configurations of the same symmetry as the reference configuration will contribute to the CI wave function. Also the number of electrons excited out of the reference to create a configuration is important as singly excited configurations make no contribution to the CI wave function if only singly excited configurations are considered; this is called Brillouin's Theorem [2]. However, singly excited configurations can become important in the presence of doubly excited configurations. Triply or higher configurations generally lead to little improvement in energy. The greatest improvement in energy is found in calculations involving

singly and doubly excited configurations; this is shown in Fig 2.3 where the energy of SiF_3^+ is plotted against the electron excitation level for a series of CI calculations.

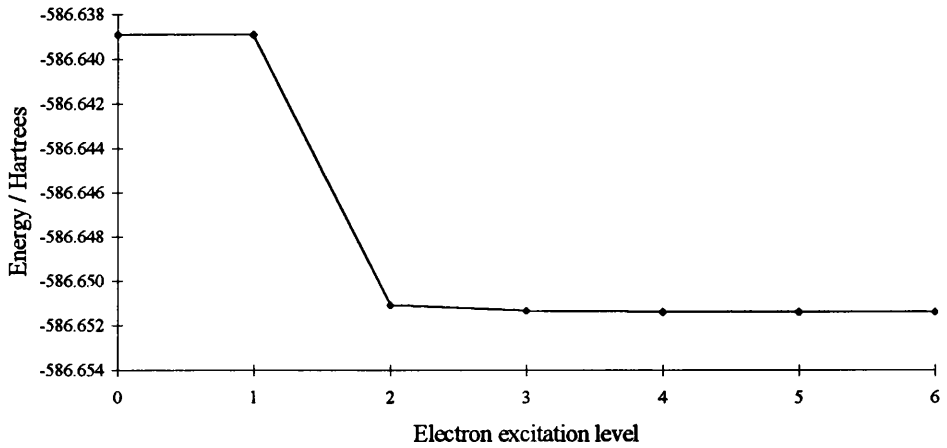

Fig 2.3 *Energy of SiF_3^+ for a series of CI calculations using an increasing level of electron excitation in the configuration creation.*

The maximum level of electron excitation possible is twice the number of electrons in the molecule, calculations which include all configurations created from all possible excitations are called Full CI. Full CI calculations provide highly accurate results but are extremely intensive computationally and are only performed on small systems, the results being used as benchmark tests for other smaller calculations.

2.5.1 Size Consistency

Restricting the number of configurations used in the CI wave function avoids large calculations and the problems of slow convergence often found with high excitation levels, but it does introduce a problem of size inconsistency. A method is said to be size consistent if it calculates the energy of a species AB at infinite bond length to be equal to the sum of the energies of A and B calculated separately by the same method. The energy of N non-interacting bodies should equal N times the

energy of a single body. However, for a singles and double CI the energy is found to vary as $\sqrt{N}$.

The discrepancy between treating two bodies at infinite separation and separately can be illustrated by a CI singles and doubles treatment of Be_2. The Be ground state is $1s^2 2s^2$. A small CI calculation which includes the double excitation $1s^2 2p^2$ in the wave function for two separate Be atoms, A and B, will contain the configurations $1s_A^2 2s_A^2$, $1s_A^2 2p_A^2$, $1s_B^2 2s_B^2$ and $1s_B^2 2p_B^2$. For Be_2 the ground state would be $1s_A^2 1s_B^2 2s_A^2 2s_B^2$ and double excitation of the $2s$ electrons creates the configurations $1s_A^2 1s_B^2 2s_A^2 2p_B^2$ and $1s_A^2 1s_B^2 2p_A^2 2s_B^2$. The configuration $1s_A^2 1s_B^2 2p_A^2 2p_B^2$ which was included for 2Be corresponds to a quadruple excitation from the Be_2 ground state. A quadruple excitation is not possible for the CI singles and doubles calculation on Be_2 so the energies obtained for Be_2 and 2Be cannot be identical.

The size consistency error is corrected for in calculations using methods developed by Siegbahn [13] or by Langhoff and Davidson [14] which estimate the contribution that higher order excitations would make to the correlation energy. For example the contribution that quadruple excitations would make to the energy ΔE_Q can be estimated from the double excitations using the formula

$$\Delta E_Q = \left(1 - C_0^2\right)\Delta E_D \qquad 2.19$$

developed by Davidson ΔE_D is the energy lowering obtained from all double excitations and C_0 the coefficient of the main reference in the CI wave function. The full CI technique mentioned earlier is fully size consistent as all possible excitations are considered but the computational expense of Full CI is so large it is better to use a CI singles and doubles calculation with the true correlation energy recovered by a correction term such as Eqn 2.19.

2.5.2 Excited States

The CI method allows the calculation of excited states relatively easily as the solution of the CI wave function has many possible values depending on which root of the equation is required. Thus the nth root corresponds to the (n-1)th excited state as the first root is the ground state.

The excited states can be distinguished depending on whether they are the lowest energy state of a particular symmetry or a higher lying state. For the first state of a given symmetry (not the ground state) the calculations can treat it analogously to the ground state. By specifying the orbital occupations that correspond to the excited state in a Hartree-Fock calculation and adding electron correlation, the first states of a given symmetry can be calculated. The calculation of higher lying states of a given symmetry is most easily performed by CI methods, other methods for recovering electron correlation collapse to the lowest energy state.

2.5.3 Multi-Reference CI

Performing CI out of a single reference configuration only gives accurate energies if the state under consideration is well described by that particular configuration. Ground state energy calculations around the equilibrium geometry are well described by single reference CI calculations as they are often dominated by the ground state configuration. However, over a range of bond lengths or for calculations requiring the evaluations of several excited states an accurate description requires the specification of more than one reference wave function.

Calculations which use more than one reference are called Multi Reference CI, MRCI, these are also called Multi Configuration SCF, MCSCF, when the atomic orbitals are also optimised in that calculation. Generally, for CI and MRCI the molecular orbitals are calculated in an initial Hartree-Fock calculation and only the weighting of each configuration is optimised. Also optimising the atomic orbitals

would obviously improve the accuracy but the added computational effort is large and so MCSCF calculations are only performed on small systems, although open shell systems sometimes require a small MCSCF calculation to provide suitable atomic orbitals to use in subsequent CI or MRCI calculations.

2.5.3.1 Table CI

In going from single reference to MRCI calculations the number of configurations produced increases by a factor approximately equal to the number of configurations making up the multi reference. MRCI calculations are therefore very expensive computationally but techniques have been developed to limit the number of configurations that are actually used in creating the CI wave function.

The Table CI method [15] is an MRCI technique that uses a configuration selection technique to limit the number of configurations in the MRCI wave function. Using a set of reference configurations specified at the start of the calculation a series of test configurations are created by a singles and doubles excitation of each reference. The energy lowering of each test configuration, relative to the value obtained from the reference configurations alone, is estimated via solution of the CI wave function created by the reference wave function plus the test species. Any test species with an energy lowering below a threshold value, typically around 10^{-5} hartrees, are discarded, and thus the MRCI wave function is created out of the reference configurations and the test configurations with energy lowerings greater than the threshold value.

The energy lowering that the discarded configurations would have made is recovered by estimating their total contribution to be a sum of their energy lowerings determined in the selection process. The energy of a calculation with no selection criteria, E, is given by the equation

$$E \approx E(T) + \sum_r \Delta E_r \qquad 2.20$$

where E(T) is the energy of the Table CI wave function and ΔE_r is the energy lowering of a test configuration.

The Table CI method will calculate more than one root of a particular symmetry providing the set of main configurations is sufficiently large to allow for a realistic representation of all the states of interest. Although the selection technique of Table CI limits the amount of electron correlation energy that is recovered it does achieve a balance in the correlation effects for different electronic states of the same system or for different nuclear conformations of the same state.

2.5.3.2 Complete Active Space SCF

In MRCI techniques such as Table CI, described above, the selection of the configurations in the multi reference is crucial to the success of the calculation. In the Complete Active SCF, CASSCF technique [16], also called Fully Optimised Reaction Space, FORS, the problem of selecting important configurations is replaced by the more tractable choice of important molecular orbitals. For a CASSCF calculation the molecular orbitals are partitioned into active and inactive spaces where the active molecular orbitals are usually some of the highest occupied and lowest unoccupied molecular orbitals from an RHF calculation. The inactive molecular orbitals are kept either doubly occupied or empty, i.e. virtual orbitals outside the of the active space remain empty and occupied orbitals outside of the active space always contain two electrons. The molecular orbitals to include in the active space are dictated by which will be important in the problem being investigated and the computational resources available. So, if several points on a potential surface are required, the active space should include all orbitals which change significantly or for which the electron correlation is expected to change.

The configurations for a CASSCF calculation are then created by performing Full CI within the active space and selecting the configurations with the correct symmetry for the system under study. As it uses a Full CI calculation the CASSCF wave function grows rapidly with the number of orbitals in the active space and 10 to 12 electrons in 10 to 12 orbitals is the limit for most calculations. A CASSCF calculation can give an unbalanced description of a system as all the electron correlation recovered is in the active space. This is not a problem if the active space includes all the valence electrons, but this is only possible for small systems. To recover electron correlation from outside the active space CI can be performed out of each of the configurations generated by the CASSCF into all the virtual molecular orbitals. This will obviously restrict the size of the active space by a greater extent and will result in CI being performed out of configurations that are not important. But, using a Full CI expansion enables the use of efficient selection techniques [17] and the routine calculation of the systems with hundreds of reference configurations.

2.6 Geometry Optimisation

As well as determining the energy at a single geometry, many electronic structure techniques can also be used to determine equilibrium geometries and transition states. By calculating the first derivative of the energy, the gradient, and also the second derivative, the hessian, minima on a molecule's potential energy surface can be located. Geometries at which the energy gradient is zero correspond to a minimum on the potential surface and to determine if they are a local minimum or the equilibrium geometry, the global minimum, a calculation of the hessian is required.

A hessian calculation at a particular geometry creates a matrix from which the vibrational modes of a molecule can be determined. At a global minimum the curvature of the potential surface is positive in all directions and at a local

minimum at least one direction on the potential surface will have negative curvature. So, as the frequency of a vibrational mode is dependent on the square root of the curvature a non-global minimum has at least one mode with a frequency that is the square root of a negative number i.e. an imaginary number. The hessian matrix thus has no imaginary frequencies at the equilibrium geometry; one imaginary frequency corresponds to a transition state and geometries with more than one imaginary frequency are local minima with no real chemical significance.

Most computational methods calculate the energy gradients analytically using derivatives of the one and two-electron integrals. These integrals require evaluation of derivatives of the basis functions with respect to the nuclear coordinates of their centres. From the analytical energy gradients the hessian can be computed and the geometry classified as described above. For the Table CI technique analytical gradients are not calculated so the gradient has to be determined numerically. The numerical gradient is calculated by taking each atom in turn and displacing it by a set amount in a given direction and recalculating the energy, the new energy is then compared to the original geometry's energy. Once each atom has been displaced in each co-ordinate, (i.e. x, y and z) then the curvature of the potential surface at the geometry can be determined. If the new energy is lower in one or more displacements this it is obviously not a global minimum. Once all possible displacements have been tried a numerical Hessian can be determined and the frequencies of the modes can be calculated.

2.7 Mulliken Population Analysis

From an electronic structure calculation information on the charge distribution of a molecule is obtained relatively easily through a Mulliken population analysis [18]. This gives a value representing the number of electrons associated with a particular atom, all electrons within the molecule are thus assigned to a particular atom even though they may not spend much time close to a nucleus.

Taking the molecular orbital wave function defined in equation 2.7, the net atomic population of a given atomic orbital, χ, is defined as

$$P_k = 2\sum_i C_{ik}^2 \chi_\kappa^2 \qquad 2.21$$

Here i labels the molecular orbital and k refers to the atomic basic function. Also, the square of the wave function represents the charge density. The electron population shared by atomic orbitals k and l is an overlap given by

$$O = 2\sum_i C_{ik} C_{il} S_{kl} \qquad 2.22$$

where S is the overlap integral between orbitals k and l defined in equation 2.10. Since P_k=O_{kl} the gross population of atomic orbital χ is given by

$$P_k = \sum_l O_{kl} \qquad 2.23$$

Thus the total electron population at any nucleus can be found by adding all the values of P_k for orbitals χ_κ which are centred on a particular atom and a charge for the atom can be calculated as the nuclear charge is known.

2.8 Software Packages

Sophisticated software packages have been developed to perform electronic structure calculations, using the *ab initio* methods described above. Graphics packages are also available either as part of the electronic structure packages or as stand alone packages that use the output from electronic structure calculations. Molecular structures, molecular orbitals, charge distribution and other molecular properties can be visualised. Each of the packages used in the calculations described in this Thesis is now briefly discussed.

2.8.1 GAMESS-US

GAMESS stands for General Atomic and Molecular Electronic Structure System. It is a software package developed separately in America and the UK, the

American version being called GAMESS-US and the UK version GAMESS-UK. GAMESS-US is maintained at the Department of Chemistry of Iowa State University and described in detail in the literature [19]. Created from several older quantum chemistry programs, particularly a package called HONDO, GAMESS-US can perform standard RHF, UHF, ROHF, CI and MRCI *ab initio* calculations as well as semi-empirical calculations. Also, geometry optimisations, vibrational frequencies calculations and Infra Red absorption spectra can be calculated along with one and two electron properties such as dipole, quadruple and higher moments, electron density distribution and polarizability. Many other types of calculation are also possible, including following reaction, co-ordinates, finding saddle points, excited state energies and spin-orbit coupling coefficients. The GAMESS-US package is very versatile allowing many different chemical properties to be calculated although it is not geared towards very high accuracy calculations.

The official GAMESS-US website has more information and is at "http://www.msg.ameslab.gov/gamess/gamess.html".

2.8.2 MOLPRO

MOLPRO is a package for ab initio molecular electronic structure calculations. It is maintained by H-J Werner and P.J Knowles at the University of Birmingham. The package is geared towards performing high accuracy calculations with extensive treatment of electron correlation through MRCI and other associated methods. As with GAMESS-US many molecular properties such as dipole moments, electron density polarisation functions etc. can be computed.

The CASSCF/MRCI software in MOLPRO uses a sophisticated configuration selection routine that allows many reference configurations to be used in the MRCI

calculation. This MRCI routine has been used extensively to generate the potential energy curves and surfaces used to study O_3^{2+} and BCl^{2+} in chapters 4 and 5.

More information on MOLPRO can be found at the website, "http://tcpc.bham.ac.uk/molpro".

2.8.3 LEVEL

LEVEL is a computer program for solving the radial Schrödinger equation for bound and quasibound levels and calculating various expectation values. It is maintained at the University of Waterloo, Ontario, Canada by Robert J LeRoy and it is version 6.1 that has been used in the studies in chapters 4 and 5.

The solutions to the Schrödinger equation are obtained using the Numerov method [20] which expresses the integrals of the Schrödinger equation in a mathematically tractable form. For the quasibound potentials vibrational level lifetimes are also calculated. The Level software is available by contacting Robert LeRoy at leroy@Uwaterloo.ca

2.8.4 MOLDEN

The molecular orbital and electron density plots produced for BCl^{2+} were made using the program MOLDEN. This package uses the output from an electronic structure calculation and depending on the information in the output can produce two or three dimensional plots of molecular orbitals and electron density. The packages GAMESS, MOLPRO and GAUSSIAN amongst others produce output that can be visualised by MOLDEN.

The MOLDEN website contains more information on the software and is "http://www.caos.kun.nl/~schaft/molden/molden.html".

2.9 Computational Resources

The computers used in the calculations presented in the subsequent chapters are:

i) A Silicon Graphics indigo 2 with a 150 MHz R4400 processor for the calculations on SiF_3^{2+} in Chapter 3.

ii) Silicon Graphics Power Challenge with six R8000 processors used for the O_3^{2+} and BCl^{2+} potential energy calculations in chapters 4 and 5.

iii) IBM RS6000 Model 43P with a 166 MHz processor used for general data manipulation and running the MOLDEN package.

References

(1) Hoffman R. *J. Chem. Phys.* **39** (1963) 1397.

(2) Szabo A. and Ostlund N. S. *Modern Quantum Chemistry*; McGraw-Hill Publishing Co.:, 1989.

(3) Hartree D. R. *Proc. Cambridge Phil. Soc.* **24** (1928) 89.

(4) Fock V. *Z. Physik* **61** (1930) 126.

(5) Gray D. E. *American Institute of Physics Handbook*; McGraw Hill: New York, 1972.

(6) Slater J. C. *Phys. Rev.* **36** (1930) 57.

(7) Boys S. F. *Proc. R. Soc. London, A* **A200** (1950) 542.

(8) Hehre W. J., Stewart R. F. and Pople J. A. *J. Chem. Phys.* **51** (1969) 2657.

(9) Clementi E. *IBM J. Res. and Dev.* **9** (1965) 2.

(10) Whitten J. L. *J. Chem. Phys.* **44** (1966) 359.

(11) Löwdin P. O. *Advan. Chem. Phys.* **2** (1959) 207.

(12) Hylleraas E. A. *Z. Physik* **48** (1928).

(13) Siegbahn P. E. M. *J. Chem. Phys.* **72** (1980) 1647.

(14) Langhoff S. R. and Davidson E. R. *Int. J. Quant. Chem.* **8** (1974) 61.

(15) Buenker R. J. *Stud. Theor. Chem.* **21** (1982) 17.

(16) Roos B., Taylor P. and Siegbahn P. E. M. *Chem. Phys.* **48** (1980) 157.

(17) Knowles P. J. and Werner H.-J. *Chem. Phys. Lett.* **115** (1985) 259.

(18) Mulliken R. S. *J. Chem. Phys.* **23** (1955) 1833.

(19) Schmidt M. W., Baldridge K. K., Boatz J. A., Elbert S. T., Gordon M. S., Jensen J. H., Koseki S., Matsunaga N., Nguyen K. A., Su S. J., Windus T. L., Dupuis M. and Montgommery J. A. *J. Comput. Chem.* **14** (1993) 1347.

(20) Smith K. *The calculation of atomic collision processes*; Wiley-Interscience: New York, 1971; Chapter 4.

Chapter 3

Electron-transfer reactions of the SiF_3^{2+} dication with the rare gases, neon, argon, krypton and xenon.

3.1. Introduction

Early experimental studies of molecular dications have concentrated on the properties of the isolated species. However, recently improvements in experimental techniques has enabled sophisticated studies into the fate of dications upon collision with atoms or molecules.[1-3] In the collision of a dication XY^{2+} with a neutral A the following two processes may be observed

$$XY^{2+} + A \rightarrow XY^{+} + A^{+} \qquad 3.1$$

$$XY^{2+} + A \rightarrow XY^{+*} + A^{+} \rightarrow X^{+} + Y + A^{+} \qquad 3.2$$

where Eq. 3.1 represents non-dissociative electron-transfer and Eq. 3.2 represents dissociative electron-transfer. In the latter reaction an unstable excited state of the product molecular cation, XY^{+*}, fragments to X^{+} + Y. Other reactions observed in dication / neutral collisions are collision-induced neutral-loss Eq. 3.3 and also bond forming reactions. [2,4-6]

$$XY^{2+} + A \rightarrow X^{2+} + Y + A \qquad 3.3$$

This study is concerned with rationalising the electron-transfer reactions of SiF_3^{2+}.

Mathematical modeling of electron-transfer reactions is possible using reaction window theory [7-13], an extension of Landau-Zener theory which is explained below. This methodology has been used in studies of the reactions of OCS^{2+}, CO_2^{2+}, SiF_2^{2+} and SiF_3^{2+} with rare gases [1,14] and was found to model the reactions successfully except when applied to SiF_3^{2+}. The lack of success was felt, in part, to be due to the greater degree of geometrical freedom of SiF_3^{2+} introducing the possibility of significant equilibrium geometry differences depending on the degree of ionisation.

In this study of SiF_3^{2+} the energetic and geometric changes associated with passing between the SiF_3 cation and dication are determined by *ab initio* computational calculations. Also, the energies of the first few excited states of these ions have been determined and used, together with the geometric and energetic information, in the Landau-Zener algorithm. Combining this information enables a more satisfactory interpretation of the experimental product ion distribution of the SiF_3^{2+}/rare gas electron transfer reactions and a more detailed insight into the electron-transfer reactions of larger dications.

As will be shown below, the key conclusion to be drawn from this study is that successful modeling of the electron-transfer reactions of polyatomic molecular dications requires the consideration of the geometry at which the reaction occurs. In these systems, this is the dication equilibrium geometry.

3.2. Preliminary Considerations: Reaction Window Theory

To successfully model the electron-transfer reactions of SiF_3^{2+} with the rare gases, and to rationalise the product ion yields observed experimentally from these reactions, a one-dimensional reaction window theory based on the Landau-Zener model of electron-transfer reactions is employed. [15-17] This methodology has been used successfully to model electron-transfer reactions of several dications including CO^{2+}, CO_2^{2+} and OCS^{2+}. [1,3,7,12] In this model the molecular dication and rare gas atom are pictured as approaching each other along a potential curve dominated by polarisation attraction. At some point this curve may cross a Coulomb repulsion curve which represents the repulsive potential between the two cationic products that are formed by the electron-transfer reaction. These two diabatic potentials are shown schematically for a generalised dication XY^{2+} in Figure 3.1.

The point at which the two curves cross, the curve crossing radius, is the theoretical optimum inter-species separation for an electron to 'hop' between the neutral and the dication. Depending on the degree of coupling between the attractive reactant curve and the repulsive product curve there may be a high or low probability of electron-transfer occurring. This coupling depends on the interspecies separation of the curve crossing. If the curve crossing is at a small interspecies separation (< ca. 3 Å), there is a strong interaction between the reactant and product diabatic potentials and a high probability of electron-transfer between dication and neutral. But, as the colliding species will pass back through the curve crossing again as they travel out along the product curve there is again a high probability of an electron being transferred between the two species and thus no net reaction will be observed.

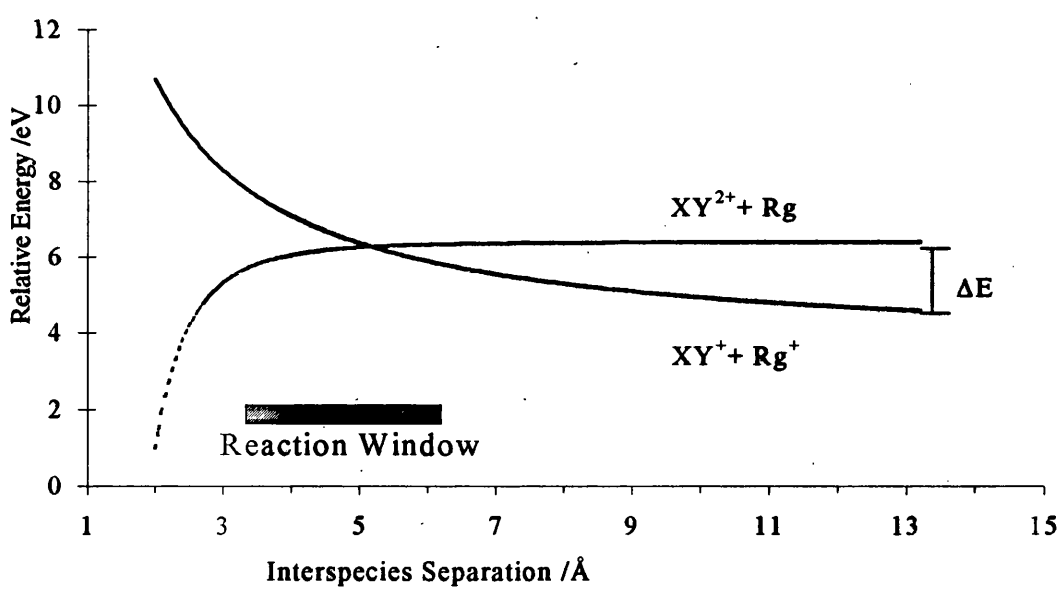

Fig 3.1 *Schematic reactant and product potential energy curves for the electron-transfer reactions of a molecular dication (XY^{2+}) with a rare gas atom (Rg). For this value of the reaction exothermicity (ΔE) the curve crossing lies within the reaction window. As discussed in the text, the reactant potential is plotted with a dotted line at small interspecies separations to indicate that in this regime the true potential may be both significantly anisotropic and deviate from a simple electrostatic potential.*

For systems where the curve crossing is at a large interspecies separation, (> ca. 6 Å), there is a weak coupling between the potentials so a low probability of an electron being transferred on either pass through the curve crossing. Between these two extremes there is a so called reaction window at approximately 3 - 6 Å. If a curve crossing lies within this 'window' the probability of an electron-transfer reaction, as given by the equations below, can approach the Landau-Zener maximum of 50%.

These concepts can be qualified as follows: an electron-transfer reaction between an atomic dication and a neutral entails entering on the reactant potential and exiting on the product potential. This involves passing through the curve crossing radius twice but only crossing between the potentials once. The overall probability for this, P, is given by

$$P = 2\delta(1-\delta) \qquad 3.4$$

where δ is the probability of the system remaining on the same diabatic potential curve through the crossing region and is given by the standard Landau-Zener equation.

$$\delta = \exp\left(\frac{-\pi|H_{12}|^2}{2\hbar|V_1' - V_2'|v_b}\right) \qquad 3.5$$

Here $|H_{12}|^2$ is the electronic coupling matrix element between the two states 1 ($A^{2+} + B$) and 2 ($A^+ + B^+$), $|V_1' - V_2'|$ is the difference between the slopes of the potential curves at the curve crossing, and v_b is the relative radial velocity of the two atoms. To model the potential curves simple electrostatics can be used to produce approximate curves with the form

$$V_1 = -Z^2e^2\alpha \,/\, 4\pi\varepsilon_0 r^4 + \Delta E \qquad 3.6$$

$$V_2 = e^2 \,/\, 4\pi\varepsilon_0 r \qquad 3.7$$

where the reactant channel V_1 is a polarisation attraction function dependent on the reactant exothermicity ΔE, see Figure 3.1, the polarizability α of the neutral the

charge Z on the ion ($Z = 2$ for a dication) and ε_0 vacuum permitivity. For the product potential, the curve is simply the Coulombic repulsion between the two monocations.

Using these curves the curve crossing radius r_c is the value of r when $V_1 = V_2$, and differentiation of the potential curves at this point gives the relative slopes. The determination of the electronic coupling matrix $|H_{12}|$ is possible via a variety of proposed empirical functions. For the reaction of a diatomic molecular dication with a neutral atom, Olsen *et al* have put forward one function using the ionisation potential $I_{(XY^+)}$ for forming the reactant dication XY^{2+} from the product ion XY^+ and the ionisation potential of the neutral reactant I_A.[18]

$$|H_{12}|^2 = 1.0\left(I_{(XY^+)} I_A\right)\left(r_c^*\right)^2 \exp(-1.72) r_c^* \qquad 3.8$$

where

$$r_c^* = \left(\frac{I_{(XY^+)}^{1/2} + I_A^{1/2}}{\sqrt{2}}\right) r_c \qquad 3.9$$

From these equations the electronic coupling $|H_{12}|$ is predicted to decrease exponentially with increasing distance that the electron must tunnel between the two reactants. As described qualitatively above, at values of r_c between three and six Angstroms the coupling switches from being strongly adiabatic ($\delta \rightarrow 0$, low probability of remaining on the reactant diabat) to diabatic ($\delta \rightarrow 1$), allowing the probability P to reach its maximum value of 0.5.

The Landau-Zener methodology was originally formulated for atom-atom systems and extension of the model to polyatom-atom systems introduces several complications. For an atom-molecule reaction the electron-hopping probability can be extended to include the Franck-Condon overlap of the vibrational states of the reactant dication with the product monocation[11]. Also, the potential surfaces for atom-molecule reactions contain an angular as well as a radial dependence; this is

ignored in simple Landau-Zener theory as it was designed for isotropic collisions. For the SiF_3^{2+} system the polarisation attraction will become markedly anisotropic at small interspecies separation. This is indicated in Figure 3.1 as a dotted region of the potential energy curve. But, as the curve crossing occurs at moderate interspecies separation, we assume that in this region the polarisation attraction curve provides a good approximation of the inter-reactant potential. Despite these complications, the basic principle of a localised avoided crossing still applies in atom-molecule collisions and reactions are still found to occur in the region dictated by Landau-Zener theory with the coupling at the crossing dependent on its interspecies separation.

In this adapted Landau-Zener model of electron-transfer the exothermicity of the reaction is a key factor in determining the likelihood of an electron-transfer reaction. The general form of the reactant and product potential energy curves does not vary with the reaction exothermicity ΔE. Thus, a small exothermicity produces a curve crossing at large interspecies separation and large exothermicity places the crossing at a small interspecies separation. This results in a "window" of exothermicities (typically between 2 and 5 eV) where the curve crossing occurs within the reaction window and electron-transfer is favoured. In electron-transfer reactions between dications and the rare gases, He and Ne have large ionisation energies making their electron-transfer reactions generally endothermic or only slightly exothermic. Hence, by the above arguments electron-transfer is often disfavoured with these reactants. However, the heavier rare gases have lower ionisation energies and thus larger exothermicities for electron-transfer with the result that electron-transfer reactions are more likely for the heavier rare gases in dication-rare gas collision experiments[1,3,12,14].

The exothermicity of the electron-transfer reactions with the heavier rare gases often is sufficiently large though that the curve crossing to the lowest state of the

product cation often occurs at small inter-species separations, outside the reaction window. That the electron-transfer reactions still occur at all can be understood if one considers the possibility of electron-transfer to excited states of the product molecular cation. Product potential curves for excited electronic states of the product molecular cation will lie higher in energy than that for the ground state, thus having a lower exothermicity and, as shown in Figure 3.2, the curve crossing for forming an excited state lies at larger interspecies separations than the ground state and may therefore lie in the reaction window. If electron-transfer occurs to an unstable excited state of the product molecular ion then this can result in the formation of fragment ions, e.g. SiF^+ and SiF_2^+ from SiF_3^+. So for collision experiments between dications and rare gases a trend is observed with increasing reaction exothermicity; that is, no electron-transfer, then monocation ground state population and finally monocation excited state population leading to dissociation. Such a trend has been noted experimentally for several dications [3,12,14] and the experimental results for SiF_3^{2+} also display such a trend as can be seen in Figure 3.3b.

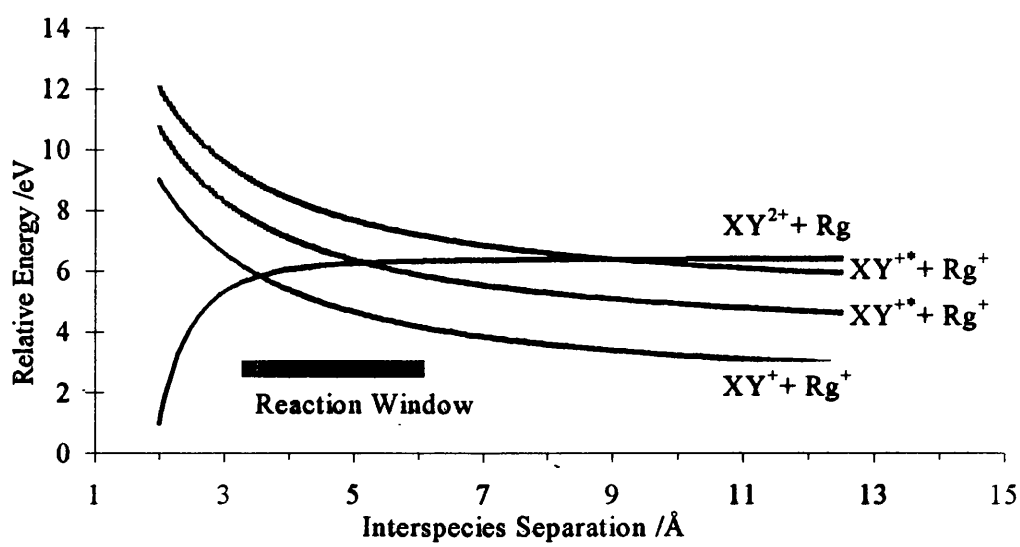

Fig 3.2 *Schematic potential energy curves for the electron-transfer reactions of a molecular dication (XY^{2+}) with a rare gas atom (Rg), where the reaction exothermicity favours the formation of excited state states of the product monocation (XY^{+*}).*

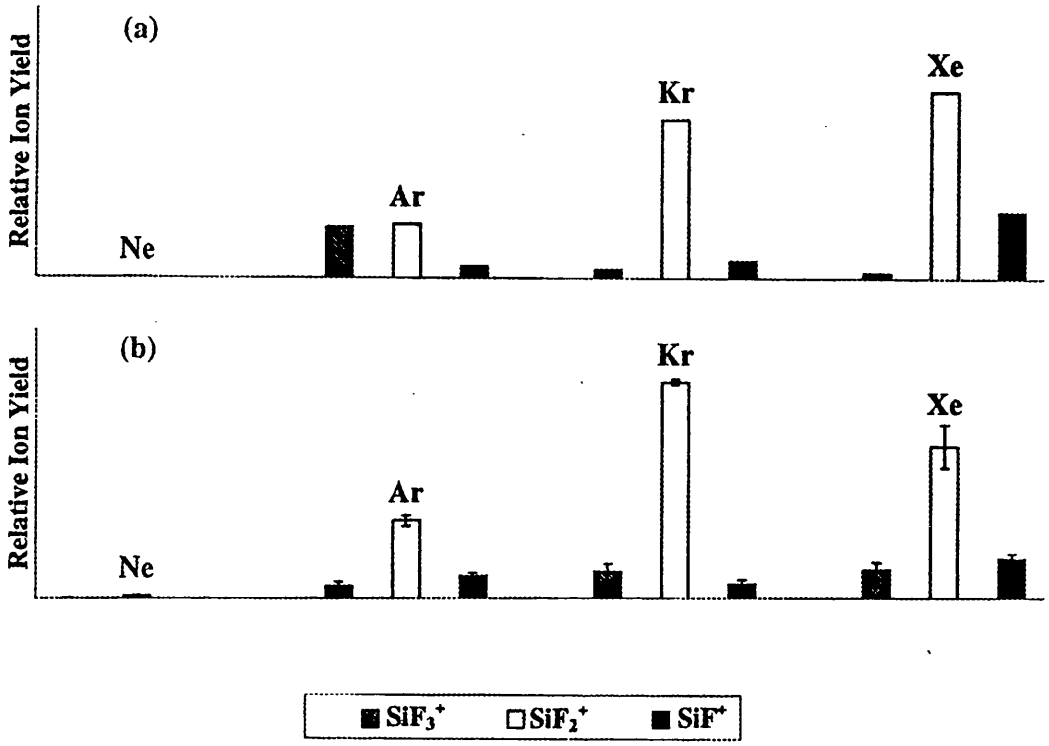

Fig. 3.3 *A comparison of (a) the relative ion yields predicted by the calculations described in the text, the results of which are displayed in Table 3.4, and (b) the actual values obtained in the experiment together with experimental uncertainties (Table 3.1) [14].*

As described below, in Section 3.3.2, using the Landau-Zener equations it is possible to quantify these qualitative ideas and derive the electron-transfer cross section for populating a given electronic state of the molecular monocation. Combining this with a knowledge of the stabilities of the accessible electronic states of the product molecular monocation it is possible to derive a theoretical product ion distribution that can be compared with experimental measurements. This procedure has been applied successfully in the modeling of the ion yields recorded following collisions of OCS^{2+} with the rare gases[1]. Unfortunately, information is often not available on the stabilities of the electronic states of the product molecular ion and in such cases the assumption is made that electronic states of the product molecular ion lying above a thermodynamic dissociation asymptote are dissociative, and dissociate to the nearest lower lying asymptote.

Evidence to support this assumption comes from studies in which molecules are excited to the energy of a dissociation asymptote and the appearance of the products associated with this asymptote are observed when the excitation energy is just above the energy of the asymptote[19]. For SiF_3^+ experimental information on the energies of the excited states is unavailable and in this study *ab initio* calculations have been performed to determine the energies of the low lying excited states of SiF_3^+.

Studies comparing low, (~ eV) and high, (~ keV), energy collision reactions between doubly charged molecules and neutrals [20] have shown that although the timescale of the low energy collisions is closer to a molecular vibrational period, the electron-transfer process itself is significantly faster. Thus, even at low collision energies the electron-transfer process between a dication and a neutral species can be considered as effectively a vertical transition. So, for the SiF_3^{2+} system the formation of the monocation occurs as a vertical transition from the dication and the excited state energies of SiF_3^+ must be determined at the equilibrium geometry of the dication not the monocation. It is important to take into consideration the geometries of the cation and dication in the electron-transfer reactions of polyatomic dications as these species have a large number of geometrical degrees of freedom and it is likely that equilibrium geometries may differ between the singly and doubly charged states. These considerations have not been important in previous studies of diatomic and triatomic dications as the equilibrium geometry of the singly charged cation has been similar to the dication. For example, in the electron-transfer reactions of OCS^{2+} and CO_2^{2+} [1] in going from cation to dication the electron is removed from a non-bonding orbital so will have little effect on the geometry of the species.

3.3 Experimental and theoretical details

As this is a theoretical study, the details of the acquisition of the experimental data that is to be modeled will not be repeated but can be found elsewhere [12,14,21,22]. The experiments form the SiF_3^{2+} dications by electron-impact ionisation and mass select them using a quadrupole mass spectrometer. The collisional reactions occur when the dications pass through an interaction region containing the rare gas. Mass-to-charge selection of the products of these collisions is carried out using a time-of-flight mass spectrometer and the ion yields from these experiments are presented in Table 3.1 and Figure 3.3b. The experimental results reported were recorded at a laboratory kinetic energy of 49 eV.

Table 3.1 *Experimental product ion yields following collisions of SiF_3^{2+} with the rare gases at E_{Lab}=49 eV (see reference [14]). The yields are expressed in parts per thousand of the parent ion signal and have been corrected for mass discrimination effects. The figures in parentheses give the uncertainty in the last figure of the tabulated ion yield.*

	Product ion					
Rare gas	Si^+	F^+	SiF^+	SiF_2^+	SiF_2^{2+}	SiF_3^+
Ne	0.6(2)	0.5(3)	0.0(1)	0.9(3)	36.5(50)	0.0(2)
Ar	0.8(3)	0.4(2)	4.2(10)	8.4(20)	28.9(35)	4.6(15)
Kr	0.0(1)	0.5(2)	5.3(15)	80.2(10)	5.1(10)	9.8(30)
Xe	0.0(1)	2.1(5)	14.7(20)	56.3(80)	22.9(40)	10.4(30)

The electron-transfer and reaction window theories are applied to the SiF_3^{2+} system using *ab initio* calculations of the cation and dication equilibrium geometries and excited state energies. The energies of several excited states of the cation SiF_3^+ at the geometry of the dication are combined with electron-transfer cross section calculations to produce a theoretical product ion ratio for the electron-transfer reaction of SiF_3^{2+} with the rare gases.

3.3.1 *Ab initio* calculations

The *ab initio* calculations on SiF_3^+ and SiF_3^{2+} ground and excited states were performed using the GAMESS_UK program suite [23] employing the 6-311G* basis set in all cases. The geometries of both SiF_3^+ (D_{3h}) and SiF_3^{2+} (C_{2v}) were optimised at the Hartree Fock level and characterised by harmonic vibrational analysis. Following the observation of no negative eigenvalues in the Hessian matrices, the geometries were re-optimised using configuration interaction (CI) at the singles and doubles level. Of the 84 molecular orbitals, 20 are occupied by the 40 electrons of SiF_3^+ and 39 electrons of SiF_3^{2+}. For all the CI calculations the 20 least stable unoccupied molecular orbitals were discarded and the 8 most stable molecular orbitals kept doubly occupied, leaving 24 (SiF_3^+) and 23 (SiF_3^{2+}) electrons to be distributed amongst the remaining 56 molecular orbitals. To calculate the ground and excited state energies of SiF_3^+ and SiF_3^{2+} multi reference CI, (MRCI) was used, employing the Table CI method of Buenker *et al.* [24], described in Chapter 2, with a configuration selection threshold of 10^{-5} hartrees.

As described below, previous work and this study have determined that SiF_3^{2+} has a C_{2v} equilibrium ground state geometry. The calculations of the electronic state energies of SiF_3^+ were performed with the monocation at the C_{2v} geometry of SiF_3^{2+} by analysis of the first two roots of the Hamiltonian in each MRCI calculation. The energies of the first two singlet states and the first two triplet states of each of the four irreducible representations of C_{2v} (A_1, A_2, B_1, and B_2) were calculated. Multiplicites greater than triplet were not calculated as these were considered to lie too high in energy to be populated in the electron-transfer reactions. That is, although there will be electronic states lying above those calculated it is felt that a sufficient number have been considered, (see below), so as to encompass all states that are energetically accessible in the electron-transfer reactions. This is shown in more detail in subsequent paragraphs.

The energies of the low-lying electronic states of the dication SiF_3^{2+} were determined in the same way as for the cation. The ground state of the dication has one unpaired electron and is of doublet multiplicity. As for the cation, the energy of the first two roots of each irreducible representation of C_{2v} were calculated giving a total of eight states as only doublet states were considered. The energy of dication's excited states was not necessary for the subsequent Landau-Zener calculations so to save computational time calculations were only performed in the ground state multiplicity.

In an electron-transfer reaction between a dication and a rare gas the amount of energy that can be transferred to the product molecular cation is the difference in energy between the ionisation potential of the rare gas and the energy difference of the cation and dication, Eq. 3.10. This energy difference is represented as ΔE in Figure 3.1.

$$\Delta E\left(XY^{2+} \rightarrow XY^{+}\right) - \Delta E\left(Rg \rightarrow Rg^{+}\right) \qquad 3.10$$

For the SiF_3^{2+} system Eq. (3.10) will have a maximum value for the rare gas with the lowest ionisation potential i.e. Xenon (IP = 12.13 eV). The energy difference between the cation and dication was determined using *ab initio* calculations. Using the setup described earlier the energy of the dication at its equilibrium geometry was determined and then the energy of the cation at this geometry was calculated, the difference between these two values being the first part of Equation. 3.10; *ab initio* calculations determined this to be 20.45 eV. Thus, the maximum possible electron excitation of SiF_3^{+} is (20.45 - 12.13), 8.32 eV. However, previous collision experiments on CF_2^{2+} [3] determined that more than one electronic state of the dication may have a lifetime long enough to be present in the dication reactant beam and so dications in various excited states were participating in the electron-transfer reactions. Thus, if excited states of SiF_3^{2+} are to be considered in the calculations then the value of $(XY^{2+} \rightarrow XY^{+})$ in Eq 3.10 will be greater than the

figure of 20.45 eV mentioned above and therefore the maximum possible electronic excitation of SiF_3^+ will be increased. The increase in the maximum possible energy transferred to the product molecular cation is equal to the electronic excitation of the dication. So, in order to account for the possibility of increased energy transferred to the cation SiF_3^+ excited states lying up to 17 eV above the cation ground electronic state were calculated. This allows for us to assess the reactivity of excited states of the dication SiF_3^{2+} lying up to 9 eV above the dication ground state.

3.3.2 Landau-Zener cross section calculations

The algorithm used to give the electron-transfer cross sections for the formation of SiF_3^+ from a given state of SiF_3^{2+} in a rare gas collision reaction is based on Landau-Zener theory. Using the *ab initio* methodology described above, the electron-transfer exothermicity for populating a given electronic state of SiF_3^+ from SiF_3^{2+} is determined. Given the polarisability α of the rare gas atom, Eqs 3.4 - 3.9 can be used to determine the curve crossing radius, $|H_{12}|^2$, r_c^*, $|V_1' - V_2'|$, δ and finally P, as a function of the radial velocity v_b. To calculate the state-to-state electron-transfer cross section, the expression for $P(v_b)$ is integrated as a function of impact parameter from 0 to the value of b for which the collision system just reaches the curve crossing radius.

Accurate prediction of the product ion intensities from these state-to state electron-transfer reactions requires the knowledge of which states of SiF_3^+ are stable and which are dissociative. This stability information is necessary as the ion ratios detected are a combination of whole ions from stable states of SiF_3^+ and fragment ions from the dissociation of unstable states of SiF_3^+. Unfortunately, for SiF_3^+ this stability information is not available so it is necessary to make some approximations. The method used, as described earlier, assumes that any excited states of SiF_3^+ lying above a thermodynamic dissociation asymptote, e.g. to

$SiF_2^+ + F$, are dissociative to the asymptote lying closest in energy below them. Given these approximations, it is possible to sum the cross sections for populating the different states of SiF_3^+ which are predicted to yield a given product ion, such as SiF_2^+. A summation is performed for each of the three accessible product channels (formation of SiF_3^{2+}, SiF_2^+ and SiF^+) yielding a total cross section for the formation of each of these products. This calculated ratio can then be compared with the experimentally observed product ion yields.

The calculations of the product ion yields must also consider the possibility of more than one long-lived electronic state of SiF_3^{2+} being present in the experimental dication beam. This is incorporated in to the Landau-Zener calculations by simply employing an appropriately adjusted value of the electron-transfer exothermicity[3]. The exothermicity of the reaction for an excited state of the dication will be greater than for the ground state by an amount equal to the energy difference between the ground state and excited state. The adjusted value of the exothermicity, ΔE, is then used in the Landau-Zener formula and calculations performed as for the ground state.

3.4 Results and Discussion

3.4.1 Geometries of the SiF_3 neutral, cation and dication

Before discussing the product ion yield calculations it is interesting to discuss the geometric properties of the SiF_3 molecule upon successive ionisations from neutral through to dication. Neutral SiF_3 has been determined by experimental studies to possess a pyramidal C_{3v} equilibrium geometry [25] that can undergo a geometrical inversion process analogous to the ammonia molecule, passing through a planar intermediate [26]. The exact geometry of this intermediate is unclear, but geometry optimisation performed with the molecule constrained to allow only planar geometries determined a C_{2v} intermediate structure with angle and

bondlengths as given in Table 3.2. These calculations of the SiF_3 planar intermediate were performed at the ROHF and UHF level of theory with the basis sets 3-21G, 3-21G* and 6-31G* because they were used to reproduce the results of earlier studies of SiF_3 [26] as a test to check that the computer packages were set up correctly and producing reliable results.

Table 3.2 *Geometries of the SiF_3 neutral, cation and dication. All values are for the equilibrium geometry except SiF_3 neutral C_{2v} which is the geometry of the planar intermediate; results for SiF_3 are for the 6-31G* basis set. Details of the D_{3h}, C_{2v} and C_{3v} structures are shown in the bottom three figures.*

		r_1 / Å	r_2 / Å	θ / °
SiF_3	C_{3v}	1.575	-	107.7
	C_{2v}	1.602	1.578	96.0
SiF_3^+	D_{3h}	1.527	-	120.0
SiF_3^{2+}	C_{2v}	1.881	1.502	102.0

Geometries for Table 3.2

D_{3h}	C_{2v}	C_{3v}
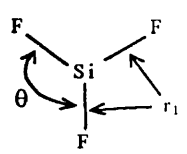	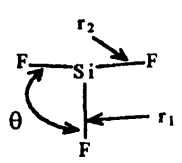	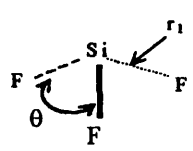

Geometry optimisation of SiF_3^+ found a planar D_{3h} equilibrium geometry and optimisation of the dication SiF_3^{2+} found a C_{2v} distorted 'T' shape with one Si-F bond significantly longer than the other two. These geometries are summarised in Table 3.2. This trend in changing equilibrium geometry with ionisation level

suggests that the shape of the molecular orbital that the ionised electron has been removed from strongly influences the equilibrium geometry of the molecule. In fact, examination of the highest occupied molecular orbital, the HOMO, of the SiF_3 neutral reveals that it contains significant silicon *p* orbital character with electron density localised above the silicon atom, a plot of the molecular orbital is shown in Figure 3.4.

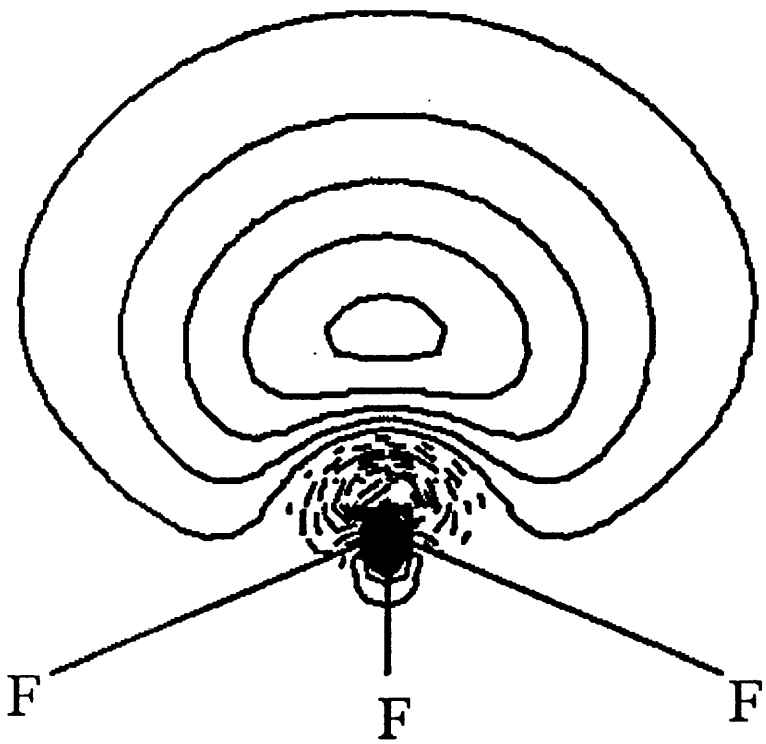

Fig. 3.4 *Molecular orbital plot of the highest occupied molecular orbital, HOMO, of SiF_3 showing the significant electron density located above the silicon atom, located at the centre of the picture, pushing the Si-F bonds 'down' to the observed C_{3v} geometry.*

The principles behind these geometry changes are similar to those used in the construction of a Walsh diagram of molecular orbital energy versus molecular geometry. Here a planar geometry is a minimum energy configuration for the

molecular orbital involved in bonding silicon to the three fluorines, call this orbital *a*, but is unstable for the out-of-plane molecular orbital with significant *p* orbital character mentioned above, orbital *b*. Changing the molecular geometry from planar D_{3h} to a pyramidal C_{3v} destabilizes orbital *a*, moving the fluorine atoms closer together increasing electrostatic repulsion between them, and stabilizes orbital *b*, as it brings the fluorine atoms away from the electron density localised above the silicon atom. Thus, the molecular geometry could be predicted if it is known whether orbital *b* is occupied or empty. For the SiF_3 neutral which has one electron in orbital *b* a C_{3v} geometry would be expected as the destabilsation of orbital *a* caused by moving the three fluorines closer together is slight compared to the stabilisation of orbital *b* achieved as the fluorines are moved away from the electron density above the silicon. For SiF_3^+ the electron is removed from orbital *b* so there is no electron density above the silicon atom and the Si—F bonds can 'relax' to the now more stable planar D_{3h} geometry.

The C_{2v} shape of the dication SiF_3^{2+} can not be described by this simple model, but a possible explanation can be obtained by drawing analogies with isoelectronic BF_3^+. The ground state of BF_3^+ has a 'T' shape similar to SiF_3^{2+} with one bond shorter than the other two [27,28]. The C_{2v} shape of BF_3^+ is attributed to a pseudo Jahn-Teller effect where moving to a C_{2v} shape allows mixing of the HOMO and same symmetry components of higher lying doubly degenerate orbitals stabilizing a distorted, non D_{3h} ground state geometry. There is as yet no experimental evidence to support this as an explanation for the ground state geometry of SiF_3^{2+} but the similarities in the molecules, (trihalogenated, isoelectronic) makes this a plausible explanation for the interesting SiF_3^{2+} ground state geometry.

Experimental evidence for a C_{2v} SiF_3^{2+} ground state comes from postulated geometries proposed to rationalize the observations of collisional excitation of fluorinated species [14]. In these collision experiments it was observed that tri-

fluorinated systems, such as CF_3^{2+} readily fragmented, losing one fluorine atom, suggesting that these molecules possessed one weakly bound fluorine atom. A distorted 'T' shape will have a one fluorine less strongly bound than the other two and so was proposed as being the most probable geometry to explain these observations. It is satisfying to note that the *ab initio* calculations on SiF_3^{2+} support this postulated geometry.

Recent high level *ab initio* calculations on the dication CF_3^{2+} have determined that it possesses a C_{2v} ground state equilibrium geometry [27,29] similar to that found in this study of SiF_3^{2+}. The reason for the reduced symmetry of the ground state of CF_3^{2+} is proposed to be the same mechanism as occurs for SiF_3^{2+} [27]

The calculations performed for this chapter have shown that the SiF_3 molecule displays interesting changes in equilibrium geometry upon successive ionisations to SiF_3^{2+}. The neutral has a pyramidal C_{3v} equilibrium geometry due to electron density in a molecule orbital with significant silicon *p* orbital character. This electron density is located above silicon (see Fig 3.4) and 'pushes down' the fluorine atoms away from a planar arrangement. Ionisation to SiF_3^+ removes the electron density from above the molecule allowing it to adopt a planar D_{3h} structure, minimising electron/electron repulsion between the fluorine atoms. Upon further ionisation to the dication SiF_3^{2+} the equilibrium geometry is a distorted 'T' shape with one bond longer than the other two. Rationalisation of this equilibrium geometry is more complicated but by analogy to isoelectronic BF_3^+ it seems likely that a pseudo Jahn-Teller distortion produces the stabilisation of this geometry.

3.4.2 Landau-Zener Calculations

As described above, the equilibrium geometry of SiF_3^+ is of D_{3h} symmetry [14,30] and the present *ab initio* calculations determine a bond length of 1.527 Å. The dication SiF_3^{2+} has a C_{2v} structure analogous to the calculated ground state

geometry of CF_3^{2+} and the experimentally determined geometry of valence isoelectronic BF_3^+ [28]. The calculated C_{2v} geometry of SiF_3^{2+} has one fluorine at a distance of 1.881 Å from the central fluorine, the other two Si–F bond lengths being 1.502 Å. The F_{axial}–Si–$F_{equatorial}$ angle is 102.0°. In the modeling of the experiments it is assumed that when SiF_3^{2+} is formed there are sufficient collisions in the ion source to relax it to its equilibrium geometry. As mentioned previously when an electron is transferred from the rare gas neutral to the dication in an electron-transfer reaction it is assumed that this occurs on a time-scale fast enough for it to be considered as a Franck-Condon transition, so forming the monocation at the same geometry as reactant dication. From the *ab initio* calculations it was determined that SiF_3^+ at the C_{2v} geometry has an energy 1.92 eV above its equilibrium (D_{3h}) geometry. Also, the dication at its ground state geometry (C_{2v}) lies 22.37 eV above the monocation at its ground state geometry (D_{3h}). These energy differences along with the calculated excited state energies of SiF_3^+ and SiF_3^{2+} are displayed in Table 3.3 and plotted in Fig. 3.5.

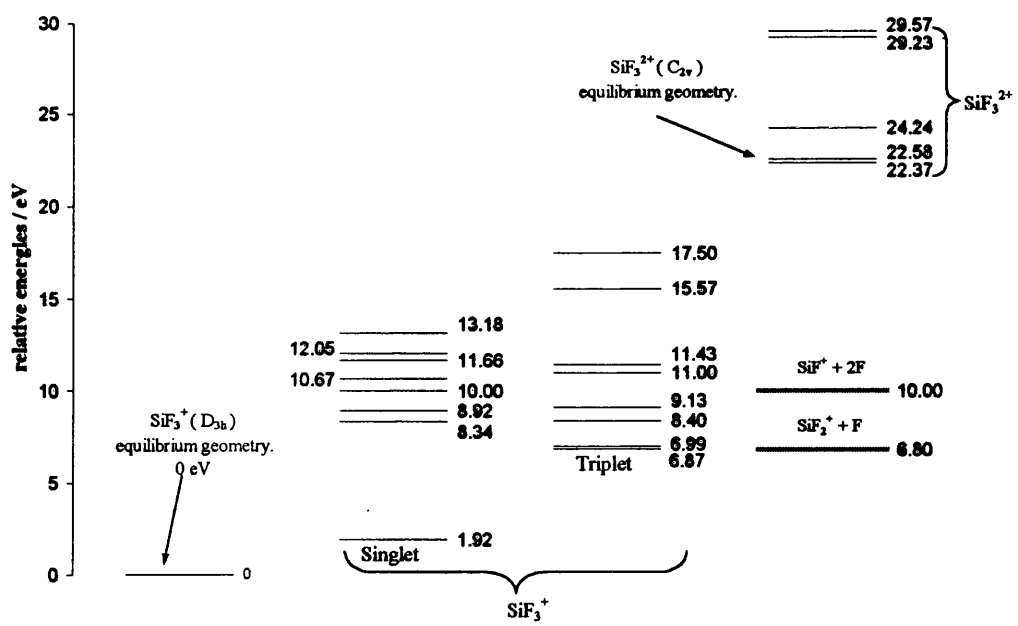

Fig. 3.5 *Plot of the electronic energies of SiF_3^+ and SiF_3^{2+} given in Table 3.3. The SiF_3^+ singlet and triplet states are all at the C_{2v} equilibrium geometry of SiF_3^{2+} except where marked. Also shown are the dissociation asymptotes giving SiF_2^+ and SiF^+ lieing at 6.8 eV and 10.0 eV respectively. The energies are plotted relative to ground state SiF_3^+ at its equilibrium D_{3h} geometry.*

Table 3.3 *Relative energies (eV) of the electronic states of SiF_3^+ and SiF_3^{2+} and their associated symmetry labels. The energy zero is taken as SiF_3^+ in its ground electronic state and at its equilibrium geometry. The energy zero is the only calculation at the D_{3h} conformation; all other energies are calculated at the C_{2v} geometry which is the ground state geometry of the dication.*

$SiF_3^{+\,a}$		$SiF_3^{2+\,b}$
Singlet	Triplet	Doublet
0 (A_1) [c]		
1.92 (A_1) [d]	6.87 (B_2)	22.37 (B_2) [e]
8.34 (B_2)	6.99 (B_1)	22.58 (B_1)
8.92 (B_1)	8.40 (A_1)	24.24 (A_1)
10.00 (A_2)	9.13 (A_2)	29.23 (A_1)
10.67 (A_1)	11.00 (B_1)	29.57 (A_2)
11.66 (B_1)	11.43 (B_2)	31.51 (B_1)
12.05 (A_2)	15.57 (A_1)	31.97 (B_2)
13.18 (B_2)	17.50 (A_2)	34.32 (A_2)

[a] *All values are for the C_{2v} geometry unless stated otherwise.*
[b] *Energies are all for the dication in its equilibrium ground state (C_{2v}) geometry.*
[c] *SiF_3^+ in its ground state equilibrium D_{3h} geometry.*
[d] *Ground electronic state of SiF_3^+ but in a distorted geometry (C_{2v} geometry of SiF_3^{2+}).*
[e] *SiF_3^{2+} ground electronic state.*

The arbitrary zero point to which all the energies given in Table 3.3 and Figure 3.5 are referenced to is taken to be the energy of SiF_3^+ in its ground state D_{3h} geometry. Using published thermodynamic data [31] it was determined that the first dissociation asymptote for SiF_3^+ results in the formation of $SiF_2^+ + F$ and lies 6.8 eV above SiF_3^+ (D_{3h}), the second dissociation asymptote lies at 10.0 eV and is for the formation of $SiF^+ + 2F$.[31] As described above, electron-transfer reactions may produce SiF_3^+ in a variety of excited states which are assumed to dissociate rapidly to the dissociation products associated with the first asymptote lying below

the given state. Thus, population of SiF_3^+ states lying between 6.8 eV and 10.0 eV will result in an SiF_2^+ signal in the mass spectrum, and population of states above 10.0 eV will give SiF^+. States of SiF_3^+ below 6.8 eV do not predissociate and so SiF_3^+ will be observed in the mass spectrum. The energies of the cation and dication electronic states along with these dissociation asymptotes are plotted relative to each other in Figure 3.5.

The experimental product ion ratios [14] displayed in Figure 3.3b show clearly the high state-selectivity of the electron-transfer reactions. As described earlier, the product ion ratios for dications are usually predicted reasonably accurately by Landau-Zener theory [1,3,12]. In this analysis of the SiF_3^{2+} system *ab initio* calculations of the monocation's electronic state energies have been used with Landau-Zener calculations to predict product ion yields for collision reactions between SiF_3^{2+} and the rare gases. However, in Figure 3.6a the predicted product ion yields when only the ground state of the dication is considered as a reactant are plotted and it can be seen that this does not achieve a satisfactory fit with the experimental ion yields (Figure 3.3b). Hence, calculations of the product ion yields which allowed multiple states of the reactant dication to be present were performed using the theoretical method outlined previously. The best fit to experimental data occurs for three electronic states of SiF_3^{2+} being present in the reactant beam. The three electronic states are at energies of 21.9 eV, 26.2 eV and 30.4 eV, and correspond to the ground state and excited states 4.3 eV and 8.5 eV above the dication ground state. Also if the three states are considered to be present in equal amounts, Figure 3.6b, a poor fit with the experimental product ratios is obtained a far better fit is obtained when the states are present in the ration of 1 : 0.8 : 0.1, this is shown in Figure 3.3a. Given the approximations used in the derivation of these ratios they should only be taken as rough estimates of the relative populations of the SiF_3^{2+} electronic states in the ion beam. However, comparisons of the experimental results and the Landau-Zener calculations clearly indicate that in the

dication reactant beam a significant number of the dications are in one excited electronic state and a smaller number in a higher lying state.

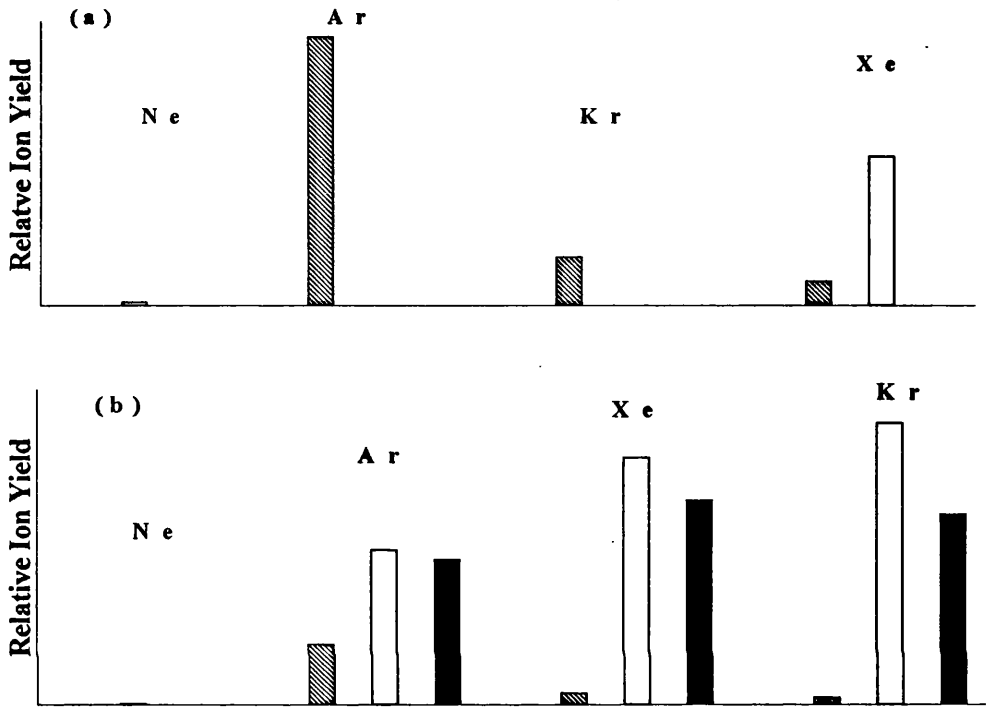

Fig. 3.6 *Plot of the product ion yields predicted by the calculations when (a) only the ground state of the dication is present and (b) three electronic state of the dication present in the ion beam in equal amounts. As for Figure 3.3 the hatched boxes are SiF_3^+, the white boxes SiF_2^+, and the black boxes for SiF^+.*

From Figure 3.6a it can be clearly seen that if excited states of SiF_3^{2+} are not included in the modeling then the ground state of the dication on its own will not form SiF^+ in any electron-transfer reactions with the rare gases. Yet SiF^+ is clearly seen in the experimental data (Table 3.1, Figure 3.3b). Also, the Landau-Zener calculations indicate that SiF_2^+ should only be observed in reactions of the ground state of SiF_3^{2+} with xenon, Figure 3.3b shows clearly that SiF_2^+ is detected experimentally for all the rare gases except neon.

Comparison of the dication electronic state energies from the Landau-Zener calculations with the *ab initio* electronic state energies in Table 3.3 shows a good

agreement, the Landau-Zener derived value of 21.9 eV being with in 0.5 eV of the calculated energy of the SiF_3^{2+} ground state and the other energies lying close to other states. It is important to realise that the *ab initio* calculations are restricted to the C_{2v} geometry of the dication ground state and the relevant excited states may have different equilibrium geometries. Hence, the restricted calculations are only employed to indicate approximately where the excited states of SiF_3^{2+} lie so as to determine if the predictions of the Landau-Zener model are reasonable.

The reactivity of the SiF_3^{2+} ground and excited states is shown diagramatically in Figure 3.7, where the electron-transfer cross sections of the three electronic states of SiF_3^{2+} are plotted as a function of the electronic energy of the SiF_3^+ product. The figure clearly shows how on collision with argon, the ground state of SiF_3^{2+} can only populate the ground state of SiF_3^+, so excited dication states must be present to form the SiF_2^+ and SiF^+ observed experimentally. This figure shows clearly the necessary presence of dication states at energies above the SiF_3^{2+} ground state to achieve a satisfactory fit with the experimental data.

3.4.2.1 Neon

From Table 3.1 it can be seen that the experimental product ion distribution for the reaction of SiF_3^{2+} with neon is dominated by collision-induced neutral loss Eq. (3), resulting in the loss of F to form SiF_2^{2+}. The Landau-Zener calculations predict such a result for neon as dication states with energies of 21.9 eV, 26.2 eV and 30.4 eV above the SiF_3^+ equilibrium geometry undergo no significant electron-transfer. The ionisation energy of neon is sufficiently large for the reactant and product potentials to cross at a large interspecies separation where the probability for electron-transfer is small. The dication state at 26.2 eV is predicted to have a small cross section for the formation of SiF_3^+, see Table 3.4, but this would be below the experimental detection limit.

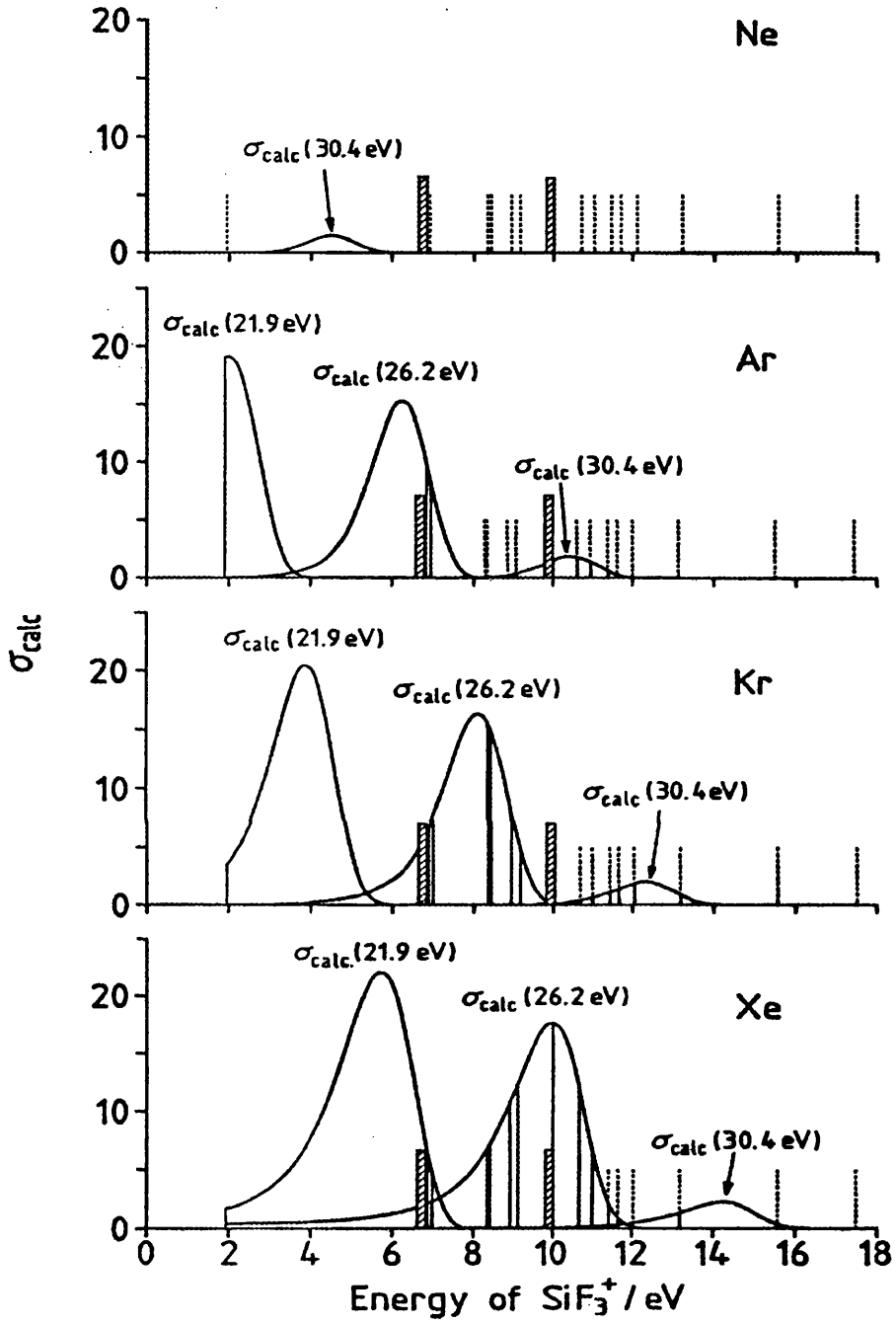

Fig. 3.7 *Landau-Zener electron-transfer cross sections σ_{calc} for each of the three dication electronic states present in the dication beam, plotted against the electronic energy of SiF_3^+. The SiF_3^+ ion is constrained to have the C_{2v} geometry of the ground state of the dication. Also shown are the monocation's electronic states and the dissociation asymptotes to $SiF_2^+ + F$ at 6.8 eV and $SiF^+ + 2F$ at 10.0 eV, which are represented as hatched boxes at the energies at which they lie. The ground state of SiF_3^+ lies at 1.92 eV. The electronic states of SiF_3^+ are represented as vertical lines from the energy axis and are extended to the value of the electron-transfer cross section at that energy to give a representation of the probability for populating the given state. The values of σ_{calc} have been scaled to be in the ratio of 1 : 0.8 : 0.1 for the dication state at the energies 21.9 eV, 26.2 eV and 30.4 eV. Plots are represented for collisions with the rare gases neon, argon, krypton and xenon.*

If there were any states of the dication lying at energies between 26.2 eV and 30.4 eV then any electron-transfer reactions would populate the ground state SiF_3^+ as these energies lie in the reaction window for the population of the cation ground state. But, in Figure 3.7 it can be seen that the calculated cross section (σ_{calc}) has a characteristic shape with a distinct maximum at a particular energy. For neon the exothermicity of the reaction with the dication state at 30.4 eV is just sufficient that the cross section envelope maxima lies between the SiF_3^+ ground state and first excited state. Due to the SiF_3^+ ground state being a closed shell system a significant amount of energy is required to un-pair the electrons resulting in a large energy gap, 4.95 eV, between the ground state and the first excited state. Thus, with neon there are no states of SiF_3^+ lying at energies which are accessible for electron-transfer with a dication state at 30.4 eV.

3.4.2.2 Argon

From Figure 3.3b it can be seen that a wider range of products are observed following the reaction of SiF_3^{2+} with argon than were observed with neon, indicating that electron-transfer reactions form SiF_3^+ in a range of electronic states. The strongest product ion signal though is for SiF_2^{2+} (Table 3.1) the collision-induced neutral loss process. As can be seen in Figure 3.6a the ground electronic state of SiF_3^{2+} is predicted to form only SiF_3^+ in an electron-transfer reaction with argon, but the excited dication states at 26.2 eV and 30.4 eV react to populate excited states of SiF_3^+ that dissociate to the SiF_2^+ and SiF^+ asymptotes. As is shown in Figure 3.7 the Landau-Zener algorithm predicts the dication state at 26.2 eV to populate two states of SiF_3^+ lying just above the SiF_2^+ asymptote. The higher lying dication state at 30.4 eV has its maximum for electron-transfer cross section just above the SiF^+ asymptote at 10.0 eV (Figure 3.7) so populating some states below 10.0 eV (which dissociate to form SiF_2^+) and a few above 10.0 eV (giving SiF^+).

Incorporating the three reactant dication states in the ratio of 1 : 0.8 : 0.1 gives a product ion distribution for reactions with argon with almost equal amounts of SiF_3^+ and SiF_2^+ and much less SiF^+. From Figure 3.3 it can be seen that the predicted product ion yield is in good agreement with experiment.

Table 3.4 *Calculated and scaled relative cross sections for the formation of SiF_3^+, SiF_2^+ and SiF^+ via electron-transfer between SiF_3^{2+} and a rare gas. The values shown are for SiF_3^{2+} states lying at 21.9, 26.2 and 30.4 eV above SiF_3^+ (D_{3h}) equilibrium geometry. The ratio of the three states in the ion beam is 1 : 0.8 : 0.1.*

	Relative electron-transfer cross sections							
Product	Neon				Argon			
Ion	21.9	26.2	30.4	Total	21.9	26.2	30.4	Total
SiF_3^+	0	0.2	0	0.2	18.9	0.1	0	19.0
SiF_2^+	0	0	0	0	0	17.5	2.7	20.2
SiF^+	0	0	0	0	0	0	4.6	4.6
	Krypton				Xenon			
	21.9	26.2	30.4	Total	21.9	26.2	30.4	Total
SiF_3^+	3.4	0.1	0	3.5	1.7	0.4	0	2.1
SiF_2^+	0	59.0	0.5	59.5	10.5	58.5	0.6	69.6
SiF^+	0	0	6.5	6.5	0	21.8	3.3	25.1

3.4.2.3 Krypton

The experimental product ion yields for the collision reaction between SiF_3^{2+} and krypton (Table 3.1) show that electron-transfer is now the dominant process, predominantly forming states of SiF_3^+ that dissociate to $SiF_2^+ + F$ (Figure 3.3b). Thus the product ion spectrum has a large SiF_2^+ signal with small amounts of SiF_3^+, SiF^+ and SiF_2^{2+}. The Landau-Zener model predicts the dication state at 26.2 eV to

have a large cross section for the formation of SiF_3^+ ions with energies between 6.8 and 10.0 eV. States at these energies should dissociate to the SiF_2^+ + F asymptote. The ground state dication has a cross section maximum below the SiF_2^+ + F asymptote at energies where SiF_3^+ has no electronic states, although there is a small cross section for the formation of ground state SiF_3^+. The highest lying dication state at 30.4 eV reacts to populate only SiF_3^+ states lying above 10.0 eV which would dissociate to SiF^+. From Figure 3.3 it can be seen that the Landau-Zener calculations for this system produce predicted product ion yields that are again in good agreement with experiment.

3.4.2.4 Xenon

The product ion distribution for xenon, as with krypton, has SiF_2^+ as the dominant product with similar, smaller amounts of SiF_3^+ and SiF^+. However, the signal for SiF_2^{2+}, formed via collision induced neutral loss, is stronger for xenon than it was for krypton (Table 3.1). The increase in the neutral loss signal on moving from krypton to xenon is probably due to the larger centre of mass collision energy with xenon.

In the Landau-Zener algorithm the lower ionisation energy of xenon produces more SiF_3^+ in the higher lying excited states than for krypton. The ground state of the dication has a small electron-transfer cross section for the formation of SiF_3^+ ground state and also a state of the cation lying just above the first dissociation asymptote. The dication state at 26.2 eV populates a variety of states either side of the asymptote at 10.0 eV (Figure 3.7) so contributing to the SiF_2^+ and SiF^+ signals. The dication state at 30.4 eV reacts solely to produce SiF_3^+ in electronic states that will dissociate to SiF^+ + 2F.

The experimental and predicted product ion yields for xenon are in reasonable agreement, although the methodology has not been as successful for xenon as it

has been for krypton and argon. The main discrepancy is the small ratio of SiF_3^+ to SiF^+ which are observed in similar amounts experimentally although with significant uncertainties. The agreement between the calculated and experimental values, although good, seems to decrease with the larger rare gas atoms. The larger rare gases are more polarisable and this would affect the polarisation attraction curve (Figure 3.1) making its shape at small interspecies separations harder to model successfully and affecting calculations.

3.5. Conclusions

The product ion yields for the electron-transfer reactions of SiF_3^{2+} with the rare gases have been interpreted by a combination of *ab initio* and Landau-Zener calculations. By investigating the SiF_3^{2+} system this work is intended to evaluate the applicability of a simple Landau-Zener algorithm to the electron-transfer reactions of large molecules, specifically those with more than three atoms and subsequently a greater degree of geometrical freedom.

The *ab initio* calculations enabled the evaluation of the energy differences between SiF_3 cationic and dicationic ground state geometries, and also the energies of their low lying excited states. Using all of these data it has been possible to achieve a satisfactory agreement between predicted and experimental product ion yields better than has been achieved in a previous study. The best agreement is obtained when the reactant beam is modeled as containing the dication in its ground electronic state and also two excited states lying at 4.25 eV and 8.5 eV above the dication ground state. The dication states are present in the reactant beam in the approximate ratio of 1 : 0.8 : 0.1. The good agreement between calculation and experiment shows that the Landau-Zener algorithm is still applicable for these larger systems, although the cation and dication geometries and excited state energies must be carefully taken nto consideratio.

References

(1) Price S. D., Rogers S. A. and Leone S. R. *J. Chem. Phys.* **98** (1993) **280**.

(2) Price S. D., Manning M. and Leone S. R. *Chem. Phys. Lett.* **214** (1993) 553.

(3) Manning M., Price S. D. and Leone S. R. *J. Chem. Phys.* **99** (1993) **8695**.

(4) Curtis J. M., Brenton A. G., Beynon J. H. and Boyd R. K. *Chem. Phys.* **117** (1987) 325.

(5) Dolejsek Z., Farnik M. and Herman Z. *Chem. Phys. Lett.* **235** (1995) **99**.

(6) Newson K. A. and Price S. D. *Chem. Phys. Lett.* **269** (1997) 93.

(7) Maier W. B., II *Chem. Phys.* **60** (1974) 3588.

(8) Spears K. G., Fehensfeld G. C., McFarland M. and Ferguson E. E. *J. Chem. Phys.* 56 (1972) 2562.

(9) Smith D., Adams N. G., Alge E., Villinger H. and Lindinger W. *J. Phys. B.* **13** (1980) 2787.

(10) Sadílek M., Vancura J., Fárník M. and Herman Z. *Int. J. Mass Spectrom. Ion Proc.* 100 (1990) 197.

(11) Kamber E. Y., Akyungor K., Safvan C. P. and Mathur D. *Chem. Phys. Lett.* 258 (1996) 336.

(12) Rogers S. A., Price S. D. and Leone S. R. *J. Chem. Phys.* **98** (1993) **280**.

(13) Griffiths W. J., Langford M. L. and Harris F. M. *Rapid Commun. Mass Spectrom.* 10 (1996) 997.

(14) Lee Y.-Y., Leone S. R., Champkin P., Kaltsoyannis N. and Price S. D. *J. Chem. Phys.* 106 (1997) 7981.

(15) Landau L. *Phys. Z. Sov. 2* **2** (1932) 46.

(16) Stueckelberg E. C. G. *Helv. Phys. Acta* **5** (1932) 369.

(17) Zener C. *Proc. R. Soc. London. Ser. A.* **137** (1932) 696.

(18) Olson R. E., Smith F. T. and Bauer E. *Appl. Opt.* **10** (1971) 1848.

(19) Eland J. H. D. *Int. J. Mass Spectrom. Ion Phys.* **9** (1972) 397.

(20) Herman Z. *Int. Reviews in Phys. Chem.* **15** (1996) 299.

(21) Price S. D., Lee Y. Y., Manning M. and Leone S. R. *Chem. Phys.* **190** (1995) 123.

(22) Lee Y. Y. and Leone S. R. *J. Phys. Chem.* **99** (1995) 15438.

(23) Guest M. F., van Lenthe J. H., Schöffel K. and Sherwood P. ; Daresbury Laboratory: Daresbury UK, 1995.

(24) Buenker R. J. *Stud. Theor. Chem.* **21** (1982) 17.

(25) Symons M. C. R. *J. Chem. Soc. Dalton Trans.* (1976) 1568.

(26) Moc J., Rudziñski J. M. and Ratajczak H. *Chem. Phys.* **159** (1992) 197.

(27) Kaltsoyannis N. and Price S. D. *Chem. Phys. Let.* **in press** (1999).

(28) Haller E., Koppel H., Cederbaum L. S., Vonniessen W. and Bieri G. *J. Chem. Phys.* 78 (1983) 1359.

(29) Hrusák J., Sändig N. and Koch W. *Int. J. Mass Spectrom. Ion Proc.* **187** (1999) 701.

(30) Hayes T. R., Shul R. J., Baiocchi F. A., Wetzel R. C. and Freund R. S. *J. Chem. Phys.* 89 (1988) 4035.

(31) Lias S. G., Bartmess J. E., Liebman J. F., Holmes J. L., Levin R. D. and Mallard W. G. *J. Phys. Chem. Ref.* (1988) **Data 17 S1**, 1.

Chapter 4

On the dissociation of the ozone dication

4.1 Introduction

The presence of ozone in the Earth's stratosphere is essential to biological life as it absorbs much of the UV radiation coming from the sun, preventing it from reaching the Earth's surface where it would be harmful. Many of the properties of this important molecule have been elucidated in recent intensive research into the chemistry and physics of ozone depletion.[1,2] However, despite this interest into O_3 little attention has been paid to the behaviour of ozone upon electron ionisation. The properties of the ozone cation O_3^+ have been studied successfully, [3] but attempts to produced long lived O_3^{2+} ions by electron-induced double ionisation of the neutral have been unsuccessful.[4] In experiments to form the ozone dication only the dissociation products of O_3^{2+} were observed, (O^+ and O_2^+) indicating that unstable regions of the dicationic potential energy surface have been populated. The nature of this instability is unclear though, and could be due to the lack of any metastable electronic states. It is also possible that the experimental set-up may be forming the dication in unstable geometries. Elucidating the dissociation mechanism of O_3^{2+} is the focus of the work described in this chapter.

Previous theoretical work on O_3^{2+} is scarce. An early study of cyclic O_3^{2+}, in electronic singlet states, determined this geometry to be unstable with respect to fragmentation to O^+ and O_2^+.[5] Two investigations into 22 electron triatomics, which include O_3^{2+}, have been reported by Pyykkö.[6,7] These calculations were restricted to linear geometries and determined that the ground singlet state is quasibound. Also, Pykkö determined that there is a dissociative triplet state that cuts this singlet state but the intersection lies away from the equilibrium geometry

and at the equilibrium geometry the triplet state is significantly higher in energy than the singlet state.

The calculations presented in this investigation determine a possible fate of O_3^{2+}, following formation from neutral O_3, by inspection of the form of the potential energy surfaces of the ground singlet and ground triplet electronic states and the geometry of the dication upon formation in the experimental set-up. Also, calculated values of the double ionisation potential and kinetic energy release are compared with reported experimental values.

4.2 State Averaging Technique

As described in Chapter 1 the metastability of dication electronic states can be considered to arise from an avoided crossing between two states of the same symmetry, the attractive $X + Y^{2+}$ curve and repulsive $X^+ + Y^+$ curve. Potential curves of this nature can, for standard *ab initio* techniques, present problems where the calculations do not converge on the required electronic state. This produces a discontinuous potential energy curve with the difficulties tending to occur in the region of the avoided crossing; this is the region that usually corresponds to the barrier maximum. The state averaging technique used in this investigation avoids this problem by using a set of orbitals that are optimised so as to minimise the energy of two or more states simultaneously,[8] and each state has a particular weighting controlling its contribution to the overall wavefunction. Generally, in the calculation of dication potential energy curves at least two states need to be included in the state averaging procedure, that is the two states corresponding to $X + Y^{2+}$ and $X^+ + Y^+$ mentioned above.

The state averaging technique has been applied successfully to calculate potential energy curves and molecular properties of many systems [9-11]. Also neutral molecules with strong ionic character such as LiF [12] require the state averagin

technique as the ground state is characterised by an ionic-neutral curve crossing between the Li^+-F^- and Li-F states.

4.3 Theoretical and computational methodology and results

All electron *ab initio* calculations were performed for the first singlet and first triplet states of O_3^{2+} using the SA-CASSCF / MRCI (State Averaged-Complete Active Space Self Consistent Field Multi Reference singles and doubles Configuration Interaction) method [13,14] implemented in the program MOLPRO. [15] The standard 6-311G basis set supplemented with two *d* and one *f* polarisation functions, was used for most calculations. However, for calculations of the kinetic energy release and double ionisation potential the basis sets 6-31G(2d) and VTZ were also employed. As described above the state averaging technique was required for a correct description of the dissociation of singlet and triplet O_3^{2+} and to produce a continuous curve through the barrier found in the potential correlating with the charge separation asymptote for the O_3^{2+} singlet state.

CASSCF geometry optimisation of the ozone neutral found a C_{2v} equilibrium geometry with bond length r(O–O) = 1.2826 Å and bond angle O–Ô–O = 116.59°, in excellent agreement with experiment: 1.2717 Å and 116.7°.[16] For the geometry optimisation a full valence active space was employed with only the 1*s* orbitals of each oxygen being kept doubly occupied (frozen).

For the potential energy surface calculations a smaller active space was employed to reduce computational time, this was necessary due to the large number of calculations required for each surface. The seven most stable valence molecular orbitals were kept doubly occupied in all of the calculations of the potential energy surfaces, leaving eight electrons to be distributed amongst the remaining eight valence molecular orbitals. Configuration Interaction employing single and double excitations from this reduced active space into the 76 external molecular orbitals

was performed in order to produce the final energy of each point on the potential energy surfaces. C_s symmetry was employed for each point on the surfaces.

The method used to determine the symmetries of the dissociation asymptotes of O_3^{2+} that correlate with the ground singlet and triplet states is as used by Katani in reference [17] and involves determining the symmetries of the constituent species in the completed molecule's symmetry. Then the fragments are combined and the direct product of the fragment symmetries gives the possible symmetries of the combined molecule (e.g. O_3^{2+}) that can dissociate to the fragments in those particular electronic states. The possible total spin values, S, of the combined molecule are obtained by vectorial addition of the individual spin values of the dissociated fragments, S_i, that is

$$S = \sum S_i . \qquad 4.1$$

So for each pair of individual spin values, S_i and S_k, partial resultants have to be formed according to the rule:

$$S_{ik} = S_i + S_k,\ S_i + S_k - 1,\ \ldots,\ |S_i - S_k| \qquad 4.2$$

which are then added according to the same rule.

Applying this to O_3^{2+} the electronic states of the dissociated species, O^+ and O_2^+, need to be resolved into the symmetry of O_3^{2+}, that is C_{2v}, using the descent in symmetry given in Table 4.1. For O_2^+ the ground state is $^2\Pi_g$ and first excited state $^4\Pi_u$ [18], for O^+ the ground state and first excited state are ^4S_u and ^2D_u respectively.[19] Taking the lowest energy dissociation asymptote i.e. ground state O^+ (^4S_u) and ground state O_2^+ ($^2\Pi_g$), the O^+ ^4S_u corresponds to quartet A_2 in C_{2v} symmetry and for O_2^+ $^2\Pi_g$ is doublet A_2 and B_2. Using the direct products given in Table 4.2 the product of these symmetries is

$$A_2(A_2 + B_2) = A_1 + B_1$$

and the possible S values, using Eq. (4.2), are

$$1.5 + 0.5,\ 1.5 - 0.5 = 2,\ 1$$

thus quintet and triplet states are possible. Thus states of O_3^{2+} that can dissociate to ground state O^+ and ground state O_2^+ are $^{3,5}A_1$ and $^{3,5}B_1$.

Table 4.1 *Descent in symmetry table for the full rotational group to C_{2v} and for linear $D_{\infty h}$ to C_{2v}. For $D_{\infty h}$ to C_{2v} the the C_{2v} system lies in the zy plane.*

Full rotation	C_{2v}	$D_{\infty h}$	$C_{2v}(z \rightarrow y)$
S_g	A_1	Σ_g^+	A_1
S_u	A_2	Σ_u^+	B_2
P_g	$A_2 + B_1 + B_2$	Σ_g^-	B_1
P_u	$A_1 + B_1 + B_2$	Σ_u^-	A_2
D_g	$2A_1 + A_2 + B_1 + B_2$	Π_g	$A_2 + B_2$
D_u	$A_1 + 2A_2 + B_1 + B_2$	Π_u	$A_1 + B_1$

Table 4.2 *Direct product table for the C_{2v} point group.*

	A_1	A_2	B_1	B_2
A_1	A_1	A_2	B_1	B_2
A_2		A_1	B_2	B_1
B_1			A_1	A_2
B_2				A_2

The energy difference between the ground and first excited state of O^+ is 3.3 eV and for O_2^+ 4.10 eV, [18,19] therefore the next dissociation asymptote for O_3^{2+} is ground state O_2^+ and first excited state O^+, i.e. O^+ ^2D_u and O_2^+ $^2\Pi_g$. As before, using Table 4.2, $^2\Pi_g$ is doublet A_2 and B_2 in C_{2v}, and ^2D_u is doublet $A_1 + 2A_2 + B_1 + B_2$. The product of these is

$$A_2(A_1 + 2A_2 + B_1 + B_2) = A_2 + 2A_1 + B_2 + B_1$$

$$B_2(A_1 + 2A_2 + B_1 + B_2) = B_2 + 2B_1 + A_2 + A_1$$

$$= 3A_1 + 3B_1 + 2B_2 + 2A_2$$

and the possible S values are

$$0.5 + 0.5,\ 0.5 - 0.5 = 1,\ 0$$

so triplet and singlet multiplicities are possible. Therefore, molecular states of O_3^{2+} that can dissociate to the second dissociation asymptote, $O^+\ ^2D_u + O_2^+\ ^2\Pi_g$, are $^{1,3}A_1$, $^{1,3}B_1$, $^{1,3}B_2$, $^{1,3}A_2$.

The ozone dication singlet ground state is a closed shell system so in C_{2v} is of A_1 symmetry. Calculations on the ground triplet state determined it to be of B_1 symmetry, so in light of the above discussion the following correlations are expected:

$$O_3^{2+}\,{}^1A_1 \rightarrow O_2^+\,{}^2\Pi_g + O^+\,{}^2D_u \qquad 4.3$$

$$O_3^{2+}\,{}^3B_1 \rightarrow O_2^+\,{}^2\Pi_g + O^+\,{}^4S_u \qquad 4.4$$

which, as shown below, are reproduced by the calculations.

In order to allow the state averaging technique to describe correctly the dissociations given in Eqns 4.3 and 4.4 at all distances of the O^+ from the O_2^+, it is necessary to include a sufficient number of states of the correct symmetry to describe fully both the associated and dissociated O_3^{2+}. It is therefore necessary to consider the arrangement of the electrons in the dissociated products, and the change in symmetry which occurs on going from those products to the associated dication. As the dissociation lowers the symmetry of O_3^{2+} from C_{2v} to C_s, the calculations of the potential energy surfaces have been performed exclusively in the latter symmetry. The symmetries of the dissociated products are, of course, R_3 for O^+ and $D_{\infty h}$ for O_2^+.

In O_2^+ the HOMO is the π_g antibonding orbital, which contains one electron. The ground electronic state of O_2^+ is therefore $^2\Pi_g$. Lowering of the symmetry to C_s lifts the degeneracy of this state and creates two new possibilities, $^2A'$ and $^2A''$, according to whether the electron is in the π_x or π_y orbital (in $D_{\infty h}$ notation) respectively. This may be represented as follows:

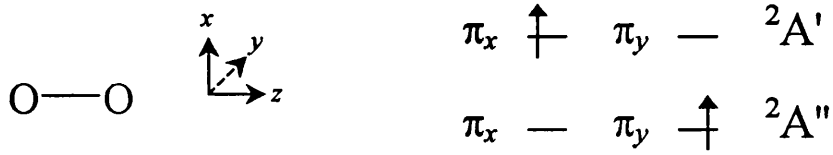

where the *xz* plane is defined to be the C_s mirror plane.

The situation is rather more complicated for O^+. O^+ has the electronic configuration $[He]2s^22p^3$, and the different arrangements of the three $2p$ electrons in the p_x, p_y and p_z orbitals will lead to several electronic states on account of differing electron/electron repulsions. The states produced by p^3 are, in fact, ^4S_u, ^2D_u and ^2P_u. The ^4S_u state (the dissociation limit of the first triplet state of O_3^{2+}) is produced by only one arrangement of the O^+ $2p$ electrons:

Lowering of the symmetry from $R_3 \rightarrow C_s$ converts the ^4S_u state to $^4A''$, as the p_z and p_x orbitals are defined to have *a'* symmetry in the above diagram and the p_y orbital *a"* (i.e. the *xz* plane forms the mirror plane of C_s). Thus in order to describe fully the dissociation of the lowest energy triplet surface of O_3^{2+} we must include $A'' \otimes (A' + A'') = A'' + A'$ states (i.e. one A" and one A') in the state averaging approach.

The dissociation limit of the lowest singlet state of O_3^{2+} is $^2D_u(O^+)$ and $^2\Pi_g(O_2^+)$. We have already considered the $^2\Pi_g$ state of O_2^+, and must now examine the arrangements of the three $2p$ electrons of O^+ which contribute to the ^2D_u state.

The eight possible arrangements of the three $2p$ electrons of O^+ which give rise to the spatial components of the ^2D_u and ^2P_u states are as follows:

m_ℓ	1	0	-1	M_L	Symmetry in C_s
	—	↑	↑↓	-2	$^2A'$
	↑	↑↓	—	+1	$^2A'$
	↑↓	↑	—	+2	$^2A'$
	↑	—	↑↓	-1	$^2A'$
	↑↓	—	↑	+1	$^2A''$
	—	↑↓	↑	-1	$^2A''$
	↑	↓	↑	0	$^2A''$
	↑	↑	↓	0	$^2A''$

The ^2D_u state is associated with five of these arrangements (microstates) - with M_L values -2, -1, 0 1, 2 and the ^2P_u state with three M_L = -1, 0, 1. However, with the exception of the $M_L = \pm 2$ microstates we can't assign a particular microstate to a particular state (this process is really just a book-keeping exercise) and, hence, it is most sensible to include all eight microstates in the state averaging approach. Thus to correctly describe dissociation of the singlet curve it is safest to include the following 16 states:

$^2\Pi_g\ (O_2^+)$		O^+		
A'	$\otimes$	4A'	=	4A'
A'	$\otimes$	4A"	=	4A"
A"	$\otimes$	4A'	=	4A"

$$A'' \otimes 4A'' = 4A'$$

i.e. 8 states of A' symmetry and 8 of A".

We saw earlier that the states of O_3^{2+} that can dissociate to ground state $O^+(^4S_u)$ and ground state $O_2^+(^2\Pi_g)$ are $^{3,5}A_1$ and $^{3,5}B_1$. Descent in symmetry from $C_{2v} \rightarrow C_s$ tells us that $A_1 \rightarrow A'$ and $B_1 \rightarrow A'$. Thus the most stable triplet state of A' symmetry is used to form the lowest energy triplet surface disscussed in this chapter. We also saw that $^{1,3}A_1$, $^{1,3}B_1$, $^{1,3}B_2$ and $^{1,3}A_2$ O_3^{2+} can dissociate to $O^+(^2D_u$) and $O_2^+(^2\Pi_g)$. The lowest energy singlet surface of O_3^{2+} may therefore be either of A' or A" symmetry. In practice it is found that the lowest energy singlet surface is of A' symmetry.

It was not initially clear that the state averaging procedure would be necessary for the calculations on O_3^{2+}. Early attempts using single reference CI and non CAS or state averaged methods were unsuccessful and displayed all the problems of root flipping and discontinuous potential energy curves described earlier. Even when the SA-CASSCF MRCI method was found to be successful almost two weeks of computer time was necessary to calculate all the points necessary for both surfaces.

The O_3^{2+} surfaces were created by keeping one bond length fixed at 1.2826 Å (the equilibrium bond length for O_3 neutral determined by the earlier CASSCF calculations) with the other ranging from 1.2 Å to 3.0 Å. The bond angle, theta, was varied between 80° and 180° at 10° intervals. This approach is illustrated in Figure 4.1 where r is the bond length that is varied. The full surfaces were generated by reflecting these points about the $\theta = 180°$ line. This created 273 points for each surface, which was then fitted to a 50 x 50 grid using a spline function. The singlet surface is shown in Figure 4.2 and the triplet surface in Figure 4.3.

This methodology in which one O–O bond length was kept fixed, was adopted both for reasons of computational economy (since only a qualitative explanation of

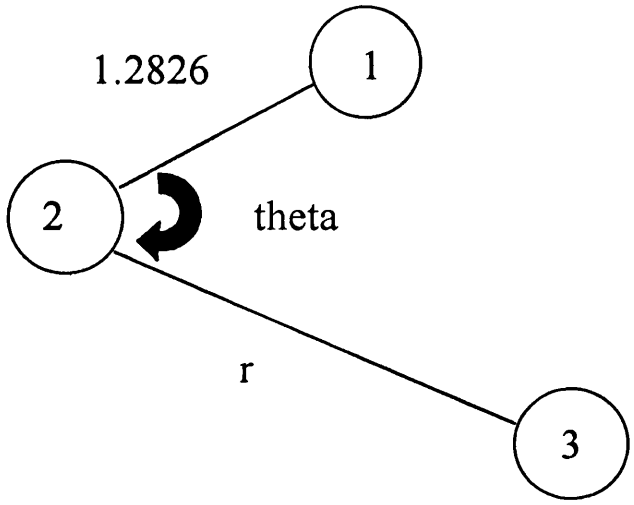

Fig 4.1 *The model of the ozone dication used in the calculations, O1 and O2 are kept at a distance of 1.2826 Å whilst the distance between O2 and O3 is allowed to vary, θ is the angle made between O3, O2 and O1.*

the experimental results is being sought), and since it is known from experiment that O_3^{2+} dissociates to O_2^+ and O^+. Thus, the cleavage of the O_2^+–O^+ bond is the crucial element of the dynamics. Further support for this approach involves the fact that the experiments that are being studied form O_3^{2+} in a vertical transition from the neutral geometry. Hence, the critical dynamics of the dissociation will occur in the region of the potential energy surface where the O–O bond length is close to that of O_3. So, although containing approximations (such as trapping some internal energy in the O_2^+ fragment), the calculations probe the key points of the O_3^{2+} potential energy surface.

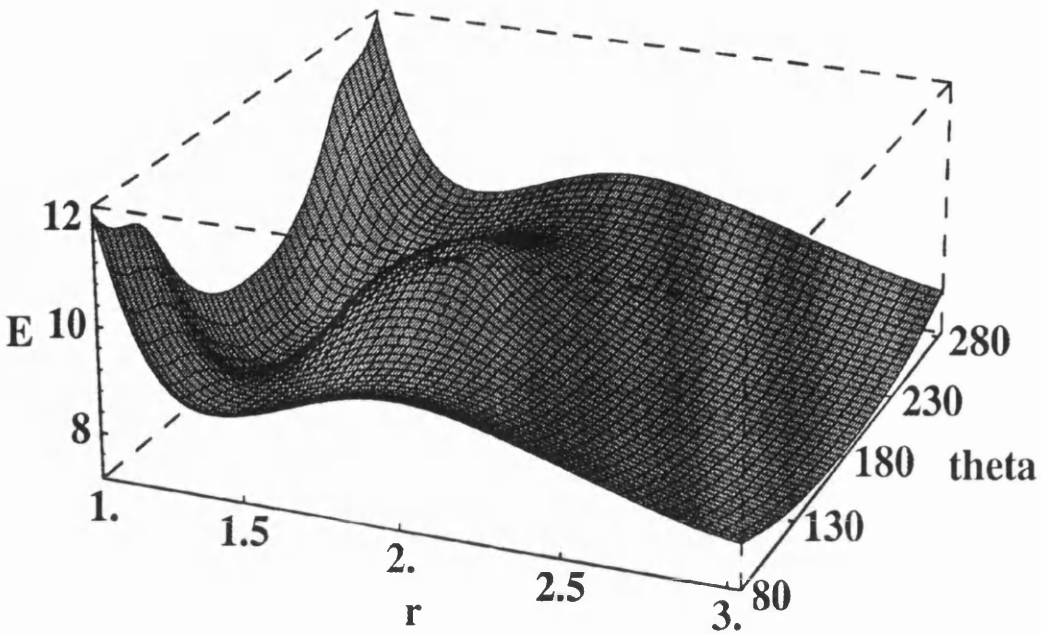

Fig. 4.2 *Potential energy surface for the ground singlet state of O_3^{2+}. Energies are in electron volts, r is in Å and is the distance of the oxygen atom that dissociates to the O^+ unit (atom 3 in Figure 4.1) from the central oxygen atom and θ the angle made between this bond and the O_2 unit (atoms 1 and 2 in Figure 4.1).*

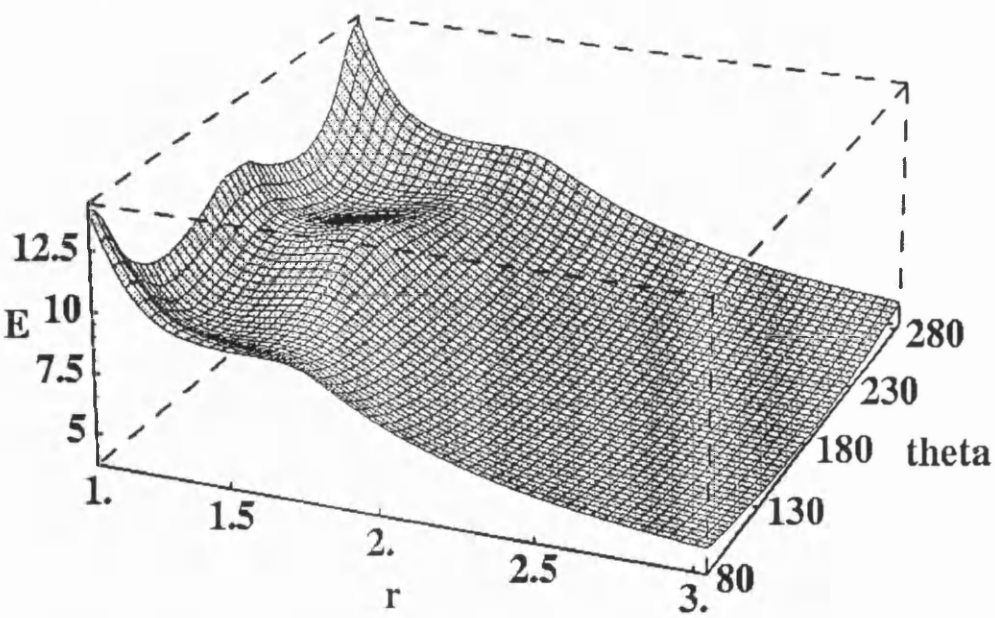

Fig. 4.3 *Potential energy surface for the ground triplet state of O_3^{2+}, E, r and θ are as described for the singlet surface.*

To allow a clearer picture of the region where the two calculated surfaces intersect they are overlaid and plotted together in Figure 4.4. Also, to ensure that the two surfaces are correctly plotted relative to each other the spectroscopically

determined separation of 3.33 eV between their asymptotes at dissociation was enforced. This was done by calculating the energy of the singlet and triplet surfaces at very large r (60 Å), where the molecule is essentially fully dissociated to O^+ and O_2^+. At this geometry the singlet surface was set to lie 3.33 eV above the triplet surface so ensuring a correct representation of the surfaces with respect to the spectroscopic measurements. This scaling involved only adding a minor offset ($\approx$ 0.1 eV) to the calculated singlet states.

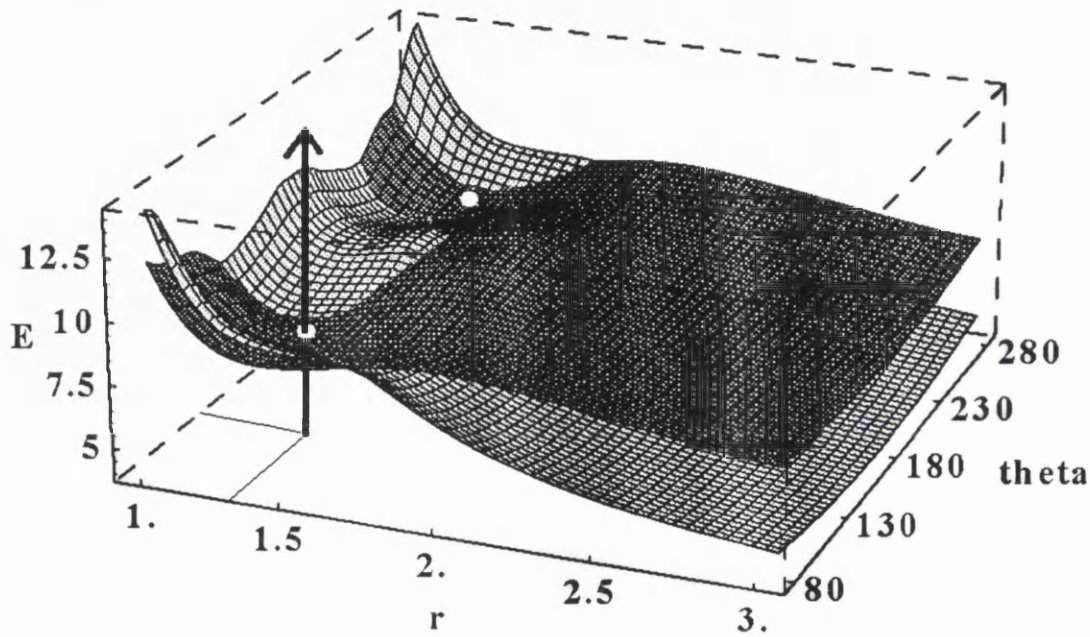

Fig. 4.4 *The singlet surface (dark grey) and the triplet surface (light grey) plotted relative to each other with the Franck Condon zone (r=1.27 Å, θ=116.7°) marked by an arrow.*

To estimate an approximate lifetime of O_3^{2+} on the singlet and triplet electronic surfaces vibrational level and lifetime calculations were performed with the computer program LEVEL [20] described in Chapter 2. In these calculations the lifetime for vibrational levels of O_3^{2+} vibrating in the dissociation co-ordinate [O_2^+ – O^+] at the equilibrium value of θ are determined. It is important to realise that the purpose of these calculations is only to provide a guide as to whether the O_3^{2+} ion is likely to be stable on a mass spectrometric time-scale, in a quasibound electronic

state, not to produce an actual model of the vibrational frequencies in the dication states.

4.4 Discussion

4.4.1 Key experimental data

As these calculations on the ozone dication were prompted by previous experimental studies of O_3 [4], the relevant conclusions from these studies will now be set out. As this is a theoretical study, the details of the acquisition of the experimental data will not be repeated but can be found elsewhere.[4] In the experiments, electron double ionisation of ozone was investigated using ion-ion coincidence spectroscopy coupled with time-of-flight mass spectrometry. O_2^+ and O^+ fragment ion pairs were detected but no stable dications were observed, indicating that any O_3^{2+} ions formed are not stable on a mass spectrometric time scale. Hence, experiment indicates that the majority of the Franck Condon zone for the population of the ground state of O_3^{2+} from O_3 lies in an unbound region of the dication's potential energy surface. From this work the experimentally determined double ionisation potential for ozone is 34 ± 2 eV and the kinetic energy release for its dissociation to $O_2^+ + O^+$ has a mean value of 7.5 ± 0.3 eV and a half-width of 4.6 eV.

4.4.2 Dissociation of O_3^{2+}

Examination of Figures 4.2 and 4.3 reveals that both of the potential energy surfaces possess minima that could support vibrational levels. The singlet surface has the largest barrier to dissociation at 2.3 eV, this is for a linear geometry with a value of r of 1.2 Å. The triplet surface has a shallow minimum for a bent configuration at an angle of 120°, the potential barrier here is 0.14 eV and the minimum is at a value of r of 1.3 Å. For the singlet surface the crude lifetime

calculations found 7 vibrational states with lifetimes $> 10^{-6}$ s at a geometry approximately that of neutral ozone (116°) and 15 at a linear geometry where the global minimum exists. However, on the triplet surface the lifetime calculations determined that the barrier to dissociation is too small, no more than three vibrational levels are supported and none have sufficient lifetimes (i.e. greater than a microsecond) to allow any triplet O_3^{2+} to be observed in simple mass spectrometry experiments. These lifetime calculation results are summarised in Table 4.3.

Table 4.3 *Number of vibrational energy levels and their associated tunneling lifetimes for O_3^{2+} ground singlet and ground triplet states at a linear geometry and at an angle of 120° corresponding to the equilibrium geometry of neutral ozone. Also shown is the potential energy barrier to dissociation at these geometries.*

		No. vibrational levels	Barrier / eV	Lifetimes		
Singlet	120°	10	0.75	$v = 0 - 6$: $> 10^{-6}$s	$v = 7$: 10^{-6}s	$v = 8$: 10^{-9}s
				$v = 9$: 10^{-12}s		
	linear	21	2.3	$v = 0 - 6$: $> 10^{-6}$s	$v = 15 - 16$: $> 10^{-8}$s	$v = 17$: 10^{-10}s
				$v = 18$: 10^{-11}s	$v = 19$: 10^{-12}s	$v = 20$: 10^{-14}s
Triplet	120°	2	0.14	$v = 0$: 10^{-9}s	$v = 1$: 10^{-12}s	
	linear	3	0.41	$v = 0$: 10^{-7}s	$v = 1$: 10^{-9}s	$v = 2$: 10^{-11}s

But if the singlet surface is predicted to be bound why is no long-lived O_3^{2+} observed experimentally? There is no experimental evidence that electron ionisation should disfavour the formation of O_3^{2+} in its singlet state, so it is proposed that the singlet O_3^{2+} ions must be being removed via a crossing to the triplet surface and subsequent dissociation. In fact, examination of Figure 4.4 reveals that around the geometry at which O_3^{2+} would be formed, via double ionisation of neutral O_3, the singlet and triplet surfaces lie very close in energy. Figure 4.5 shows detail from Figure 4.4 showing that the separation of the singlet

and triplet states at an angle of 116 ° (the equilibrium geometry of neutral O_3) is only a few tenths of an eV. Crossing between the singlet and triplet states would normally be a forbidden transition but spin orbit coupling between the two states is likely to be strong enough to allow such a transition. Indeed, in some dication systems it has been established that spin orbit coupling between bound and unbound states provides a mechanism for rapid dissociation, and that the spin-orbit lifetimes are much shorter than tunnelling lifetimes. This dissociation mechanism is the predominant mechanism for decay of quasibound dication states crossed by unbound states of differing multiplicities and has been studied in HCl^{2+} and HS^{2+} [21,22].

Applying this mechanism to the double ionisation of ozone then any dications formed must either be in the triplet state, in which case they dissociate rapidly, or in the singlet state and cross rapidly to the triplet state before having time to stabilise on the singlet surface. Therefore, a possible route to forming stable O_3^{2+} would be to populate the singlet surface closer to the global minimum which is at a linear geometry and away from the crossing to the triplet surface. This might be achieved by forming the dication at a geometry closer to linear, i.e. via ionisation of the monocation which has a C_{2v} equilibrium geometry with $\theta = 130°$ and $r = 1.26$ Å.

4.4.3 Kinetic energy release and double ionisation potential calculations

The experimental study of the ozone dication determined values for the kinetic energy release and double ionisation potential and so a series of *ab initio* calculations were performed to compare with these experimental quantities. First, an optimised geometry of the ozone neutral was determined. Then the energy of the dication was calculated at this geometry and the energy difference between it and the neutral was taken as a measure of the vertical double ionisation potential. The energies of the dissociation products O^+ and O_2^+, with O_2^+ at its equilibrium

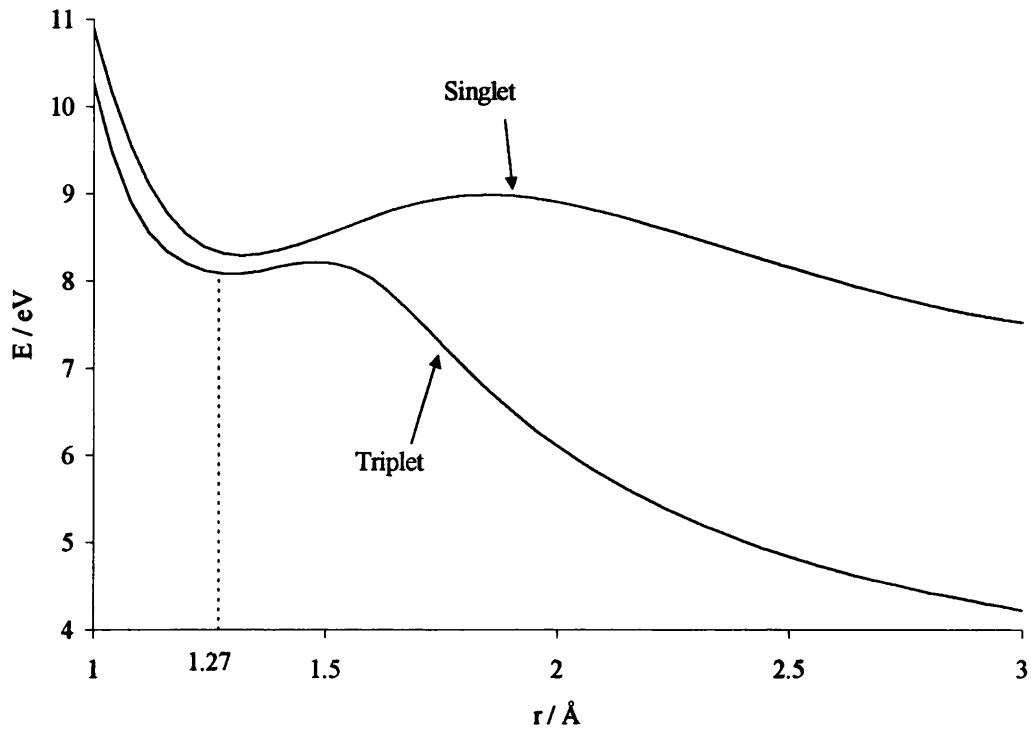

Fig. 4.5 *Detail from Figure 4.4 showing the separation of the singlet and triplet states of O_3^{2+} at an angle of 116° (see Figure 4.1). A bond length r of 1.27 Å is the equilibrium geometry of neutral ozone.*

geometry, were also calculated. The energy difference between the ground state of O_3^{2+} and the $O^+ + O_2^+$ asymptote may be compared with the kinetic energy release observed by experiment.

The experimentally determined values of the kinetic energy release and double ionisation potential are 34 ± 2 eV and 7.5 ± 0.3 eV respectively. Previous theoretical studies of O_3^{2+} determined the vertical double ionisation potential to be around 35-36 eV [6,7]. From Table 4.4 it can be seen that the *ab initio* calculations performed here agree well with experiment determining the double ionisation potential to lie between 34.69 eV and 35.03 eV, depending on the size of basis set used.

For the kinetic energy release the calculated values are between 9.63 eV and 9.79 eV overestimating the experimental value by approximately 2 eV. This discrepancy implies that the fragmentation products O^+ and O_2^+ are not being

Table 4.4 *Calculated and experimental values[4] of (a) the double ionisation potential and (b) the kinetic energy release of O_3^{2+}. Values are shown for three basis sets and are in units of electron volts.*

		6-31G(2*d*)	6-311G(2*d,f*)	VTZ	Expt.
(a)	$O_3 \rightarrow O_3^{2+}$	34.69	35.03	34.9	34 ± 2
(b)	$O_3^{2+} \rightarrow O_2^+ + O^+$	9.79	9.69	9.63	7.5 ± 0.3

formed in their ground electronic or vibrational states as the extra 2 eV could be stored as internal energy of O^+ and O_2^+. For O^+ the first excited electronic state lies 3.4 eV above its ground state and for O_2^+ the first electronic state is 4.1 eV above its ground state [18,19], so a larger discrepancy would be expected between the experimental and calculated kinetic energy release if the dissociation products were being formed in excited electronic states. However, the fragmentation of O_3^{2+} from the Franck Condon zone into O^+ and O_2^+ forms O_2^+ at a bond length significantly longer than its equilibrium geometry allowing the possibility of vibrational excitation. Using the Morse potential as given in Equation 4.5 it is possible to determine the potential vibrational excitation in O_2^+ when formed away from its equilibrium geometry.

$$V = D_e\left\{1 - e^{-\alpha(R-R_e)}\right\}^2 \qquad 4.5$$

$$\alpha = \left(\frac{\mu}{2D_e}\right)^{1/2}\omega, \omega = \omega_e 2\pi c$$

Published spectroscopic constants for O_2^+ [23] give $De = 6.663$ eV, $\omega_e = 1904.7$ cm^{-1}, $R_e = 1.1164$ Å and the reduced mass $\mu = 1.3284 \times 10^{-26}$ kg. The equilibrium bond length of O_3 is 1.2717 Å and using all of these values in the Morse potential gives a value of V of 0.843 eV. Also, as a check on the Morse

potential calculations, MRCI calculations on O_2^+ using a VTZ basis set at the optimised bond length of 1.12 Å and at 1.217 Å give an energy difference of 0.78 eV. Hence it is possible that O_2^+ is being formed with considerable vibrational excitation which could account for the discrepancy between the calculated values and the experimental values. Indeed, the large width of the kinetic energy release distribution observed experimentally may result from the large variation in the vibrational energy content of the O_2^+ product with the small variations in the O—O bond length in the neutral O_3 molecule at the instant of ionisation. This rapid variation comes about as the O—O bond length in O_3 is well away from the equilibrium bond length in O_2^+, hence small changes in r(O—O) of O_3 result in large changes in the vibrational excitation of O_2^+. This is shown schematically in Figure 4.6 where the curve centered about r_1 is equivalent to O_2^+ and the other curve O_3, so here small changes in r about the equilibrium geometry of O_3 require little energy but the equivalent change in r for O_2^+ which is not at its equilibrium geometry translates to significant vibrational excitation.

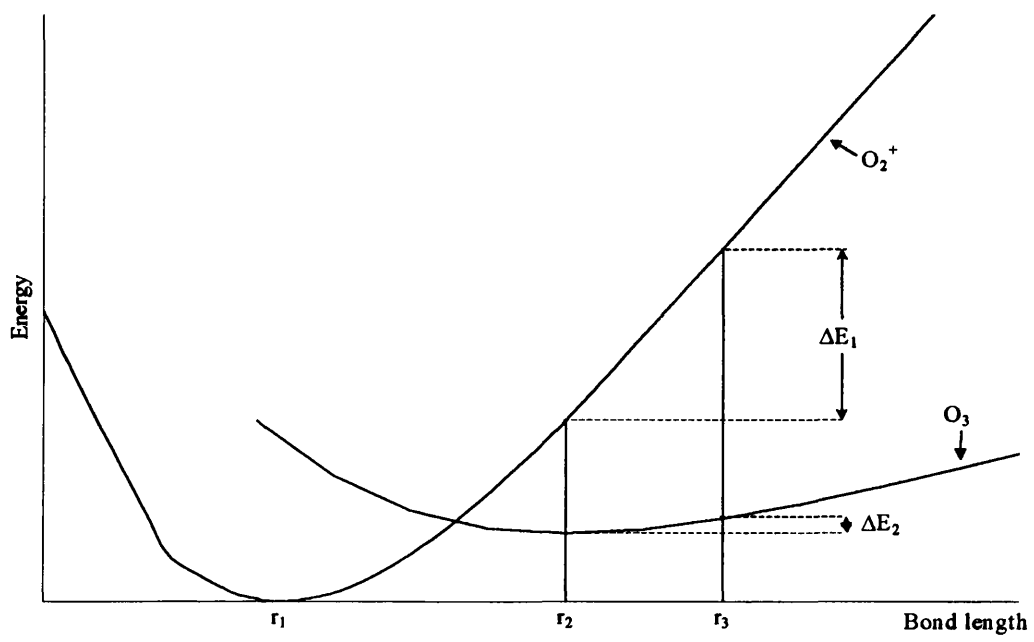

Fig. 4.6 *Schematic diagram of two potential energy curves, one with a minimum at r_1 (representing O_2^+, see text) and the other at r_2 (representing O_3, see text). Lines marked on the diagram show that a displacement from r_2 to r_3 results in a greater change in energy for the curve centered about r_1, ΔE_1, than the curve centered about r_2,, ΔE_2.*

4.5 Conclusion

Ab initio calculations on the ground singlet and triplet electronic states of the ozone dication, O_3^{2+}, have demonstrated a possible mechanism to explain the instability of the dication upon formation by double ionisation of neutral ozone. The dication's ground singlet state is determined to have a large barrier to dissociation able to support several long lived vibrational states but it is crossed by the lowest triplet potential energy surface which is only very weakly bound supporting no long-lived vibrational states. The intersection of the two surfaces occurs at a geometry close to the geometry of neutral ozone and, as this is the geometry at which the dication would be formed in experiment, dissociation via a crossing to the triplet state seems the most likely fate of any O_3^{2+} formed.

The calculations suggest that long-lived dications could be created if they are formed at geometries where the triplet surface lies further in energy from the singlet surface and so would be less strongly coupled to it, making a crossing between the two surfaces unlikely. Such stability is most strongly favoured at linear geometries where the singlet surface has its global minimum.

References

(1) Horvath M., Bilitzky L. and Huttner J. *Topics in inorganic chemistry*; Elsevier: Amsterdam, 1995; 20.

(2) Steinfeld J. I., Adler-Golden S. M. and Gallagher J. W. *J. Phys. Chem. Ref. Data* **16** (1987) 911.

(3) Newson K. A., Luc S., Mason N. J. and Price S. D. *Int. J. Mass Spectrom. Ion Proc.* **148** (1995) 203.

(4) Newson K. A. and Price S. D. *Int. J. Mass Spectrom. Ion Proc.* **153** (1996) 151.

(5) Chablo A. and Cruickshank D. W. J. *J. Mol. Struct.* **70** (1981) 95.

(6) Pyykkö P. *Chem. Phys. Lett.* **156** (1989) 337.

(7) Pyykkö P. and Zhao Y. *J. Phys. Chem.* **95** (1990) 7753.

(8) Docken K. K. and Hinze J. *J. Chem. Phys.* **57** (1972) 4928.

(9) Yamaguchi Y. and Schaefer H. F. *Chem. Phys.* **225** (1997) 23.

(10) Suzuki Y., Noro T., Sasaki F. and Tatewaki H. *Theo. Chem. Journal of Mol. Structure* **462** (1999) 351.

(11) Fujii T. S. and Iwata S. *Chem. Phys. Letters* **251** (1996) 150.

(12) Bauschlicher C. W. and Langhoff S. R. *J. Chem. Phys.* **89 (7)** (1988) 4246.

(13) Knowles P. J. and Werner H.-J. *Chem. Phys. Lett.* **115** (1985) 259.

(14) Werner H.-J. and Knowles P. J. *J. Chem. Phys.* **82** (1985) 5053.

(15) MOLPRO is a package of *ab initio* programs written by H.-J. Werner and P. J. Knowles with contributions from J. Almöf, R. D. Amos, A. Berning, M. J. O. Deegan, F. Eckert, S. T. Elbert, C. Hampel, R. Lindh, W. Meyer, A. Nicklass, K. Peterson, R. Pitzer, A. J. Stone, P. R. Taylor, M. E. Mura, P. Pulay, M. Schuetz, H. Stoll, T. Thorsteinsson, and D. L. Cooper

(16) Tsuneda T., Nakano H. and Hirao K. *J. Chem. Phys.* **103** (1995) 6520.

(17) Katani M. *Proc. Phys. Math Soc. Japan* **19** (1937) 460.

(18) Eland J. H. D. *Photoelectron Spectroscopy*; Second ed.; Butterworth and Co.:, 1984.

(19) Moore C. E. *Atomic energy levels*; US Govt. printing office Circular NBS 467:, 1949.

(20) Leroy R. J. *LEVEL 6.1 University of Waterloo Chemical Physics Research Report No. CP-555R* University of Waterloo, Ontario, Canada, 1996.

(21) Bennett F. R. and McNab I. R. *Chem. Phys. Lett.* **251** (1996) 405.

(22) Parlant G., Senekowitsch J., ONeil S. V. and Yarkony D. R. *J. Chem. Phys.* **94** (1991) 7208.

(23) Herzberg G. and Huber K. P. *Constants of Diatomic molecules*; Von Nostrand Reinhold Company:, 1979.

Chapter 5

An *ab initio* study of the structure and stability of low lying electronic states of the dication BCl^{2+}

5.1 Introduction

Computational analysis of molecular dications that have not yet been studied experimentally often provides important information on the likely stability of the ion and potential routes for successful synthesis. For BCl^{2+} synthesis via electron impact ionisation of BCl_3 is likely to be a successful synthetic route but to aid experimental studies it was decided to undertake a computational study of BCl^{2+} in order to provide information on the likely stability and electronic state energies to guide future experimental work.

The existence of long lived metastable states of doubly charged molecules is a common feature among many polyatomic and diatomic molecules. The double charge on polyatomics is readily shared amongst all the atoms so that the overall repulsion between individual positive charges is small. For a doubly charged diatomic however, the high charge per atom might be expected to break the molecule apart. Nevertheless, as indicated in Chapter 1 the existence of doubly charged diatomics indicates that sometimes the chemical binding wins out over the large electrostatic repulsions.

Potentially the dication BCl^{2+} could possess several long lived electronic states, as XY^{2+} species containing at least one atom from group 2 or 13 are relatively stable due to the standard oxidation states +2 or +3 of these atoms. For example BeF^{2+}, MgF^{2+}, MgN^{2+} and $MgNe^{2+}$ are predicted to have bound states [1,2]. So for BCl^{2+} metastable states should be favoured through the formation of the attractive structures $B^{2+}Cl$ and $B^{3+}Cl^{-}$. Also the isoelectronic molecule C_2 has several strongly

bound electronic states [3] which often provides a good guide to dicationic bonding being able to overcome the coulomb repulsion of the charges.

In this chapter 35 potential energy curves of BCl^{2+} have been calculated by state average CASSCF calculations. Of the 35 states, 10 were found to be quasibound with the $^1\Sigma^+$ ground state possessing the largest barrier to dissociation at 2.57 eV and an equilibrium bond length of 1.541 Å. For the quasibound states subsequent MRCI calculations were performed and vibrational energy levels and tunnelling lifetimes calculated. Analysis of the electronic states and molecular orbitals provides information on important electronic configurations and their charge distributions. This allows discussion of possible origins of the stability of the dicationic states.

5.2 Technical Details

The correlation consistent triple zeta (VTZ) basis set of Dunning *et al* [4], which incorporates diffuse *d* and *f* functions has been used to describe each atom in the *ab initio* calculations. The potential curves for elongation of the B-Cl bond were created using calculations performed at 0.2 Å intervals from 1.2 Å to 6.0 Å. Extra calculations were also performed at 10 Å, 15 Å and 50 Å to obtain information on the energy separations of the dissociation asymptotes and for the subsequent vibrational energy level calculations. The calculated points were then fitted to a spline curve creating points with a 0.05 Å separation. The computer program MOLPRO running on a Silicon Graphics Power Challenge was used in all the *ab initio* calculations. For the vibrational energy level and lifetime calculations the program LEVEL was used, see Chapter 2 for more information on these programs.

The state averaging SA-CAS technique as described in Chapter 4 was used in all the *ab initio* calculations to correctly model the molecular orbitals throughout the potential curves. In all the *ab initio* calculations the first four σ moecular orbtals

were kept doubly occupied and all the configurations created came from the distribution of the remaining 12 electrons amongst the next 10 molecular orbitals. For the quasibound states the subsequent MRCI calculations were performed by carrying out a singles and doubles CI calculation out of each reference created by the previous SA-CASSCF calculation.

Table 5.1 *Calculated and experimental values for the energy separation (in eV) of the first few electronic states of the ions B^+ and Cl^+. Experimental values are taken from spectroscopic data [5] and calculated values from the potential curves at very long bond length (50 Å) representing the molecule at dissociation.*

		Experimental	Calculated
B^+	$^1S_g\ (s^2p^2)$	0	0
	$^3P_u\ (s^2p^2)$	4.63	4.66
Cl^+	$^3P_g\ (3s^23p^4)$	0	0
	$^1D_g\ (3s^23p^4)$	1.44	1.50
	$^1S_g\ (3s^23p^4)$	3.46	3.45

5.3 Atomic energies, dissociation channels and correlating molecular states

Experimental and calculated values of the energy separations of the electronic states of B^+ and Cl^+ are given in Table 5.1. The calculated values are taken from the potential curve calculations at 50 Å simulating a dissociated molecule. Although these are not calculations on the individual atoms the agreement with experimental values is very good, within 0.01 eV for Cl^+ ^1S_g, showing that these calculations are a good representation of the molecule at dissociation. Table 5.2 shows the first six dissociation asymptotes of BCl^{2+} and the correlating molecular states. Asymptotes I to III are for the ground state of B^+ (^1S_g) with the first 3 states of Cl^+ (^3P_g, ^1D_g, ^1S_g), and asymptotes IV to VI for the first excited state of B^+ (^3P_u) with the first three states of Cl^+. The majority of states of BCl^{2+}, (18 out

of 35), decay to asymptote IV due to it correlating with singlet, triplet, and quintet states.

Table 5.2 *Relative energies (in eV) for the first six dissociation asymptotes of BCl^{2+}. Also shown are the electronic states of the product ions B^+ and Cl^+ and the correlating molecular states.*

Asymptote	Products		Calculated	Experimental	Correlating
	B^+	Cl^+			molecular states
I	^1S_g	^3P_g	0	0	$1^3\Sigma^-$; $1^3\Pi$
II	^1S_g	^1D_g	1.50	1.44	$X^1\Sigma^+$; $1^1\Pi$;$1^1\Delta$
III	^1S_g	^1S_g	3.45	3.46	$1^1\Sigma^+$
IV	^3P_u	^3P_g	4.66	4.63	$2^1\Sigma^+$; $1,2^1\Sigma^-$; $2,3^1\Pi$, $2^1\Delta$;
					$1^3\Sigma^+$; $2,3^3\Sigma^-$; $2,3^3\Pi$; $1^3\Delta$
					$1^5\Sigma^+$; $1,2^5\Sigma^-$; $1,2^5\Pi$; $1^5\Delta$
V	^3P_u	^1D_g	6.18	6.07	$2,3^3\Sigma^+$; $4^3\Sigma^-$; $4,5,6^3\Pi$;
					$2,3^3\Delta$; $1^3\Phi$
VI	^3P_u	^1S_g	8.09	8.09	$4^3\Sigma^+$; $7^3\Pi$

5.3.1 Determination of correlating states

The method used to determine the molecular electronic states of BCl^{2+} that correlate with each dissociation asymptote is similar to that used in chapter 4 on the ozone dication. By combining the spin and angular momentum of the dissociated species the resulting molecular electronic states are determined by vector addition of these individual L and S values.

The possible molecular Λ values are obtained by algebraic addition of the M_{Li} values of the individual atoms as in Eqn. 5.1.

$$\Lambda = \left| \sum M_{Li} \right| \qquad 5.1$$

where for each atom M_{Li} takes the values L_i, L_i-1 … -L_i. The combined molecule BCl^{2+} is of $C_{\infty v}$ symmetry so states with $\Lambda = 0$ can be either Σ^+ or Σ^-. If at least

two M_{Li} values are not zero then the Σ states occur in pairs of Σ^+ and Σ^-. When all $M_{Li} = 0$ then the one Σ state that arises that is not part of a pair is either Σ^+ or Σ^- depending of whether the sum of Eqn. 5.2 is even or odd respectively.

$$L_1 + L_2 + L_3 + \ldots + \sum l_{i1} + \sum l_{i2} + \sum l_{i3} + \ldots \qquad 5.2$$

The sum $\sum l_i$ are extended over all the electrons in each atom so even or odd $\sum l_i$ corresponds to even or odd parity (g or u).

The possible total spin values, S, that the completed molecule can take are determined by the same method used for ozone, using vector addition of the individual spin values, as shown in Eqn. 4.1.

Applying this to BCl^{2+} it is possible to determine the symmetry and number of states correlating with each dissociation asymptote. For the first asymptote, ground state B^+ ^1S_g has $L_1 = 0$, $S_1 = 0$, $\sum l_i = g$ (even) and ground state Cl^+, ^3P_g, has $L_1 = 1$, $S_1 = 1$, $\sum l_i = g$ (even). For the Λ values $M_{L1} = 0$, and $M_{L2} = 1, 0, -1$ giving $\Lambda = 1, 0$ so one Σ and one Π state result. Applying equation 5.2 to the Σ state gives $(1 + 0 + g + g)$, overall odd, so a Σ^- state. Combining the multiplicities as described in equation 4.1 gives $S = |1+0| = 1$, so triplet states. Bringing this all together gives the result that one $^3\Sigma^-$ state and one $^3\Pi$ state correlate with the first dissociation asymptote. Table 5.3 summarises the determination of the correlating states for all the dissociation asymptotes.

5.4 Molecular orbital composition and charge distribution

The $^1\Sigma^+$ ground state of BCl^{2+} is the most strongly bound of all the electronic states calculated with a barrier to dissociation of 2.57 eV, this is discussed in more detail in the next section. At 1.6 Å the molecular orbital configuration in this state is $5\sigma^2 6\sigma^2 2\pi^4$, the dominant configuration changing to $5\sigma^2 6\sigma^2 2\pi^2 7\sigma^2$ from 2.60 Å

onwards (which is just beyond the barrier maximum). Plots of the valence molecular orbitals, 5σ 6σ 2π and 7σ are given in Figure 5.1.

Table 5.3 *Summary of the determination of the molecular states of BCl^{2+} that correlate with the first six dissociation asymptotes, see text for details.*

B^+				Cl^+				BCl^{2+}		
	L_1	S_1	Σl_i		L_2	S_2	Σl_2	Λ	S	Result[a]
^1S_g	0	0	*even*	^3P_g	1	1	*even*	0, 1	1	$^3\Sigma^-$, $^3\Pi$
^1S_g	0	0	*even*	^1D_g	2	0	*even*	0, 1, 2	0	$^1\Sigma^+$, $^1\Pi$, $^1\Delta$
^1S_g	0	0	*even*	^1S_g	0	0	*even*	0	0	$^1\Sigma^+$
^3P_u	1	1	*odd*	^3P_g	1	1	*even*	0(3), 1(2), 2	2, 1, 0	$^{5,3,1}\Sigma^+$, $^{5,3,1}\Sigma^-(2)$, $^{5,3,1}\Pi(2)$, $^{5,3,1}\Delta$
^3P_u	1	1	*odd*	^1D_g	2	0	*even*	0(3), 1(3), 2(2), 3	1	$^3\Sigma^+(2)$, $^3\Sigma^-$, $^3\Pi(3)$, $^3\Delta(2)$, $^3\Phi$
^3P_u	1	1	*odd*	^1S_g	0	0	*even*	0, 1	1	$^3\Sigma^+$, $^3\Pi$

[a]*Number in parenthesis indicates the number of states when greater than one.*

By analysis of the atomic orbital contribution to each of the molecular orbitals it was possible to approximately determine on which atom the majority of the electron density lies for each molecular orbital. Table 5.4 shows such an analysis of the first 11 molecular orbitals of BCl^{2+} at the ground state equilibrium geometry of 1.6 Å. Molecular orbitals 5σ, 6σ and 2π are located primarily on chlorine and 7σ on boron. A similar analysis of the BCl^{2+} molecular orbitals at a bond length of 6.0 Å is shown in Table 5.5 showing that 5σ switches to being localised on boron at long bond lengths. Under a simplifying assumption that at 1.6 Å the 5σ, 6σ and 2π electron density is located primarily on chlorine and 7σ on boron then the $^1\Sigma^+$

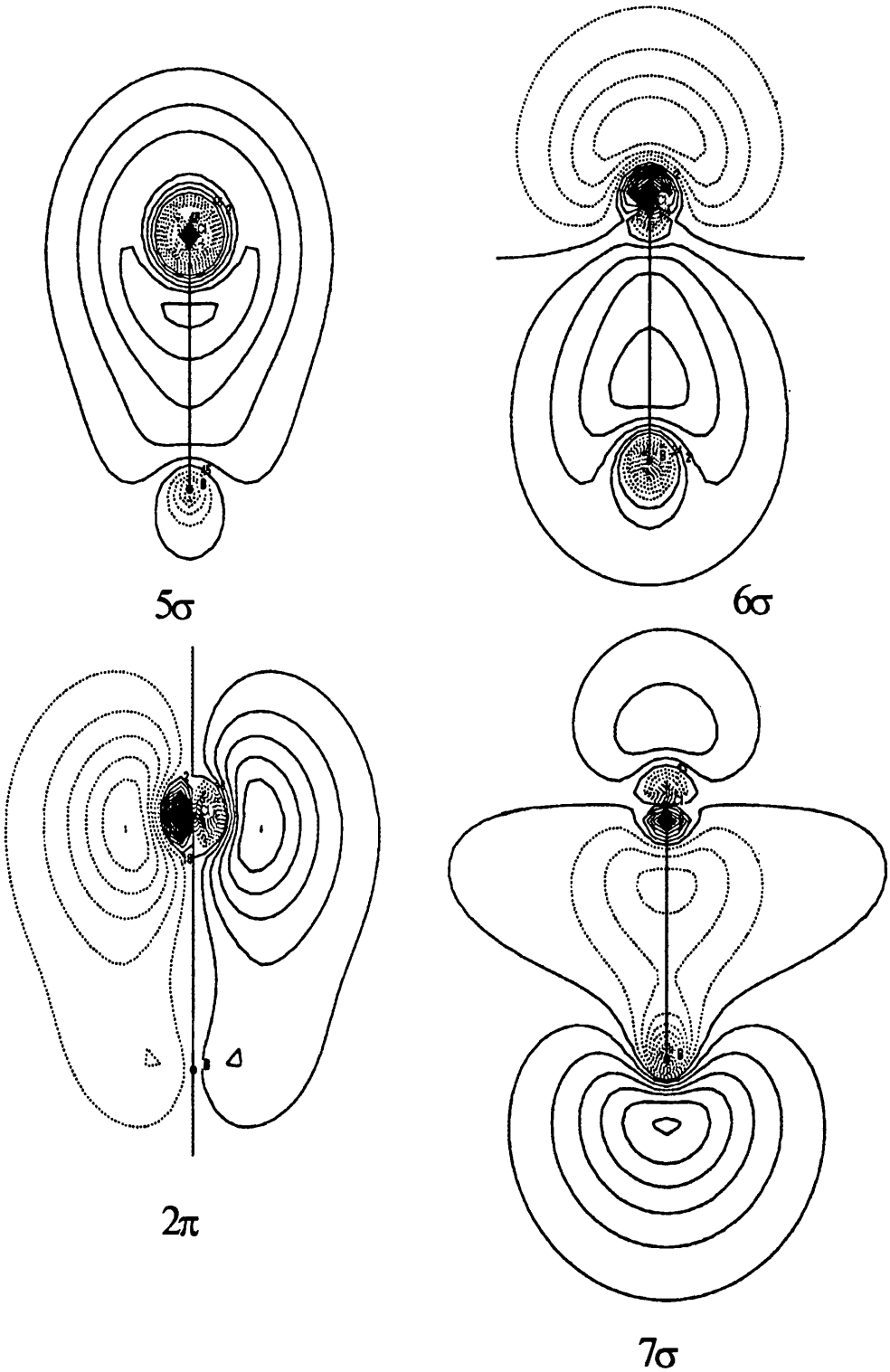

Fig 5.1 *Plot of the molecular orbitals 5σ, 6σ, 2π and 7σ of BCl^{2+} at 1.6 Å, the chlorine atom lies above the boron in each of the plots.*

state has 6 valence electrons on chlorine and none on boron, corresponding to the ionic structure $B^{3+}Cl^{-}$.

Table 5.4 *Energy and atomic orbital contribution of the first 11 molecular orbitals of BCl^{2+} at a bond length of 1.6 Å. The atom upon which the majority of the electron density lies is also shown.*

Energy / h	Molecular orbital	Atomic orbital contribution	Electron density location
-105.7	1σ	Cl s	Cl
-11.4	2σ	Cl s	Cl
-8.85	3σ	Cl p_z	Cl
-8.85	1π	Cl $p_x p_y$	Cl
-8.38	4σ	B s	B
-1.85	5σ	Cl $s p_z$	Cl
-1.29	6σ	Cl $s p_z$	Cl
-1.09	2π	Cl $p_x p_y$	Cl
-0.735	7σ	B s	B
-0.516	3π	B $p_x p_y$	B
-0.184	8σ	Cl $s p_z$	Cl

In figure 5.2 electron density plots of BCl^{2+} at a series of bond lengths between 1.6 Å and 3.0 Å show the increase of electron density between boron and chlorine as the atoms approach each other. In Table 5.6 the charge in each atom, as calculated from a Mulliken population analysis, at the bond lengths plotted in Fig 5.2 are shown. At 3.0 Å there is an approximately equal +1 charge on boron and chlorine but as the atoms approach each other the charge increases on boron and decreases on chlorine suggesting a transfer of electron density from boron to the more electronegative chlorine. This change in the charge on each atom suggests a charge transfer mechanism to account for bonding in BCl^{2+}.

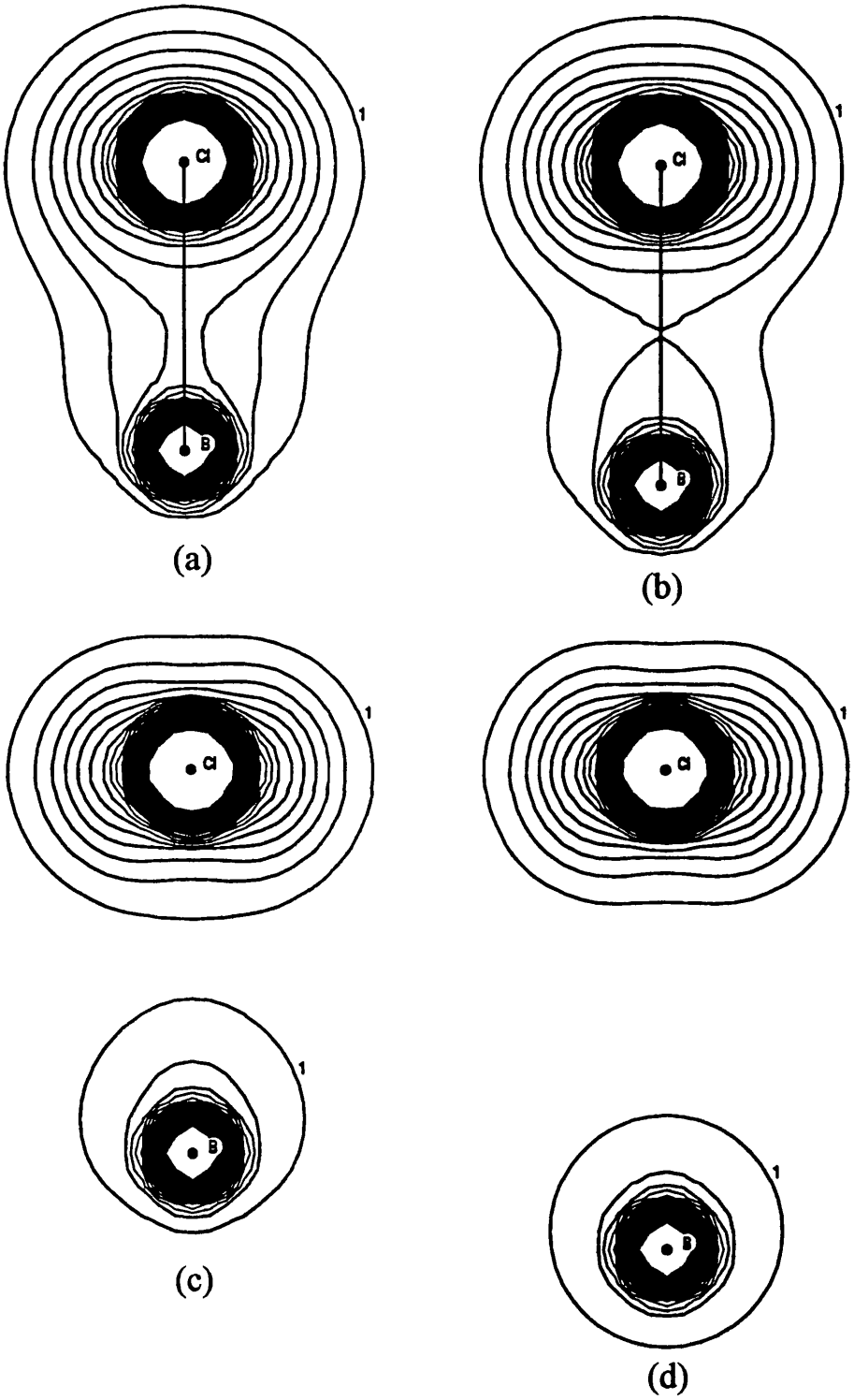

Fig 5.2 *Electron density plots of BCl^{2+} at the bond lengths (a) 1.6 Å, (b) 2.0 Å, (c) 2.4 Å and (d) 3.0 Å.*

Table 5.5 *Energy and atomic orbital contribution of the first 11 molecular orbitals of BCl^{2+} at a bond length of 6.0 Å, the atom upon which the majority of the electron density lies is also shown.*

Energy / h	Molecular orbital	Atomic orbital contribution	Electron density location
-105.4	1σ	Cl s	Cl
-11.16	2σ	Cl s	Cl
-8.63	3σ	Cl p_z	Cl
-8.63	1π	Cl $p_x p_y$	Cl
-8.24	4σ	Cl s	Cl
-1.56	5σ	B s	B
-0.844	6σ	Cl p_z	Cl
-0.843	2π	Cl $p_x p_y$	Cl
-0.822	7σ	B s	B
-0.360	3π	B $p_x p_y$	B
-0.360	8σ	Cl $s p_z$	Cl

Table 5.6 *Charge on the boron and chlorine atoms of BCl^{2+}, at the bond lengths of the plots in figure 5.2, showing the increase of the positive charge on boron as the atoms approach each other and how the electron density is transferred to chlorine.*

Atom	Bond length / Å			
	1.6	2.0	2.4	3.0
boron	+1.216	+1.141	+1.125	+1.040
chlorine	+0.783	+0.858	+0.875	+0.961

5.5 Molecular states of BCl^{2+}

Potential curves have been calculated for all 35 electronic states of BCl^{2+} that dissociate to the first six dissociation asymptotes given in Table 5.2. The output from the SA-CASSCF calculations gives the configurations which have the greatest contribution to each electronic state and also the extent to which the

configuration contributes. Several different electronic configurations are found to contribute to the molecular electronic states. These configurations are listed in Table 5.7 where they are grouped into three sections, *A*, *B* and *C* where using the simplifications described previously all *A* configurations have a charge distribution ($B^{2+}Cl$), *B* configurations ($B^{+}Cl^{+}$) and *C* configurations ($B^{3+}Cl^{-}$).

Table 5.7 *Important configurations of* BCl^{2+}

Label	Configuration[a]	Charge distribution[b]
*A*1	$6\sigma 2\pi^4 7\sigma$	$B^{2+}Cl$
*A*2	$6\sigma^2 2\pi^3 3\pi$	$B^{2+}Cl$
*A*3	$6\sigma^2 2\pi^3 7\sigma$	$B^{2+}Cl$
*A*4	$6\sigma 2\pi^4 3\pi$	$B^{2+}Cl$
*A*5	$6\sigma 2\pi^3 7\sigma 8\sigma$	$B^{2+}Cl$
*B*1	$6\sigma^2 2\pi^2 3\pi^2$	$B^{+}Cl^{+}$
*B*2	$6\sigma^2 2\pi^2 7\sigma 3\pi$	$B^{+}Cl^{+}$
*B*3	$6\sigma 2\pi^3 7\sigma^2$	$B^{+}Cl^{+}$
*B*4	$6\sigma^2 2\pi^2 7\sigma^2$	$B^{+}Cl^{+}$
*B*5	$6\sigma 2\pi^3 3\pi^2$	$B^{+}Cl^{+}$
*B*6	$6\sigma 2\pi^3 7\sigma 3\pi$	$B^{+}Cl^{+}$
*C*1	$6\sigma^2 2\pi^3 8\sigma$	$B^{3+}Cl^{-}$
*C*2	$6\sigma^2 2\pi^4$	$B^{3+}Cl^{-}$

[a] The 1-5 σ and 1π orbitals are doubly occupied throughout.
[b] At a short BCl bond length as described in the text.

The dominant molecular orbital configurations at two bond lengths, 1.6 and 6.0 Å are given for all 35 states in Table 5.8. Of the electronic states calculated, 4 singlet and 6 triplet states were found to be metastable, all quintet states are unbound.

Table 5.8 *Relative energies (in eV) with respect to asymptote I and the dominant configurations, in %, at two BCl bond lengths.*

	R = 1.6Å		R = 6.0Å	
State	ΔE	Configuration[a]	ΔE	Configuration[a]
$X^1\Sigma^+$	4.80	70 C2; 21 A2	3.82	91 B4
$1^3\Pi$	5.66	94 A3	2.13	91 B3
$1^1\Pi$	5.98	96 A3	3.86	58 B3; 41
$1^3\Sigma^+$	8.98	55 A1; 36 A2	6.88	25 B1; 75 B6
$1^3\Delta$	10.13	37 A1; 57 A2	6.88	25 B1; 75 B6
$1^1\Delta$	10.26	81 A1; 15 A2	3.87	33 B4; 64 $2\pi^4 7\sigma^2$
$1^3\Sigma^-$	10.28	94 A2	2.09	91 B4
$2^3\Sigma^+$	10.34	94 A2	8.54	98 $6\sigma^2 2\pi^2 7\sigma 8\sigma$
$2^3\Sigma^-$	10.46	82 A2; 12 B4	6.80	98 $6\sigma^2 2\pi^2 7\sigma 8\sigma$
$1^1\Sigma^-$	10.54	94 A2	6.80	98 $6\sigma^2 2\pi^2 7\sigma 8\sigma$
$1^1\Sigma^+$	10.57	95 A2	5.35	57 B4; 38 $2\pi^4 7\sigma^2$
$1^5\Pi$	12.21	99 B2	6.83	95 A5
$2^3\Pi$	13.07	94 B2	6.83	95 A5
$2^1\Delta$	13.40	81 B4; 10 B1	6.89	99 B6
$3^3\Pi$	13.72	80 A4	6.84	95 B2
$2^1\Pi$	13.91	87 B2	6.84	20 B2; 56 A5
$2^1\Sigma^+$	14.23	11 B1; 80 B4	6.89	99 B6
$4^3\Pi$	14.43	99 B2	8.58	13 B2; 87 A5
$5^3\Pi$	14.60	65 B2; 22 B3	8.58	100 B2
$1^5\Sigma^+$	14.70	7 B1; 93 B6	6.87	93 B6
$6^3\Pi$	15.27	86 B2; 7 B3	8.58	87 B2; 13 A5
$1^5\Delta$	15.32	100 B6	6.68	100 B6
$1^5\Sigma^-$	15.32	96 B6	6.79	98 $6\sigma^2 2\pi^2 7\sigma 8\sigma$
$3^1\Pi$	15.40	92 A4	6.84	66 B2; 19
$1^3\Phi$	15.75	40 B2; 37 B3	8.64	64 B2; 36 $2\pi^4 7\sigma 8\sigma$
$3^3\Sigma^-$	16.48	95 B6	6.88	98 B6
$3^3\Sigma^+$	16.52	94 B6	8.59	36 $2\pi^4 7\sigma 8\sigma$; 65
$7^3\Pi$	16.57	82 B2; 10 C1	10.11	62 B2; 35 $2\pi^4 7\sigma 3\pi$
$4^3\Sigma^-$	16.60	96 B6	8.54	98 $6\sigma^2 2\pi^2 7\sigma 8\sigma$
$2^3\Delta$	16.71	15 B1; 69 B6	8.62	50 B1; 49 B6
$3^3\Delta$	17.54	7 B1; 83 B6;	8.62	49 B1; 48 B6
$2^5\Sigma^-$	17.58	98 $6\sigma^2 2\pi^2 7\sigma 8\sigma$	6.88	98 B6
$4^3\Sigma^+$	17.91	66 B1; 33 B6	10.07	60 $6\sigma^2 2\pi^2 7\sigma 8\sigma$; 30
$2^1\Sigma^-$	18.01	7 B1; 87 B6	6.89	98 B6
$2^5\Pi$	19.25	99 B5	6.83	95 B2

[a] *Configurations are defined in Table 5.6. Relative weights are given in percent.*

Table 5.9 lists equilibrium data for the quasibound states. In this table the energy of the minima before the potential barrier, T_e, is given relative to the asymptote I, the dissociation energy, D_e, is the energy difference between the metastable minima and the dissociation asymptote and D_{eff} is the barrier height; these terms are explained in figure 5.3. As can be seen from the data in Table 5.9 half of the metastable states are relatively well bound with dissociation barriers, D_{eff}, greater

than 0.5 eV. Of the metastable states, six correlate with asymptote IV , two to asymptote II, one to asymptote I and one to asymptote V.

Table 5.9 *Calculated data for the metastable states of BCl^{2+}.*[a]

State	Asymptote	T_e[b]	R_e	D_e	D_{eff}[c]	Configuration[d]
$X^1\Sigma^+$	II	4.00	1.56	-2.56	2.57	70 *C*2; 21 *A*2
$1^3\Pi$	I	4.87	1.83	-4.87	0.33	94 *A*3
$1^1\Pi$	II	5.12	1.83	-3.68	1.06	96 *A*3
$1^3\Sigma^+$	IV	8.27	1.83	-3.61	0.99	55 *A*1; 36 *A*2
$2^3\Pi$	IV	8.41	2.55	-3.75	0.06	94 *B*2
$2^3\Sigma^-$	IV	9.08	1.83	-4.42	0.53	82 *A*2; 12 *B4*
$1^1\Sigma^-$	IV	9.20	1.92	-4.54	0.23	94 *A*2
$2^1\Delta$	IV	9.24	2.10	-4.58	0.22	81 *B*4; 10 *B*1
$2^3\Sigma^+$	V	9.28	1.38	-3.10	0.93	94 *A*2
$1^3\Delta$	IV	9.40	2.01	-4.74	0.49	37 *A*1; 57 *A*2

[a] *R_e is in Å, all other values in eV.*
[b] *With respect to asymptote I of column 2.*
[c] *Effective dissociation barrier.*
[d] *Numbers are the relative contribution in percent.*

The potential energy curves for the calculated electronic states are plotted in figures 5.4 - 5.9 and are grouped together as singlet and triplet Σ^+ (3 and 4 states respectively), singlet and triplet Σ^- (2 and 4 states), singlet Π (3 states), triplet Π (7 states), singlet and triplet Δ (2 and 3 states) and the quintet states (one Σ^+, two Σ^-, two Π, one Δ). As the electronic states are plotted together according to symmetry the $1^3\Phi$ state is not plotted as it is the only state of this symmetry and also it is not a quasibound state; it is listed in Table 5.8. Also, the ground state $X^1\Sigma^+$ is included in each plot as a guide to the relative energies and shapes of the excited state curves.

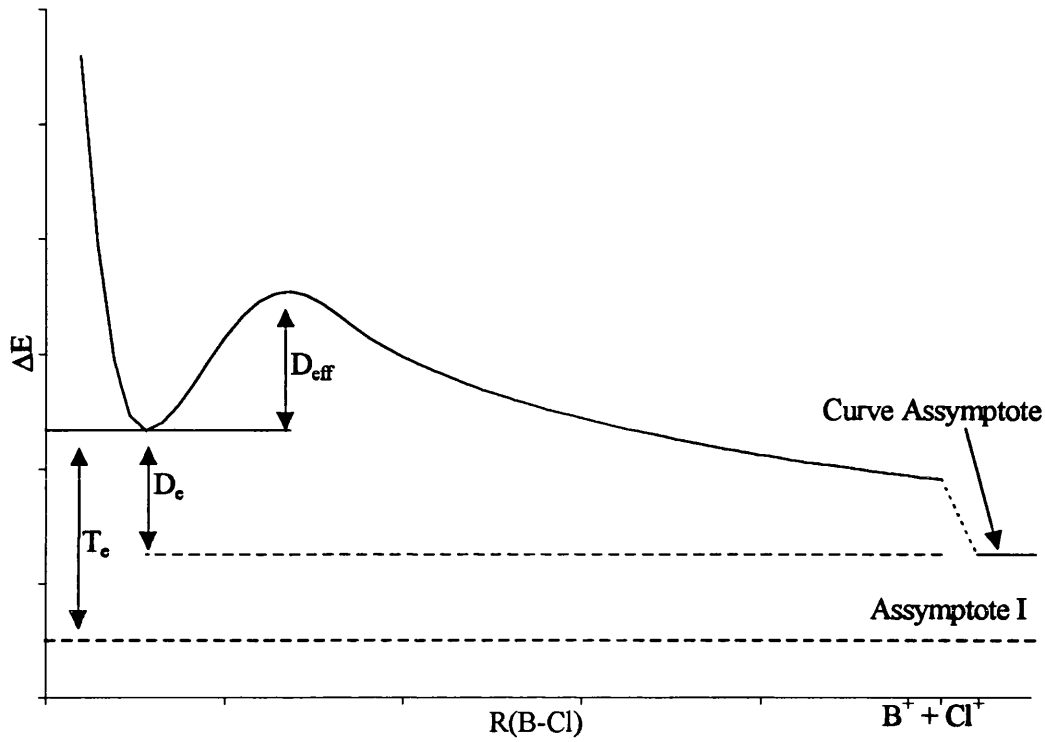

Fig 5.3 *Figure explaining terms used in tale of equilibrium data Table 5.9, note far right hand side of plot represents BCl^{2+} fully dissociated to B^+ and Cl^+.*

5.5.1 $^1\Sigma^+$ and $^3\Sigma^+$ states

The potential curves of $^1\Sigma^+$ and $^3\Sigma^+$ plotted in Figure 5.4 include the BCl^{2+} ground state $X^1\Sigma^+$ which is the most strongly bound of the calculated electronic states. At 2.57 eV the dissociation barrier of $X^1\Sigma^+$ is the largest of all the metastable states and is more than twice that of any other quasibound state. The high stability of $X^1\Sigma^+$ results from the contribution of the attractive *C*2 and *A*2 configurations (see Tables 5.8 and 5.7). For the other $^1\Sigma^+$ states, $1^1\Sigma^+$ is mostly attractive *A*2 and has a shape at small *R* suggesting a small barrier could form but an avoided crossing with $2^1\Sigma^+$ at 2 Å prevents this forming. The $2^1\Sigma^+$ is mostly composed of the repulsive *B*1 and *B*4 configurations and is unbound but with a slightly distorted curve shape due to the avoided crossing mentioned above.

Two of the $^3\Sigma^+$ states are quasibound, ($1^3\Sigma^+$,$2^3\Sigma^+$), and are dominated by the attractive *A* configurations. The two other higher lying $^3\Sigma^+$ states ($3^3\Sigma^+$ and $4^3\Sigma^+$) are unbound and like the unbound $^1\Sigma^+$ states are dominated by the repulsive *B* configurations.

5.5.2 $^1\Sigma^-$ and $^3\Sigma^-$ states

The singlet and triplet Σ^- states are plotted in Fig 5.5. The $1^1\Sigma^-$ and $2^3\Sigma^-$ are quasibound but only very weakly with D_e values of 0.23 and 0.53 eV respectively and are a mixture of mostly attractive *A*2 and some repulsive *B4* configuration. As with the Σ^+ states the unbound Σ^- states ($2^1\Sigma^-$, 3 and $4^3\Sigma^-$) are predominantly *B* configurations and the bound states, although only slightly bound, are predominantly *A* configurations with some *B*.

Table 5.10 *Dominant configurations, in %, at increasing bond lengths for the molecular states 1 $^3\Sigma^-$, $3^3\Pi$ and $3^1\Pi$*

	Configurations		
R / Å	$1^3\Sigma^-$	$3^3\Pi$	$3^1\Pi$
1.6	94 *A*2	80 *A*4	92 *A*4
2.0	86 *B*4; 6 *B*1	64 *B*2; 15 *B*3	47 *B*3; 26 *C*1
2.4	90 *B*4; 4 *B*1	77 *B*2; 7 *C*1	64 *B*2; 12 *C*1
2.8	91 *B*4; 4 *B*1	76 *B*2	65 *B*2

The exception to this is $1^3\Sigma^-$ which is unbound yet is predominantly made up of attractive *A*2 configurations. In Table 5.10 the dominant configurations at bond lengths from 1.6 → 2.8 Å are given for $1^3\Sigma^-$ and it can be seen that the important configurations change from *A* to *B* after 1.6 Å. Therefore this change to repulsive *B* configurations results in the unbound nature of $1^3\Sigma^-$. Note that this approach assumes that the electron density within each of the molecular orbitals remains constant over the bond length change. This is reasonable assumption as this is only

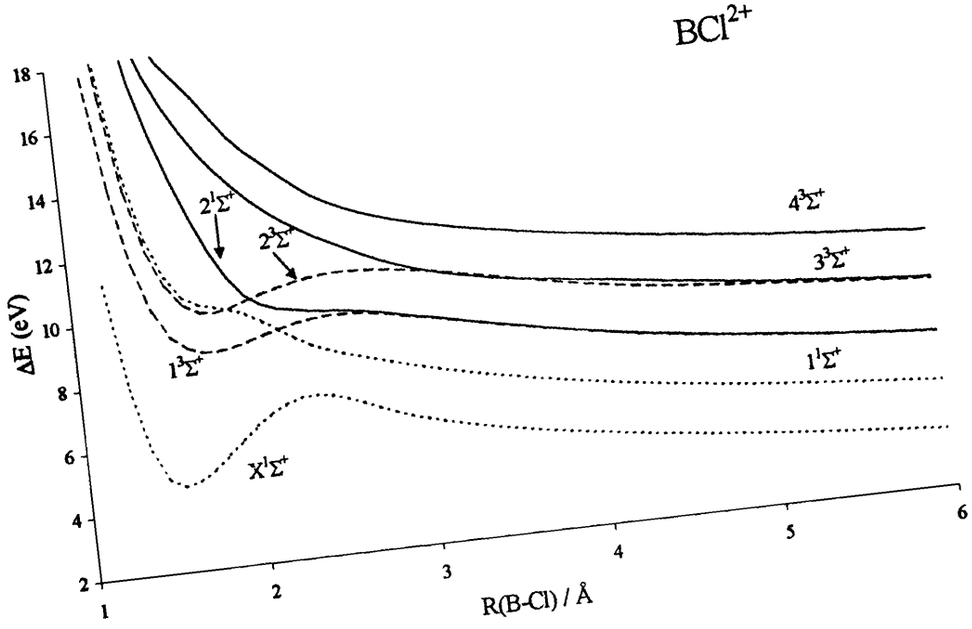

Fig 5.4 *Potential curves for the* $^{1,3}\Sigma^{+}$ *states of* BCl^{2+}

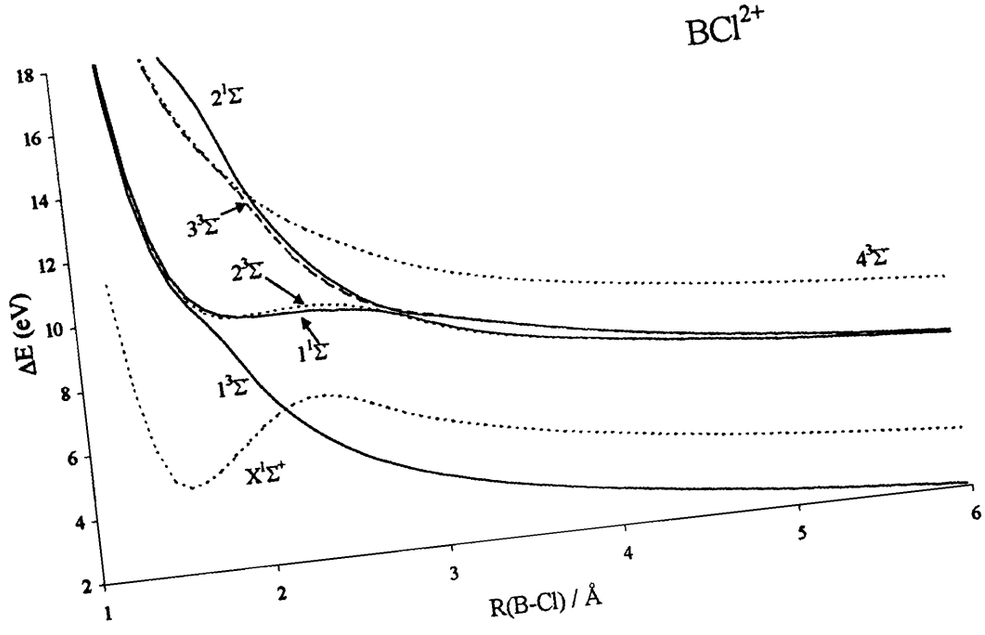

Fig 5.5 *Potential curves for the* $^{1,3}\Sigma^{-}$ *states of* BCl^{2+}

intended as a guide and the change to the repulsive *B* configuration occurs within only 0.4 Å

5.5.3 $^1\Pi$ and $^3\Pi$ states

The singlet and triplet Π states are plotted in Figs. 5.6 and 5.7 respectively. Although there are more Π states than any other symmetry calculated there is only one quasibound $^1\Pi$ state (1 $^1\Pi$) and only two quasibound triplet states (1 and 2 $^3\Pi$). The D_e values of the quasibound $^3\Pi$ states are 0.33 and 0.06 eV for 1 $^3\Pi$ and 2 $^3\Pi$ respectively, the value for 2 $^3\Pi$ is the smallest of all the quasibound states and is so small that the state could effectively be considered unbound.

As with Σ^+ and Σ^-, the quasibound Π states are dominated by attractive *A* configurations and the unbound states (including $2^3\Pi$) are completely repulsive *B* configurations, notably *B*2 for the $^3\Pi$ states. However, a few Π states go against the trends displayed by Σ^+ and Σ^- states, the $3^1\Pi$ and $3^3\Pi$ are unbound yet are mostly of *A* configurations. The dominant configurations of $3^1\Pi$ and $3^3\Pi$ at a series of bond lengths are shown in Table 5.10 to try to determine if *B* configurations dominate at longer bond lengths. And, like $1^3\Sigma^-$ the $3^1\Pi$ and $3^3\Pi$ states are dominated by *B* configurations just beyond 1.6 Å.

5.5.4 $^1\Delta$ and $^3\Delta$ states

The singlet and triplet Δ states comprise only five states and are plotted in Fig. 5.8. This is the smallest number of states for any of the symmetries calculated. From the D_{eff} data given in Table 5.9 it can be seen that only two of the $^{1,3}\Delta$ states are quasibound with one being moderately bound, $1^3\Delta$ $D_{eff} = 0.49$ eV, and one weakly bound, $2^1\Delta$ $D_{eff} = 0.49$ eV. The shallow minimum of $2^1\Delta$ is one of the smallest of all the quasibound states and results from an avoided crossing between $1^1\Delta$ and $2^1\Delta$. The unbound states, $2^3\Delta$ and $3^3\Delta$, are composed mostly of repulsive *B* configurations (Table 5.8) and the quasibound state $1^3\Delta$ of attractive *A*

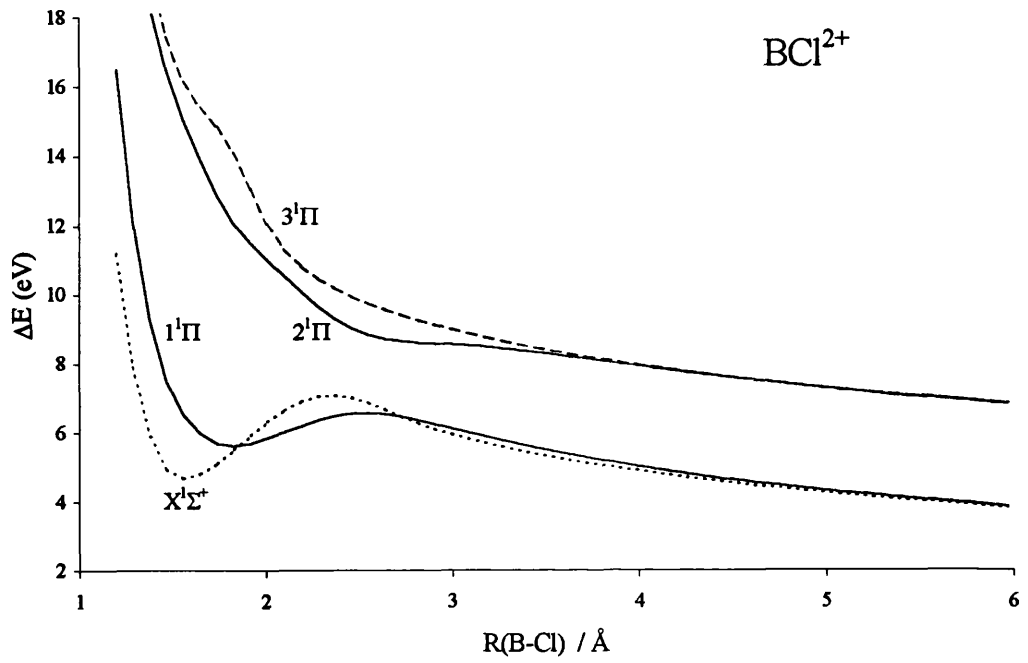

Fig 5.6 *Potential curves for the $^1\Pi$ states of BCl^{2+}*

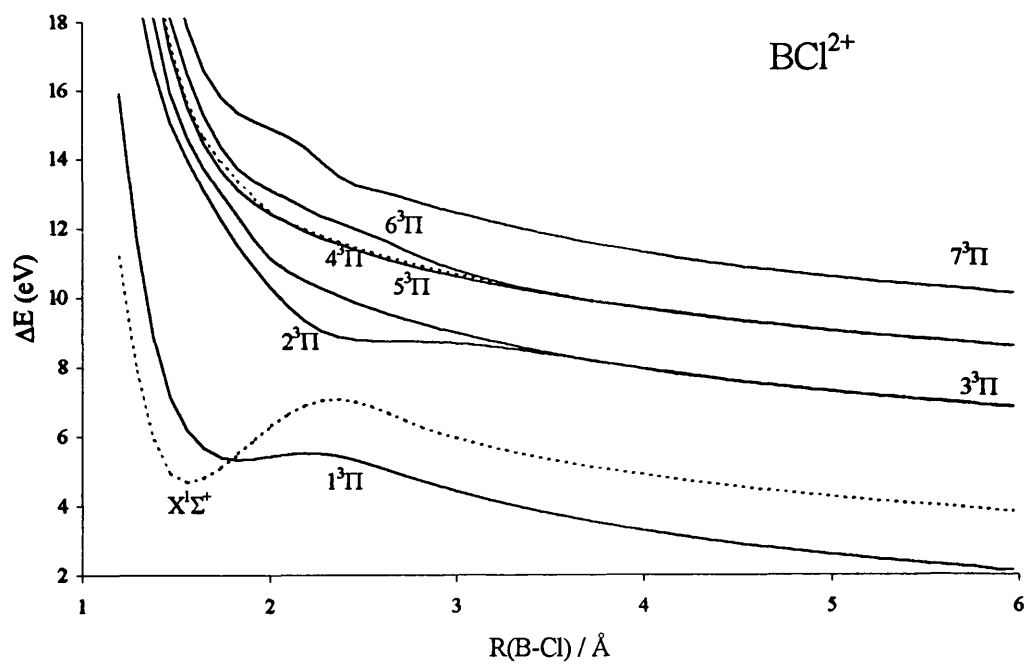

Fig 5.7 *Potential curves for the $^3\Pi$ states of BCl^{2+}*

configurations. The $2^1\Delta$ state consists mostly of repulsive *B* configurations so would be expected to be unbound but is quasibound as an avoided crossing with $1^1\Delta$ forces it into a small barrier with respect to dissociation. Similarly, $1^1\Delta$ is composed of attractive *A* configurations but is not quasibound. This is again due to the avoided crossing altering the shape of the potential curve.

5.5.5 Quintet states

In Fig. 5.9 all the quintet states calculated are plotted together, comprising of one $^5\Sigma^+$, two $^5\Sigma^-$, two $^5\Pi$, one $^5\Delta$. All the quintet states are unbound and like other unbound states of the other multiplicities the quintet states are all composed of B configurations (Table 5.8).

5.6 Tunneling lifetimes and stabilities

As mentioned earlier all electronic states of BCl^{2+} were initially determined by SA CAS calculations and only those states that possessed a potential barrier were subsequently recalculated using the more sophisticated CASSCF / MRCI method. The results of the MRCI calculations were then used in determining the vibrational level energies and tunneling lifetimes of the metastable states by use of the computer program LEVEL [6]. The results of these calculations are summarised in Table 5.11.

The MRCI calculations of the quasibound states are plotted in Figures 5.10 - 5.13. They are grouped together in a similar way to the SA CAS calculations with Fig. 5.10 $^1\Sigma^+$ and $^1\Sigma^-$ states, Fig. 5.11 $^3\Sigma^+$ and $^3\Sigma^-$ states, Fig. 5.12 $^{1,3}\Pi$ states and 5.13 $^{1,3}\Delta$ states. Plotting the quasibound states separately allows them to be seen clearly and it is also possible to compare the MRCI curve shapes with the SA CAS calculations. Studying the SA CAS and MRCI calculations it can be seen that the curve shapes and barrier heights are very similar, although the MRCI curves lie ~ 1eV lower in energy in the region plotted. The difference in energy in this region

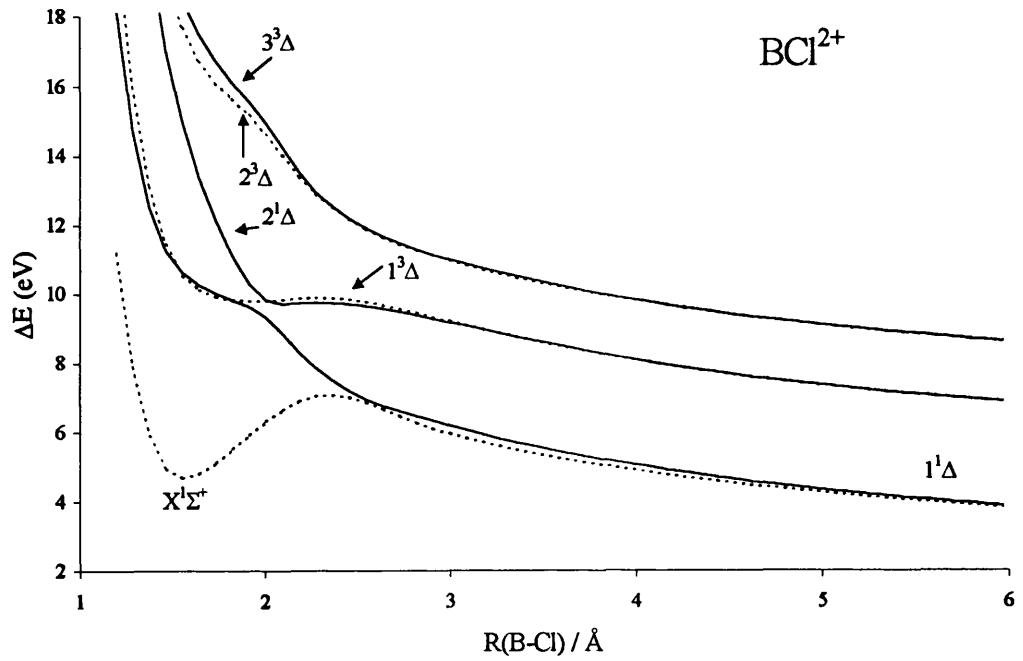

Fig 5.8 *Potential curves for the $^1\Delta$ and $^3\Delta$ states of BCl^{2+}*

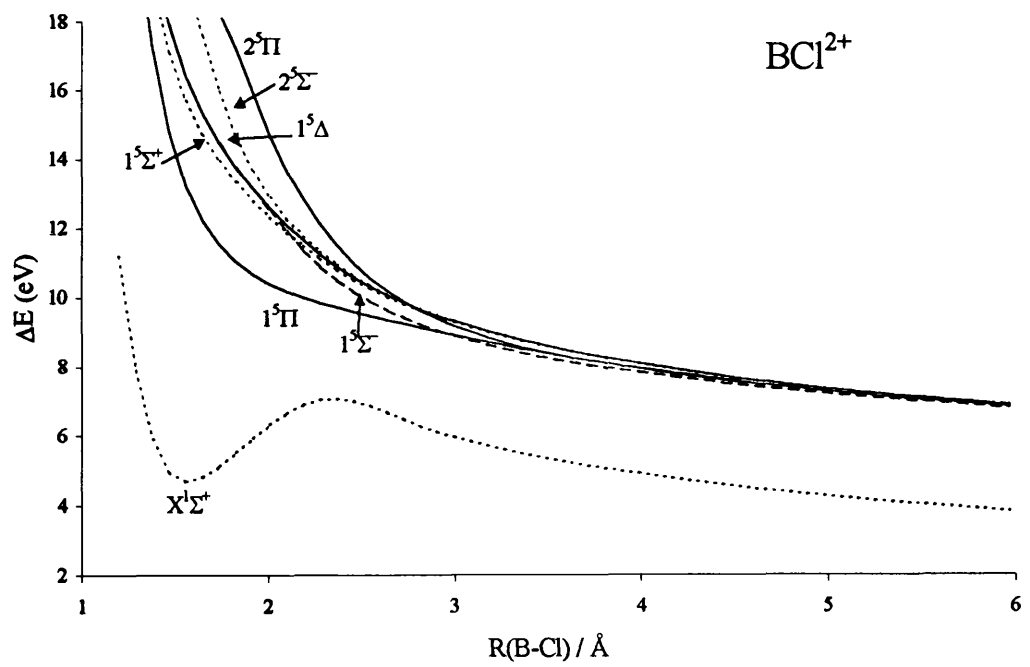

Fig 5.9 *Potential curves for the quintet states of BCl^{2+}.*

is a little surprising as they are both referenced to their own zero points, i.e. the zero point on the SA CAS curves is a SA CAS calculation at 50 Å, and the MRCI zero point is an MRCI calculation at 50 Å.

Table 5.11 *Number of vibrational levels and tunnelling lifetimes for the quasibound states of BCl^{2+}.*

State	No. vibrational levels	Lifetime		
$1^1\Sigma^+$	23	$v = 0 - 17$: $>10^3$s $v = 20$: 10^{-7}s	$v = 18$: 10^{-1}s $v = 21$: 10^{-10}s	$v = 19$: 10^{-4}s $v = 22$: 10^{-12}s
$1^3\Pi$	5	$v = 0$: 10^2s $v = 3$: 10^{-9}s	$v = 1$: 10^{-2}s $v = 4$: 10^{-11}s	$v = 2$: 10^{-5}s
$1^1\Pi$	14	$v = 0 - 8$: $>10^3$s $v = 11$: 10^{-5}s	$v = 9$: 10^2s $v = 12$: 10^{-8}s	$v = 10$: 10^{-2}s $v = 13$: 10^{-11}s
$1^3\Sigma^+$	14	$v = 0 - 8$: $>10^3$s $v = 11$: 10^{-4}s	$v = 9$: 10^2s $v = 12$: 10^{-8}s	$v = 10$: 10^{-1}s $v = 13$: 10^{-10}s
$2^3\Pi$	2	$v = 0$: 10^{-8}s	$v = 1$: 10^{-12}s	
$2^3\Sigma^-$	8	$v = 0 - 2$: $>10^3$s $v = 5$: 10^{-8}s	$v = 3$: 10^{-1}s $v = 6$: 10^{-10}s	$v = 4$: 10^{-5}s $v = 7$: 10^{-12}s
$1^1\Sigma^-$	4	$v = 0$: 10^2s $v = 3$: 10^{-10}s	$v = 1$: 10^{-2}s	$v = 2$: 10^{-7}s
$2^1\Delta$	2	$v = 0$: 10^{-3}s	$v = 1$: 10^{-9}s	
$2^3\Sigma^+$	14	$v = 0 - 9$: $>10^4$s $v = 12$: 10^{-8}s	$v = 10$: 10^1s $v = 13$: 10^{-11}s	$v = 11$: 10^{-4}s
$1^3\Delta$	8	$v = 0 - 2$: $>10^6$s $v = 5$: 10^{-6}s	$v = 3$: 10^1s $v = 6$: 10^{-10}s	$v = 4$: 10^{-3}s $v = 7$: 10^{-12}s

The most strongly bound of the BCl^{2+} states are the four states $X^1\Sigma^+$ (Fig. 5.10), 1,2 $^3\Sigma^+$(Fig. 5.11), and $1^1\Pi$ (Fig. 5.12), all having essentially infinite lifetimes for

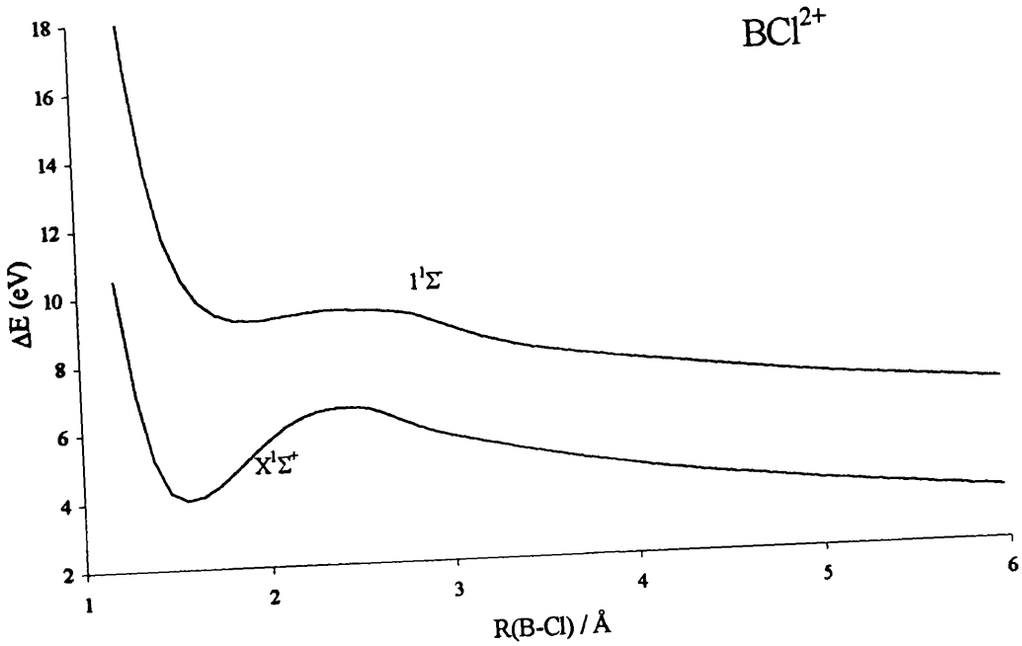

Fig 5.10 *Potential curves for the quasibound $^1\Sigma^+$ and $^1\Sigma$ states of BCl^{2+}.*

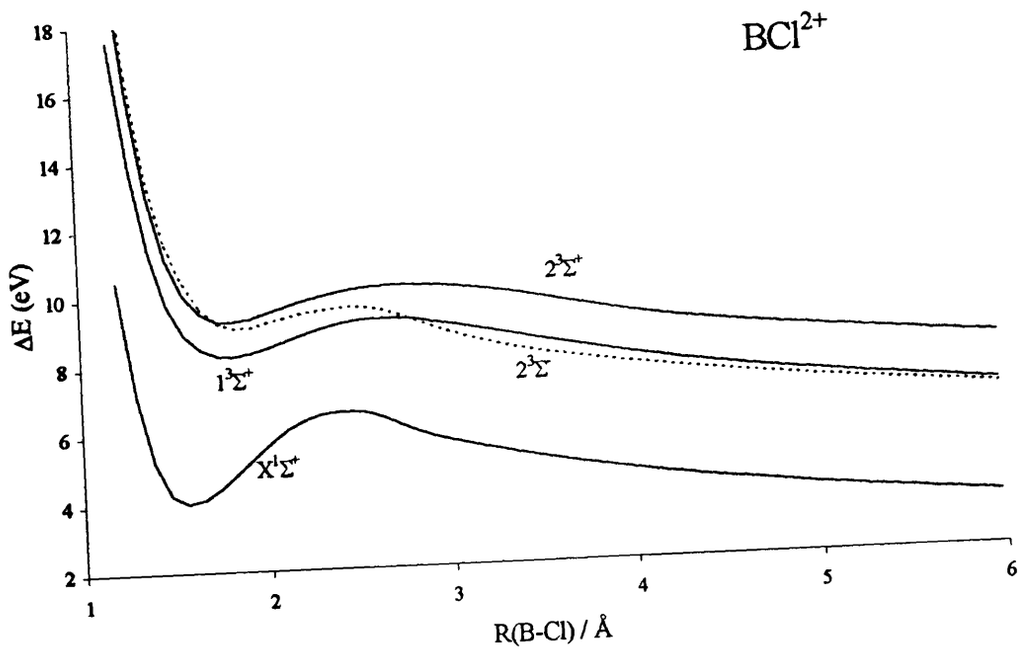

Fig 5.11 *Potential curves for the quasibound $^3\Sigma^+$ and $^3\Sigma$ states of BCl^{2+}.*

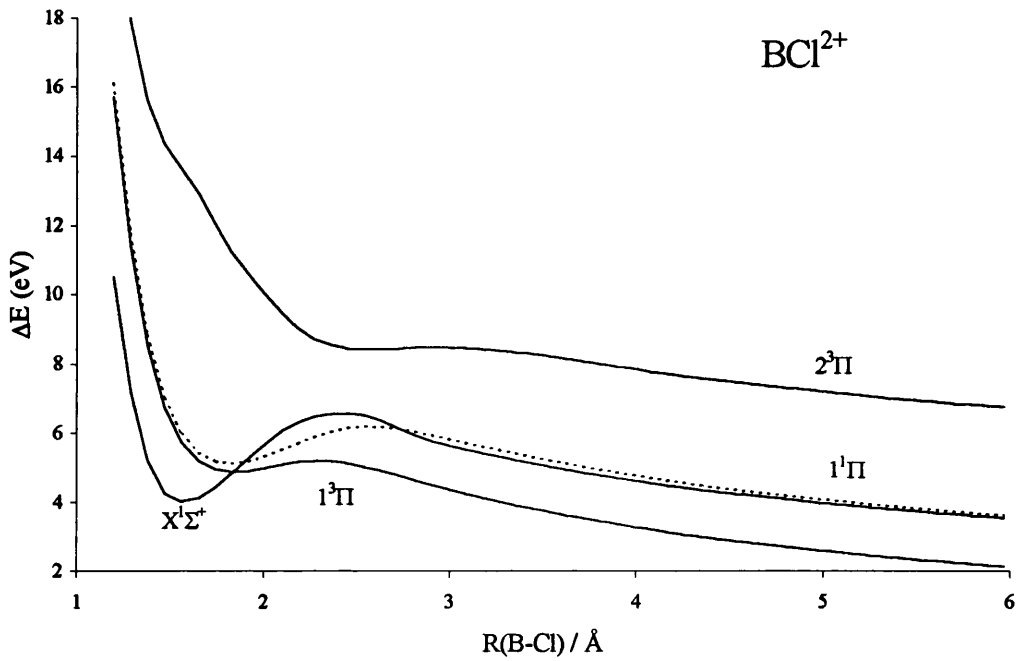

Fig 5.12 *Potential curves for the quasibound $^1\Pi$ and $^3\Pi$ states of BCl^{2+}.*

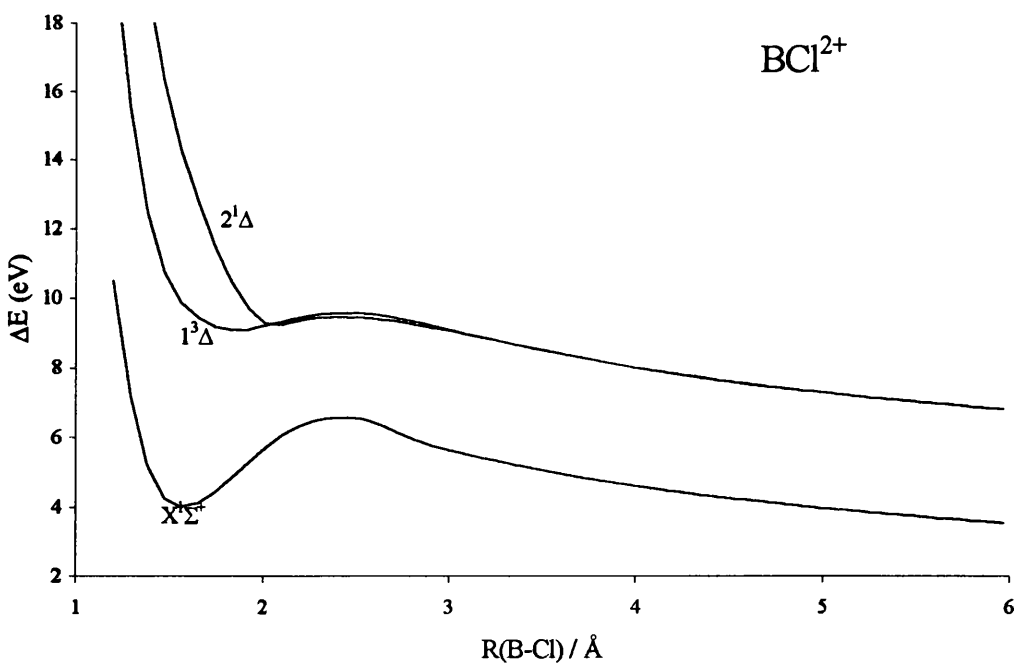

Fig 5.13 *Potential curves for the quasibound $^1\Delta$ and $^3\Delta$ states of BCl^{2+}.*

their first few vibrational levels. Less strongly bound but still relatively stable are $1^1\Sigma^-$ (Fig. 5.10), $2^3\Sigma^-$ (Fig. 5.11), $1^3\Pi$ (Fig. 5.12) and $1^3\Delta$ (Fig. 5.13), these states all have lifetimes of $> 10^2$ s for at least their ground vibrational state. The two most weakly bound states with the lowest number of bound vibrational states are $2^3\Pi$ (Fig. 5.12) and $2^1\Delta$ (Fig. 5.13) although the lifetimes of the $v = 0$ vibrational levels for these states differ significantly. The lifetime of $v = 0$ for $2^1\Delta$ is $\sim 10^{-2}$ s which is potentially detectable in mass spectrometric studies but for $2^3\Pi$ the lifetime of $v = 0$ is $\sim 10^{-8}$ s which is far too short for the parent ion to be detectable experimentally. It is interesting to notice that $2^1\Delta$ and $1^1\Sigma^-$ have almost identical D_{eff} values, 0.22 and 0.23 eV respectively, but the $v = 0$ lifetime for $2^1\Delta$ is shorter by five orders of magnitude, this difference in stability is due to the sharp barrier for $2^1\Delta$ caused by the avoided crossing with $1^1\Delta$ (Fig. 5.8). The sharp barrier of $2^1\Delta$ creates a small barrier width and the lifetime is dependent on the distance an atom must 'tunnel' through the barrier, so a smaller barrier width will reduce the lifetime.

5.6.1 Predissociation

The large number of long lived vibrational levels found for the quasibound states of BCl^{2+} suggest that once formed the dication would be kinetically stable with several accessible long lived electronic states. But the large number of unbound states that are present are likely to intersect with several of the quasibound states providing a mechanism for predissociation and a subsequent shortening of dication lifetime. In Fig 5.14 all the calculated states are plotted together with the quasibound states as solid lines and the unbound states as dotted lines and it can be seen that about half the quasibound states lie in regions with many intersecting dissociative states. As mentioned in Chapter 4 studies on the dications HCl^{2+} [7] and HS^{2+} [8] have shown that predissociation via crossing to an unbound state can be a route for depopulating quasibound states. From inspection of Fig 5.14 it can

be seen that crossing from a quasibound state to an unbound state is likely to leave only $X^1\Sigma^+$, $1^3\Pi$, $1^1\Pi$ and perhaps $1^3\Sigma^+$ and $2^3\Sigma^+$, observable.

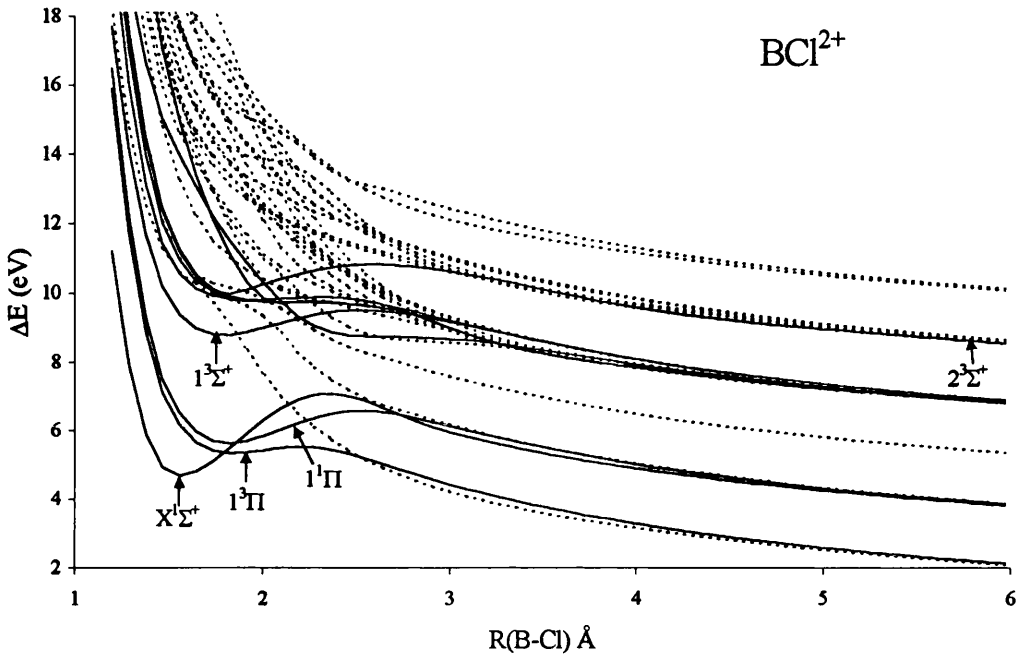

Fig 5.14 *Plot of all the calculated electronic states of BCl^{2+} dissociating to the first 6 dissociation asymptotes. The 10 quasibound states are plotted with solid lines and the unbound states with dotted lines, only certain states are labelled as the plot is used as a guide to which quasibound states are likely to be long lived, see text.*

The quasibound states $X^1\Sigma^+$, $1^3\Pi$ and $1^1\Pi$ are plotted in Fig 5.15 along with the unbound state $1^3\Sigma^-$ which is the only state that intersects these quasibound states. Also the first ten vibrational levels are overlaid onto the $X^1\Sigma^+$ state.

Examination of $X^1\Sigma^+$ shows that it is crossed by bound $1^1\Pi$ and $1^3\Pi$ and unbound $1^3\Sigma^-$. Taking into account where $X^1\Sigma^+$ is crossed by other states the BCl^{2+} ground state would be very stable in the first 4 or 5 vibrational levels, i.e. up to a vibrational excitation of approximately 0.7 eV. Between the $v = 5$ and $v = 6$ vibrational levels $X^1\Sigma^+$ is crossed by the $1^3\Pi$ state so vibrational excitation of the ground state to these levels could lead to crossing to the $1^3\Pi$ state. From Table 5.11 it can be seen that $1^3\Pi$ has only 5 vibrational levels so a crossing to this

state is likely to lead to rapid dissociation if any state other than the ground vibrational state of $1^3\Pi$ is populated due to the short lifetimes of these vibrational levels. Between the $v = 7$ and $v = 8$ vibrational levels $X^1\Sigma^+$ is crossed by the $1^1\Pi$ state and from Table 5.11 it can be seen that the $1^1\Pi$ state is strongly bound, supporting 14 vibrational levels so crossing to this state would not lead to predissociation. Near the barrier maximum of $X^1\Sigma^+$ it is intersected by the unbound $1^3\Sigma^-$ state, but as this is in a region where the tunneling lifetimes of the $X^1\Sigma^+$ vibrational states would be very short, (in the microsecond or less range), BCl^{2+} would rapidly dissociate whether it crossed to the $1^3\Sigma^-$ state or not.

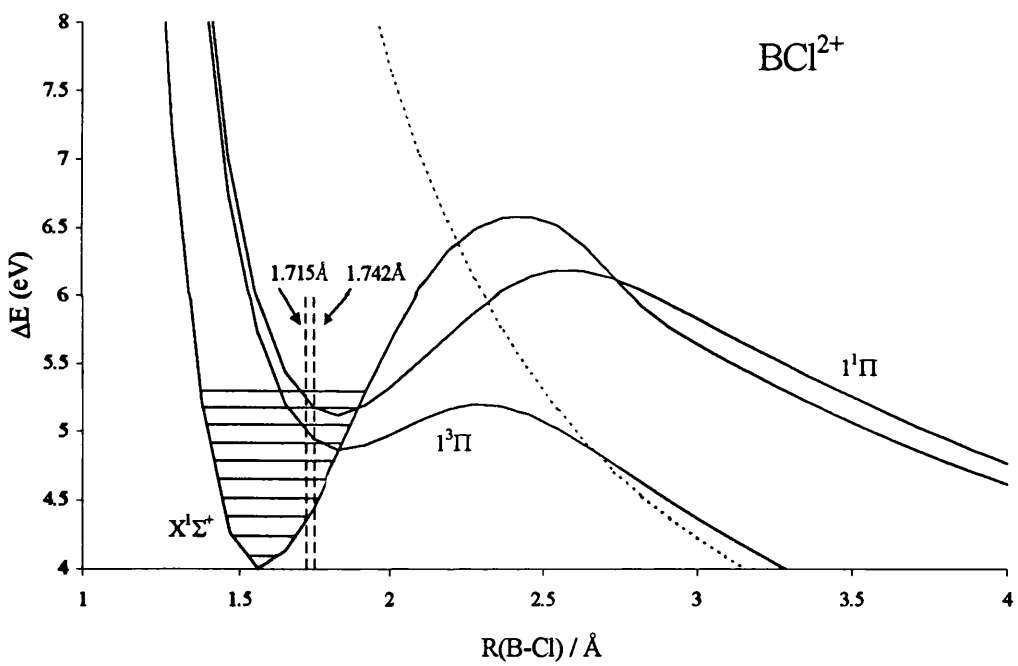

Fig 5.15 *Detail of the strongly bound $X^1\Sigma^+$, $1^1\Pi$ and $1^3\Pi$ states along with $1^3\Sigma$ the only unbound state to intersect with these quasibound states. The first 10 vibrational levels of $X^1\Sigma^+$ and the bond lengths of BCl_3 (1.742 Å) and BCl (1.715 Å) are also marked on.*

The $1^3\Sigma^+$ and $2^3\Sigma^+$ states are both strongly bound with 14 vibrational levels, see Table 5.11, and from inspection of Fig 5.14 they are seen to lie just at the edge of a region of many unbound states so it is possible that they could be observable. Detail from Fig 5.14 showing the region around $1,2^3\Sigma^+$ is shown in Fig 5.16 and it can be seen that a significant number of states cross $2^3\Sigma^+$ so there is a high

likelihood of crossing to one of these states, rapidly dissociating the molecule. The $1^3\Sigma^+$ state is crossed by fewer states than $2^3\Sigma^+$ but the crossings are evenly spaced along the curve and so it seems likely that this state also would not survive for any significant length of time.

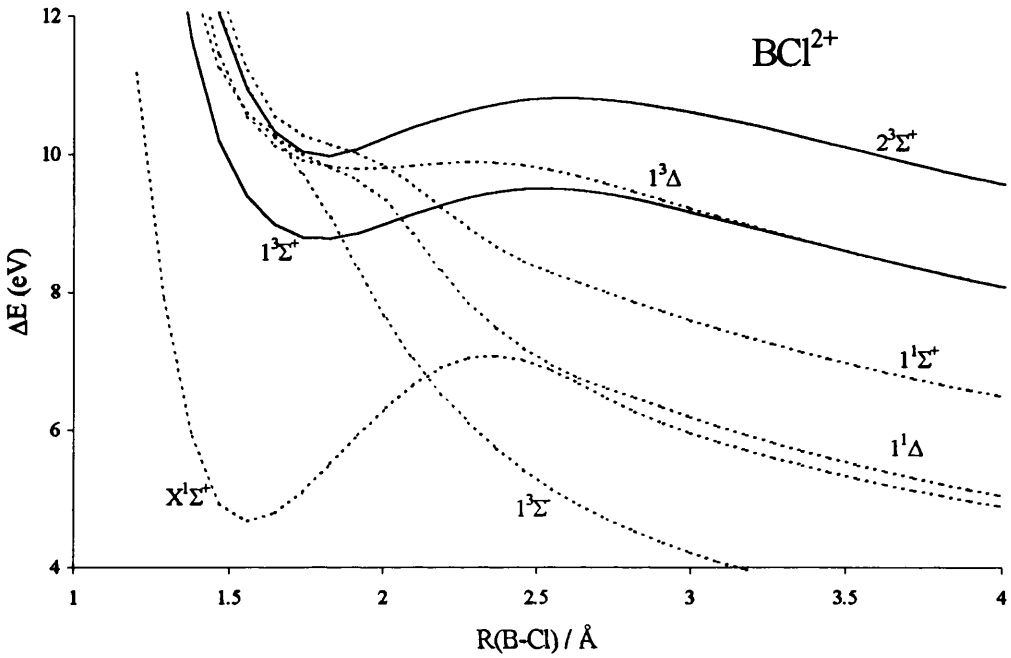

Fig 5.16 *Detail of the strongly bound 1 and $2^3\Sigma^+$ states, showing the one dissociative state ($1^3\Sigma$) intersecting $1^3\Sigma^+$, and some of the many unbound states crossing $2^3\Sigma^+$.*

5.7 Formation of BCl^{2+}

Experimental synthesis of BCl^{2+} is most likely to involve electron ionisation of gaseous BCl_3. This is the process generally used in the formation of CF^{2+} from CF_4 as it obtains high ion yields[9,10]. By this process BCl^{2+} could form via two routes, either double ionisation then fragmentation (Eqn 5.3) or neutral fragmentation then subsequent double ionisation (Eqn 5.4).

$$BCl_3 \rightarrow BCl^{2+} + 2Cl + 2e^- \qquad 5.3$$

$$BCl_3 \rightarrow 2Cl + BCl \rightarrow BCl^{2+} + 2Cl + 2e^- \qquad 5.4$$

So via Eqn. 5.3 the BCl^{2+} molecule would be formed at the bond length of BCl_3, 1.742 Å, and via Eqn. 5.4 at the bond length of BCl, 1.715 Å. These two bond lengths are marked on Fig. 5.15 showing where they cross the $X^1\Sigma^+$, $1^3\Pi$ and $1^1\Pi$

states. The two bond lengths are so similar that it seems unnecessary to discuss them separately but to assume that the behaviour of BCl^{2+} would be similar if formed at either 1.742 Å or 1.715 Å.

Assuming BCl^{2+} is formed at the equilibrium bond lengths mentioned above, i.e. little vibrational excitation of the precursor, then in the ground state $X^1\Sigma^+$ it should be stable and the dication should be observed as the BCl and BCl_3 bond lengths correspond to the third vibrational level which is very long lived. If BCl^{2+} is formed in the $1^3\Pi$ state then it is likely to dissociate rapidly due to the state's short vibrational lifetimes. Slightly higher in energy lies the $1^1\Pi$ state which is strongly bound and excitation to this state should result in long lived BCl^{2+} ions. So, from the discussion above, experiments to form BCl^{2+} from BCl_3 should observe the following trend with increasing ionization energy of the precursor, stable BCl^{2+} ions, B^+ Cl^+ fragments (dissociation via $1^3\Pi$), stable BCl^{2+} ($1^1\Pi$) then B^+ Cl^+ fragments again as excitation is to the region with many unbound states.

5.8 Summary and Conclusions

This study of BCl^{2+} has determined that it possesses several quasibound electronic states that should be accessible experimentally via ionization of gaseous BCl_3. Also, by studying the electron density distribution of the molecular orbitals, possible bonding mechanisms for the stable electronic states have been proposed. Of the 35 states calculated 10 are predicted to be thermodynamically unstable but kinetically stable with four of these states having barriers to dissociation greater than 0.9 eV.

The ground state $X^1\Sigma^+$ has the largest barrier to dissociation at 2.57 eV and subsequently the greatest number of long lived vibrational energy levels, 18, with lifetimes > 10^{-3} s (the limit for a state to be observable in mass spectrometric studies). Of the other quasibound states only $1^1\Pi$ is likely to be observable due to

the large number of unbound electronic states that intersect with the quasibound states providing a mechanism for predissociation.

Analysis of the electron density distribution of the molecule at a series of bondlengths shows a movement of electron density from boron to chlorine suggesting a charge transfer mechanism could stabilise the molecule. Also, from the electron density distribution of the molecular orbitals it appears that the most important configurations describing the metastable states are ones with a charge distribution of B^{2+} Cl and B^{3+} Cl^{-} due to the attraction between the unlike charges. The unbound states consist mostly of configurations of the form $B^{+}Cl^{+}$ with the coulomb repulsion between the like charges destabilizing the molecule.

The calculations suggest that formation of BCl^{2+} via ionization of BCl_3 should produce stable BCl^{2+} assuming sufficient vibrational relaxation of the precursor. Also experiments should observe the following product trend BCl^{2+}, $B^{+}Cl^{+}$, BCl^{2+} then $B^{+}Cl^{+}$ with increasing ionization energy of BCl_3 as excitation occurs to different electronic states.

References

(1) Kolbuszewski M. and Wright J. S. *Chem. Phys. Lett.* **218** (1994) 338.

(2) Kolbuszewski M. and Wright J. S. *Can. J. Chem.* **71** (1993) 1562.

(3) Ballik E. A. *Astrophys. J.* **137** (1963) 84.

(4) Kendall R. A., Jr T. H. D. and Harrison R. J. *J. Chem. Phys.* **96** (1992) 6796.

(5) Moore C. E. *Atomic energy levels*; US Govt. printing office Circular NBS 467:, 1949.

(6) Leroy R. J. *LEVEL 6.1 University of Waterloo Chemical Physics Research Report No. CP-555R* University of Waterloo, Ontario, Canada, 1996.

(7) Bennett F. R. and McNab I. R. *Chem. Phys. Lett.* **251** (1996) 405.

(8) Parlant G., Senekowitsch J., ONeil S. V. and Yarkony D. R. *J. Chem. Phys.* **94** (1991).

(9) Zabka J. and Herman Z. *Czeckoslovak Journal of Physics* **49** (1999) 373.

(10) Manning M., Price S. D. and Leone S. R. *J. Chem. Phys.* **99** (1993) 8695.

Chapter 6

Future work

6.1 Chapter 3: Electron transfer reactions of the SiF_3^{2+} dication with the rare gases neon, argon, krypton and xenon

In the study into the electron transfer reactions of SiF_3^{2+}, there are several areas where more study would be beneficial. As discussed in the Chapter 3, Landau-Zener theory, in our application to atom-molecule reactions contains approximations as it does not account for vibrational states or angular dependence of the potential curves. More advanced formulations of Landau-Zener theory have been developed that incorporate Frank Condon overlap of vibrational states [1] and these could be used to improve the SiF_3^{2+} study.

The *ab initio* calculations on the electronic states of SiF_3^{2+} could be used to produce potential energy curves and to determine the stability of the states. This information could be applied to the product ion yield calculations where previously all excited states were assumed to be unstable. The calculations also determined that excited states of SiF_3^{2+} are present in the reactant ion beams. These excited states could have markedly different equilibrium geometries to the dication ground state, thus forming the cation at a different geometry to that considered in the study. At present Zdenek Herman *et al* in Prague are performing detailed calculations on SiF_3^{2+} to calculate potential surfaces for electronic states of the molecule.

6.2 Chapter 4: On the dissociation of the ozone dication

In the calculations to create the ozone dication singlet and triplet surfaces one of the bonds is kept at a fixed length for all calculations. Allowing this bond to relax by optimising the energy of each calculation would produce more accurate

surfaces. Also, only the first singlet and first triplet electronic states were studied, higher lieing excited states could also be involved in the dissociation of the ozone dication and investigating these could elucidate more detail of the ozone dication dissociation.

At the geometry at which the dication is formed the coupling between the singlet and triplet states is assumed to be sufficient to allow the rapid crossing between the two states. Spin-orbit coupling calculations at the crossing would allow a lifetime of the singlet state to be determined. The dissociation of O_3^{2+} could also be investigated using collision dynamics calculations. A series of potential energy surfaces for the ground singlet states were calculated to be used in a collision dynamics study but no results are available from this study yet.

A conclusion from the O_3^{2+} study is that formation of the dication via single ionisation of the cations could form stable O_3^{2+} ions. No experimental work has yet been performed to investigate this but it would be interesting to test this conclusion.

6.3 Chapter 5: *ab initio* study of the structure and stability of low lying electronic states of the dication BCl^{2+}

The study of BCl^{2+} undertakes some discussion of the mechanism of stability of the dication and it would be interesting to investigate such mechanisms further. Also, spin-orbit coupling calculations on the intersecting electronic states would improve the discussion on the likely stability of the dication upon formation. The calculations suggest that BCl^{2+} would be detected in mass spectrometric studies but no such experimental work has been carried out as yet, although some is planned by Dr Price's research group. Some of the low lying electronic states could also be amenable to laser spectroscopic study similar to that performed on HCl^{2+} [2] giving experimental infomation on the electronic energy levels.

References

(1) Kamber E. Y., Akyungor K., Safvan C. P. and Mathur D. *Chem. Phys. Lett.* **258** (1996) 336.

(2) Hochlaf M., Hall R. I., Penet F., Kjeldson H., Lablanquie P., Lavollee M. and Eland J. H. D. *Chem. Phys.* **207** (1996) 159.

Appendix

LEVEL - Principles and Concepts

1 Introduction

LEVEL is a FORTRAN computer program for solving the radial Schrödinger equation for bound and quasibound levels of any smooth one dimensional potential. The program can also calculate expectation values, centrifugal distortion constants for specified levels and generate radiative lifetimes for transitions between vibration-rotation levels of a given potential to levels of either the same or another potential. LEVEL was written by Robert J. LeRoy who maintains and updates the code and is presently at the University of Waterloo, Canada. Copies of the source code can be obtained by contacting LeRoy at Leroy@uwaterloo.ca.

1.1 Vibration and Rotation of molecules

1.1.1 Vibration

A particle undergoing harmonic motion experiences a restoring force, F, proportional to its displacement from equilibrium, x,

$$F = -kx \qquad 1.1$$

Where k is the force constant. The potential energy, V, and the force, F, are related by $F = -dV/dx$, thus the potential energy of the system is

$$V = \tfrac{1}{2}kx^2. \qquad 1.2$$

The Schrödinger equation for the particle is given by

$$-\frac{\hbar^2}{2m}\frac{d^2\Psi}{dx^2} + \tfrac{1}{2}kx^2\Psi = E\Psi \qquad 1.3$$

and the permitted energies of the harmonic oscillator, E_v, are

$$E_v = (v + \tfrac{1}{2})\hbar\omega \qquad v = 0, 1, 2, \ldots \qquad 1.4$$

ω is the angular velocity and is given by

$$\omega = \left(\frac{k}{m}\right)^{1/2}$$

Thus the energy level separations are given by $\hbar\,\omega$, and the particle has a minimum energy, the zero point energy E_0, of $\frac{1}{2}\hbar\,\omega$.

1.1.2 Rotation

For a body rotating about a given axis, x, the energy is given by $E = \frac{1}{2}I_x\omega_x^2$ where ω_x is the angular velocity and I_x the moment of inertia. Extending this to rotation about three axes the energy term becomes

$$E = \tfrac{1}{2}I_x\omega_x^2 + \tfrac{1}{2}I_y\omega_y^2 + \tfrac{1}{2}I_z\omega_z^2 \qquad 1.5$$

The classical formula for angular momentum about an axis, x, is $J_x = I_x\omega_x$, so for the three axes

$$E = \frac{J_x^2}{2I_x} + \frac{J_y^2}{2I_y} + \frac{J_z^2}{2I_z}. \qquad 1.6$$

For a spherical rotor, a molecule with all three moments of inertia equal e.g. CH_4, the classical expression of the energy is

$$E = \frac{1}{2I}\left(J_x^2 + J_y^2 + J_z^2\right) = \frac{J^2}{2I} \qquad 1.7$$

where J is the magnitude of the angular momentum and $J^2 = J_x^2 + J_y^2 + J_z^2$. A quantum expression for the energy is achieved by making the replacement $J^2 \rightarrow J(J+1)\,\hbar^2$ $J = 0, 1, 2 \ldots$ The quantized energy for a spherical rotor is thus

$$E_J = J(J+1)\frac{\hbar^2}{2I} \quad J = 0, 1, 2, \ldots \qquad 1.8$$

Expressing the energy in terms of the rotational constant B, where $hcB = \hbar^2/I$, the energy of a rotational state is given by the rotational term $F(J)$

$$F(J) = BJ(J+1) \quad B = \hbar/4\pi cI \qquad 1.9$$

For a symmetric rotor, a molecule with two equal moments of inertia e.g. NH_3, $I_x = I_y \neq I_z$ where z is the principal axis. The classical expression for the energy here is

$$E = \frac{J_x^2 + J_y^2}{2I_x} + \frac{J_z^2}{2I_z} \qquad 1.10$$

Which when expressed in terms of $J^2 = J_x^2 + J_y^2 + J_z^2$ by dividing through by $J_z^2 / 2I_z$ becomes

$$E = \frac{J_x^2 + J_y^2 + J_z^2}{2I_z} + \frac{J_z^2}{2I_x} - \frac{J_z^2}{2I_z}$$
$$= \frac{J^2}{2I_z} + \left(\frac{1}{2I_x} - \frac{1}{2I_z}\right) J_z^2 \qquad 1.11$$

This is expressed quantum mechanically by replacing J^2 by $J(J+1)\hbar^2$, and also by using the fact that the component of angular momentum about any axis is restricted to the values

$$J_z = K\hbar \quad K = 0, \pm 1, \pm 2, \ldots \pm J \qquad 1.12$$

The rotational terms $F(J)$ for a symmetric rotor are then

$$F(J, K) = BJ(J+1) + (A-B)K^2$$
$$J = 0, 1, 2, \ldots \; K = 0, \pm 1, \pm 2, \ldots \pm J \qquad 1.13$$
$$A = \frac{\hbar}{4\pi c I_x} \qquad B = \frac{\hbar}{4\pi c I_z}$$

For a linear rotor where the moment of inertia about the axis is zero e.g. CO_2 and HCl, Eqn. 1.13 can be used with $K = 0$. The rotational terms are thus

$$F(J) = BJ(J+1) \qquad 1.14$$

also, for a diatomic the moment of inertia, I, equals μR^2 where μ is the reduced mass and is given by $\frac{1}{\mu} = \frac{1}{m_1} + \frac{1}{m_2}$, the rotational energies can then be written as

$$E_J = J(J+1)\frac{\hbar^2}{2\mu R^2} \quad J = 0, 1, 2, \ldots$$

1.1.3 Diatomic Molecular Vibration

Close to the minimum of a typical molecular potential energy curve, around the equilibrium geometry, the curve is well represented by a parabola. The potential energy can be written as for the harmonic oscillator,

$$V = \tfrac{1}{2}k(R-R_e)^2 \qquad 1.15$$

where k is the force constant of the bond, R_e the equilibrium bond length and R the atom-atom separation. The Hamiltonian for the motion of two particles of masses m_1 and m_2 moving with this potential energy is

$$H = -\frac{\hbar^2}{2m_1}\frac{d^2}{dx_1^2} - \frac{\hbar^2}{2m_2}\frac{d^2}{dx_2^2} + V \qquad 1.16$$

and using the reduced mass, μ, the Schrödinger equation for this system can be written as

$$-\frac{\hbar^2}{2\mu}\frac{d^2\Psi}{dx^2} + V\Psi = E\Psi \qquad 1.17$$

The vibrational energy levels are given by

$$E_v = (v + \tfrac{1}{2})\hbar\omega \qquad v = 0, 1, 2, \ldots$$
$$\omega = \left(\frac{k}{\mu}\right)^{1/2} \qquad 1.18$$

Which can be expressed in wavenumbers using the vibrational terms G.

$$G(v) = (v + \tfrac{1}{2})\bar{\nu} \qquad \bar{\nu} = \left(\frac{\omega}{2\pi c}\right) \qquad 1.19$$

1.1.3.1 Anharmonicity

At high vibrational excitation the diatomic potential energy curve deviates significantly from a parabola and becomes anharmonic as the force constant is no longer proportional to the displacement. Also, as the curve becomes less confining than a parabola at higher excitation the energy levels become less widely spaced.

One approach to more accurately represent this anharmonic potential energy curve is to use a Morse potential

$$V = D_e\left\{1 - e^{a(R-R_e)}\right\}^2 \qquad a = \left(\frac{\mu}{2D_e}\right)^{\frac{1}{2}}\omega \qquad 1.20$$

which resembles a parabola around R_e and allows for dissociation by tending toward an asymptote, lying at energy D_e, at large R. Solving the Schrödinger equation for the Morse potential gives the permitted vibrational energy levels

$$G(v) = (v + ½)\bar{\nu} - (v + ½)^2\chi_e\bar{\nu} \qquad \chi_e = \left(\frac{a^2\hbar}{2\mu\omega}\right) \qquad 1.21$$

where χ_e is the anharmonicity constant and the number of vibrational levels is finite.

The Morse potential is still an approximation and in practice a more general expression for the vibrational energy levels is

$$G(v) = (v + ½)\bar{\nu} - (v + ½)^2\chi_e\bar{\nu}^2 + (v + ½)^3\gamma_e\bar{\nu}^3 + \ldots \qquad 1.22$$

Several other functions have been produced to model a typical molecular potential energy curve. Examples of these include the Lennard-Jones (n,6)-potential [1] which has the form

$$V = \frac{C_n}{r^n} - \frac{C_6}{r^6} \qquad 1.23$$

where C_n and C_6 are arbitrary coefficients chosen to give a best fit to experimental data. The potential curve shape forms as a consequence of competition between the attractive $-C_6/r^6$ term and the repulsive $+C_n/r^n$ term. Generally n is chosen to be between 10 and 12 so that at short range $+C_n/r^n$ dominates the curve giving a steep repulsive wall. At large r the $-C_6/r^6$ term dominates so that the curve is attractive, and at intermediate distances a potential well forms due to competition between the r^{-6} and r^{-n} terms.

Representing the repulsion term as $\frac{1}{r^n}$ is often found to be a poor representation of a typical curve and an exponential term is more realistic. To account for this the exponential – R^{-6} function, also know as "Buckingham" or "Hill" type potential [2] can be used, this is given by

$$V = Ae^{-Br} - \frac{C}{r^6} \qquad 1.24$$

where A, B and C are again constants chosen to fit experimental data.

One method of determining the potential without imposing any assumed analytic form is the Rydberg-Klein-Rees, RKR, method [3-5]. Here the potential is determined using experimental vibrational and rotational spectroscopic terms.

2 Solving for the Vibrational Wavefunction

At the heart of the LEVEL program is the determination of the eigenvalues and eigenfunctions of the radial Schrödinger equation

$$-\frac{\hbar^2}{2\mu}\frac{d^2\Psi_{v,J}(R)}{dx^2} + V_J(R)\Psi_{v,J}(R) = E_{v,J}\Psi_{v,J}(R) \qquad 2.1$$

where $\Psi_{v,J}(R)$ incorporates vibration and rotation. The vibration and rotation quantum numbers are v and J respectively and the potential, $V_J(R)$, is a sum of the rotationless potential plus a centrifugal term.

In solving Eqn. 2.1 the equation is integrated numerically using the Numerov algorithm as the Numerov formula can be used to solve numerically differential equations of the form $y'' = F(x, y)$. Taking the one dimensional Schrödinger equation as given in Eqn. 1.3, this can be written as

$$\Psi'' = \frac{d^2\Psi(x)}{dX^2} = -\frac{2\mu}{\hbar^2}(E - V(x))\Psi(x) = f(x)\Psi(x) \qquad 2.2$$

here $F(x, y)=f(x)y$ and the Numerov formula for this case is

$$y_{n+1} = \left[2y_n - y_{n-1} + \frac{h^2}{12}\left(10 f(x_n) y_n + f(x_{n-1}) y_{n-1}\right) \right] \cdot \left[1 - \frac{h^2}{12} f(x_{n+1}) \right]^{-1} + R_{n+1} \qquad 2.3$$

$x_n - x_{n-1} = h$ and n labels the successive points at which y is computed. The residual term R_{n+1} can be computed from

$$R_{n+1} \cong -h^6 \left(\frac{d^6 y}{dx^6} \right)_{n+1} \Big/ 240$$

Using the Numerov method an iterative process can be used to determine numerically the wavefunction and subsequently the eigenfunctions and eigenvalues can be computed by methods outlined below.

The method used to locate accurately the eigenvalues and eigenfunctions is based on the Cooley procedure [6]. This method involves two series of calculations of the wavefunction for a trial energy, one proceeds inwards from $R_{MAX} \rightarrow R_{MIN}$ and the other outwards from $R_{MIN} \rightarrow R_{MAX}$. The values R_{MAX} and R_{MIN} must lie sufficiently inside the classically forbidden region of the potential that the wavefunction has decayed by several orders of magnitude, ($\sim 10^9$), relative to its amplitude in the classically allowed region. For the inward calculation an arbitrary small value (effectively zero) is assigned to $\Psi_{R_{MAX}}$ and the numerical integration carried out inwards to an arbitrary point R_x. The outward integration begins with a boundary condition of $\Psi_{R_{MIN}} = 0$ and a small value to the next point, the numerical integration is then performed outwards to R_x. A correction to the trial energy can then be determined by the discontinuity in the slopes of the outward and inward wavefunctions at R_x, the process is then repeated for this new energy and another correction term determined. This procedure is repeated in an iterative process until the successive values of the energy differ by less than a set value.

The Cooley procedure is rapid and applicable to any function and for a single minimum potential it is insensitive to the choice of R_x provided that it lies within the classically allowed region. Also, a maximum number of iterations should be set as the process can eventually oscillate between two values.

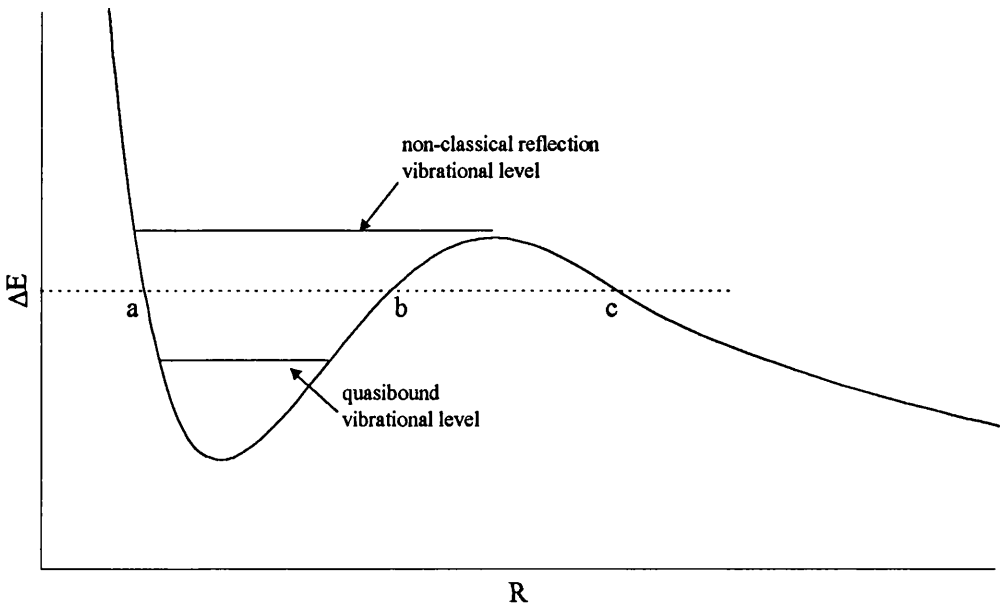

Fig 1.1 *Schematic potential energy curve with three turning points a, b and c marked for a particular energy. Also marked are two vibrational levels, a quasibound level lying above the asymptote but below the barrier maximum, the other lying above the barrier maximum and existing, despite it having sufficient energy to overcome the potential barrier, due to quantum mechanical anti-tunneling effects.*

To determine the highest vibrational levels of a potential a near dissociation expansion (NDE) function is employed [7] that estimates the energy of vibrational levels that lie near and above the barrier maximum. NDE's are based around the theory that vibrational levels lying very near the barrier maximum have properties that depend on the long range inverse power tail of the potential and simple analytical expressions can be devised for the vibrational energy levels spacings and other properties. Levels can occur above the barrier maximum as a result of anti-tunneling effects also known as non-classical reflection, where the quantum mechanical effects allow a vibrational state to exist even though classically it has sufficient energy to pass over the barrier, an example is shown schematically in

Fig 1. The lifetimes of such states of a quasibound potential are very short but they are important in calculations to determine the vibrational energy required to dissociate a molecule.

3. Treatment of quasibound levels

Quasibound or orbiting resonance levels are vibrational states that lie above the dissociation asymptote but below a local maximum in the potential, see Fig 1. These levels require special treatment as the finite width of the potential barrier means that these levels are able to quantum mechanically tunnel through the barrier resulting in the states possessing a finite lifetime before dissociation.

The energies of the quasibound vibrational states correspond approximately to the eigenvalues the potential would have if the asymptote was the barrier maximum energy. It is possible to use "exact" quantum mechanical methods to determine these quasibound levels but these methods are lengthy and time consuming [8]. A more efficient technique is to impose an approximate boundary condition where the wavefunction is required to have some chosen behaviour at the outer boundary and also at R=0. With these boundary conditions imposed it is then possible to determine the eigenvalues and eigenfunctions of the wavefunction by techniques such as the Cooley method described above. Among the most successful boundary conditions found, and the one used in LEVEL, is that the wavefunction behaves as an Airy function of the second kind [8] at the second turning point, marked b in Fig 1.

To determine the lifetimes of the quasibound vibrational levels LEVEL uses a uniform semi-classical approximation. In the classically forbidden region of the potential within the barrier, between points b and c in Fig 1, LEVEL uses the semi-classical result that the wavefunction dies off exponentially with an exponent of

$$-\sqrt{\frac{2\mu}{\hbar^2}}\int_{R_2(v,J)}^{RMX(v,J)}\left[V_J(R)-E_{v,J}\right]^{\frac{1}{2}}dR \qquad 3.1$$

The limits of this integration are set so that $R_2(v,J)$ is the outer end of the classically accessible region for this level, b in Fig 1.1, and RMX is set within the barrier at a point such that the wavefunction amplitude is less than $\sim 10^{-9}$ of its amplitude in the classically allowed region. The uniform semi-classical approximation for calculating the lifetimes requires the evaluation of an integral similar to that in Eqn 3.1, in the classically forbidden region within the barrier.

4. Potential generation

The potential used by LEVEL in its calculations is stored as an array of finely spaced points that are determined either from turning points given by the user, one of several internal analytic functions or a user entered function. For user entered turning points LEVEL fits either a polynomial function to the points or a spline function. The spline function is a function that is often used to fit a smooth curve to a set of points, it uses the constraint that the second derivative of the fitted curve is zero at each read in point. Also, LEVEL adds the condition that for distances shorter than the second of the read in turning points the potential is extrapolated inward with an exponential function fitted to the last three points. The asymptotic tail of the potential can also be fitted to an exponential or an inverse power function.

LEVEL has several in built functions that can be used to create the potential, these functions only require a few variables to be entered to generate the potential. Among the in-built functions are the Lennard-Jones and Morse potentials mentioned above and also several other more sophisticated functions. It is also possible to replace the potential generating subroutine by a user's own code to generate a potential using a function of their own.

5. Other properties calculated

As well as vibration-rotation energy levels and tunneling lifetimes LEVEL can also calculation centrifugal distortion constant for the calculated levels. Also, it is possible to calculate radiative lifetimes for a transition between levels of two different potentials or among levels of one potential. The Franck-Condon factor for the coupling of the two states the states $\Psi_{v'J'}$ and $\Psi_{v''J''}$ is calculated by the equation

$$FCF = \left|\langle \Psi_{v'J'} | \Psi_{v''J''} \rangle\right|^2 \qquad 5.1$$

and the rate of spontaneous emission from the higher lying state is calculated from the Einstein A coefficient where

$$A = 3.1361861 \times 10^{-7} \left[S(J',J'')/(2J'+1)\right] \nu^3 \left|\langle \Psi_{v'J'} | M(R) | \Psi_{v''J''} \rangle\right|^2 \qquad 5.2$$

In Eqn. 5.2 *M(R)* is the dipole moment and ν the emission frequency, *S(J',J'')* the overlap integral is originally set up for singlet - singlet transition with the selection rules $\Delta\Lambda$=0, $\pm$1 but can be generalised for other multiplicities.

References

(1) Lennard-Jones J. E. *Proc. R. Soc. London, Ser. A* **106** (1924) 463.

(2) Hill T. C. *J. Chem. Phys.* **16** (1948) 399.

(3) Rees A. L. G. *Proc. Phys. Soc. (London)* **A59** (1947) 998.

(4) Rydberg R. *Ann. Physik* **73** (1931) 376.

(5) Klein O. *Z. Physik* **76** (1932) 226.

(6) Cooley J. W. *Math. Computations* **15** (1961) 363.

(7) LeRoy R. J. *J. Chem. Phys.* **101** (1994) 10217.

(8) LeRoy R. J. and Liu W.-K. *J. Chem. Phys.* **69** (1978) 3622.